

Efficient Canonical Correlation Analysis with Sparsity

Zixuan Wu*

Department of Statistics, University of Chicago
and

Elena Tuzhilina

Department of Statistics, University of Toronto
and

Claire Donnat

Department of Statistics, University of Chicago

July 16, 2025

Abstract

In high-dimensional settings, Canonical Correlation Analysis (CCA) often fails, and existing sparse methods force an untenable choice between computational speed and statistical rigor. This work introduces a fast and provably consistent sparse CCA algorithm (ECCAR) that resolves this trade-off. We formulate CCA as a high-dimensional reduced-rank regression problem, which allows us to derive consistent estimators with high-probability error bounds without relying on computationally expensive techniques like Fantope projections. The resulting algorithm is scalable, projection-free, and significantly faster than its competitors. We validate our method through extensive simulations and demonstrate its power to uncover reliable and interpretable associations in two complex biological datasets, as well as in an ML interpretability task. Our work makes sparse CCA a practical and trustworthy tool for large-scale multimodal data analysis. A companion R package has been made available.¹

Keywords: Multi 'omics analysis; Multivariate Analysis; Sparsity; High-Dimensional Statistics; Unsupervised Learning;

*C.D. gratefully acknowledges support from the National Science Foundation under Award Number 2238616, the National Institute for Theory and Mathematics in Biology, as well as the resources provided by the University of Chicago's Research Computing Center. E.T. was supported by Natural Sciences and Engineering Research Council of Canada under grant RGPIN-2023-04727; the University of Toronto Data Science Institute Catalyst grant; and the University of Toronto McLaughlin Center under grant MC-2023-05.

¹The package can be found at the following link: <https://github.com/donnate/ccar3>

1 Introduction

In an era of increasingly prevalent multimodal datasets, from genomics to imaging and beyond, methods that can effectively uncover shared information across different data views are indispensable. Canonical correlation analysis (CCA), a classical technique introduced by Hotelling (1936), remains a cornerstone for identifying linear associations between two sets of variables. Given two datasets $X \in \mathbb{R}^{n \times p}$ and $Y \in \mathbb{R}^{n \times q}$ assumed to be jointly sampled from a centered multivariate normal distribution with covariance Σ , CCA finds r linear projections of X and Y which are maximally correlated in expectation. Mathematically, this objective can be expressed as:

$$\forall j \leq r, \quad u_j^*, v_j^* = \underset{u \in \mathbb{R}^p, v \in \mathbb{R}^q}{\operatorname{argmax}} u^\top \Sigma_{XY} v \quad (1)$$

subject to $u^\top \Sigma_X u = 1, \quad v^\top \Sigma_Y v = 1$ and $\forall l < j, \quad u_l^\top \Sigma_X u = 0, \quad v_l^\top \Sigma_Y v = 0$.

In practice, the population covariance matrices $\Sigma_X, \Sigma_Y, \Sigma_{XY}$ are replaced by their empirical counterparts ($\widehat{\Sigma}_X = \frac{1}{n} X^\top X$, $\widehat{\Sigma}_Y = \frac{1}{n} Y^\top Y$ and $\widehat{\Sigma}_{XY} = \frac{1}{n} X^\top Y$, respectively). For each pair of resulting canonical directions, u_j^* and v_j^* , the corresponding variates, Xu_j^* and Yv_j^* , represent projections of the two datasets onto a subspace that captures shared information. The resulting diagonal matrix $\Lambda^* = \operatorname{diag}(\lambda_1^*, \dots, \lambda_r^*)$, where, for each j , $\lambda_j^* = u_j^{*\top} \Sigma_{XY} v_j^*$, encodes correlations between pairs of canonical variates.

Canonical correlation analysis has found widespread applications across diverse disciplines, including sociology, economics (Fan and Konold, 2018; Thorndike, 2000; Dos Santos and Brandi, 2014; Mazuruse, 2014), and extensively in biology (Lê Cao et al., 2009; Revilla et al., 2021; Rodosthenous et al., 2020; Safo et al., 2018; Jiang et al., 2023; Lin et al., 2013), where the rise of multimodal 'omics' data has renewed interest in CCA as an integrative analysis tool. We refer the reader to Section 5 and Appendix C for examples of the use of CCA in biological settings.

Although canonical correlation analysis is a popular tool for scientific discovery, its reliability in increasingly common high-dimensional settings (i.e. when $\max(p, q) \geq n$) is a growing concern. In fact, this method is known to often produce unstable results and inconsistent canonical directions in such scenarios (Gao et al., 2017). This issue, long discussed in statistical circles, is now being highlighted in applied research (Helmer et al., 2024; McIntosh, 2021; Nakua et al., 2024). For example, recent work by Helmer et al. (2024) studying the reliability of CCA in neuroscience settings highlights that empirically, the “stability of CCA [...] in high-dimensional datasets is questionable”: the correlations found on training data do not match those on held-out data, indicating overfitting and inconsistent canonical directions. Such failures to generalize critically undermine CCA’s role in generating reliable insights and discovering associations.

CCA in High-Dimensions. To address this challenge, several sparse CCA approaches have been developed. These approaches impose structural constraints on the canonical directions, assuming only a subset of variables contribute to defining the canonical variates. The sparse variants of CCA thus simultaneously perform variable selection while estimating the CCA subspaces $U^\star = [u_1^\star | \dots | u_r^\star]$ and $V^\star = [v_1^\star | \dots | v_r^\star]$, where the \star notation indicates the underlying population quantities. Existing solutions to sparse CCA can be broadly classified into two categories: heuristic methods vs. theory-based methods ². Heuristic approaches typically rely on alternating algorithms to impose sparsity (usually in the form of an ℓ_1 penalty), holding one direction fixed to estimate the other. These algorithms tend to be fast but sensitive to initialization. Among these, the approach of Witten et al. (2009) has become particularly popular due to its simplicity and computational tractability. Yet this method relies on a crucial and often overlooked simplification: it assumes that

²A more comprehensive and detailed review of sparse CCA method is provided in Section A.

the covariance matrices Σ_X and Σ_Y are diagonal. While this assumption simplifies the optimization problem, it ignores the true geometry of the data and can lead to spurious or misleading associations—particularly when the variables exhibit strong dependencies.

In contrast, recent theoretical work has established consistent procedures for sparse CCA that respect the full covariance structure (Gao et al., 2015, 2017; Gao and Ma, 2023), though these methods often rely on computationally intensive steps — such as a Fantope-based initialization — that scale poorly with the dataset size. More recently, Donnat and Tuzhilina (2024) proposed a computationally efficient alternative by reframing CCA as a reduced-rank regression problem, offering consistent estimators when one of the datasets is low-dimensional. However, their method does not support sparsity in both X and Y .

Contributions. In this paper, we build upon the idea presented in Donnat and Tuzhilina (2024), viewing the estimation of canonical directions through the lens of a reduced-rank regression. However, we stress that our formulation of the reduced-rank regression problem is distinct. It is designed to handle more general scenarios when both X and Y are high-dimensional datasets; thus, our approach substantially extends beyond the original framework. Our main contributions are threefold:

(1) We show in Section 2.1 that the matrix product $B = U^* \Lambda^* V^{*\top}$ can be estimated by solving the optimization problem:

$$\hat{B} = \operatorname{argmin}_{B \in \mathbb{R}^{p \times q}} \left\| \frac{1}{n} X B Y^\top - I_n \right\|_F^2 \quad \text{subject to} \quad \operatorname{rank}(B) = r. \quad (2)$$

Here I_n denotes the identity matrix of size n . To extend applicability to high-dimensional contexts (Section 2.2), we incorporate an ℓ_1 penalty (or ℓ_1 -group penalty, when applicable) on the matrix B .

(2) We establish the statistical consistency of our estimates in Section 3 and provide

theoretical guarantees that our method recovers the correct support of the true canonical subspaces U^* and V^* with high probability, further validating the practical utility of sparse CCA as a hypothesis-generating tool. While our method presents a minor loss in statistical efficiency compared to established methods such as Gao et al. (2017); Gao and Ma (2023), it offers significantly improved computational efficiency.

(3) We illustrate the effectiveness of our approach through simulation studies (Section 4) and applications to four real-world datasets (Section 5), demonstrating its accuracy and capability to identify scientifically relevant associations across a variety of fields.

Notations. For any $t \in \mathbb{Z}^+$, let $[t]$ denote the set $\{1, 2, \dots, t\}$. For a set S , we let $|S|$ denote its cardinality and S^c its complement. For any $a, b \in \mathbb{R}$, define $a \vee b = \max(a, b)$ and $a \wedge b = \min(a, b)$. For a vector $u \in \mathbb{R}^d$ (denoted by a lowercase letter), we define the Euclidean norm $\|u\| = \sqrt{\sum_i u_i^2}$, the ℓ_0 -norm $\|u\|_0 = \sum_i \mathbf{1}_{\{u_i \neq 0\}}$, and the ℓ_1 -norm $\|u\|_1 = \sum_i |u_i|$. For a matrix $A = (a_{ij}) \in \mathbb{R}^{p \times k}$ (denoted by an uppercase letter), let A_i denote its i -th row. For two index subsets $S_1 \subseteq [p]$ and $S_2 \subseteq [k]$, we denote by $A_{S_1 S_2}$ the submatrix of A consisting of the rows and columns indexed by S_1 and S_2 , respectively. The support of A , denoted $\text{supp}(A)$, is the index set of its nonzero rows, i.e. $\text{supp}(A) = \{i \in [p] : \|A_i\| > 0\}$. The i -th largest singular value of A is denoted $\sigma_i(A)$, with $\sigma_{\max}(A) = \sigma_1(A)$ and $\sigma_{\min}(A) = \sigma_{\text{rank}(A)}(A)$. The Frobenius norm and the operator norm of A are defined as $\|A\|_F = \sqrt{\sum_{i,j} a_{ij}^2}$ and $\|A\|_{\text{op}} = \sigma_1(A)$, respectively. The $\ell_{1,1}$ norm of the matrix A is denoted as $\|A\|_{11} = \sum_{i,j} |A_{ij}|$, and its $\ell_{2,1}$ norm is defined as the sum of its row norms: $\|A\|_{21} = \sum_{i=1} \|A_i\|$. The pseudo-inverse of a matrix A is denoted by A^\dagger . If A is positive semi-definite, $A^{1/2}$ denotes its principal square root. For two matrices $A, B \in \mathbb{R}^{p \times k}$, the trace inner product is given by $\langle A, B \rangle = \text{Tr}(A^\top B)$.

Parameter Space. In this work, we assume the *canonical pair model* described by Gao et al. (2017). Under this formalism, we observe n independently and identically distributed (i.i.d.) pairs of vectors $(X_i, Y_i)_{i=1}^n$ drawn from a joint multivariate Gaussian distribution $\mathcal{N}_{p+q}(0, \Sigma)$. Here, $\Sigma = \begin{pmatrix} \Sigma_X & \Sigma_{XY} \\ \Sigma_{XY}^\top & \Sigma_Y \end{pmatrix}$ and the cross-covariance matrix Σ_{XY} admits the reparametrization

$$\Sigma_{XY} = \Sigma_X U^* \Lambda^* V^{*\top} \Sigma_Y. \quad (3)$$

and the matrices $U^* = [u_1^* | \dots | u_r^*] \in \mathbb{R}^{p \times r}$ and $V^* = [v_1^* | \dots | v_r^*] \in \mathbb{R}^{q \times r}$ store the r canonical directions column-wise. The diagonal matrix $\Lambda^* = \text{diag}(\lambda_1^*, \dots, \lambda_r^*)$ contains the corresponding canonical correlations, ordered in decreasing order: $\lambda_1^* \geq \lambda_2^* \geq \dots \geq \lambda_r^*$.

Throughout this paper, we consider scenarios where the leading canonical direction vectors are row-wise sparse. More precisely, we define by $\mathcal{F}(s_u, s_v, p, q, r; M)$ the set of all covariance matrices Σ that satisfy Equation 3 and such that:

1. *the support of U^* and V^* is small*, i.e. $|\text{supp}(U^*)| \leq s_u$ and $|\text{supp}(V^*)| \leq s_v$, where the support of a matrix is defined as the set of its non-zero rows;
2. *the covariances are well-conditioned*, i.e.

$$\sigma_{\min}(\Sigma_X) \wedge \sigma_{\min}(\Sigma_Y) \geq \frac{1}{M} \quad \text{and} \quad \sigma_{\max}(\Sigma_X) \vee \sigma_{\max}(\Sigma_Y) \leq M,$$

where $M > 0$ is a constant independent of the dimension.

The probability space considered throughout this paper is, therefore, given by

$$\{(X_i, Y_i) \stackrel{\text{i.i.d.}}{\sim} \mathcal{N}_{p+q}(0, \Sigma) \mid \Sigma \in \mathcal{F}(s_u, s_v, p, q, r; M)\}. \quad (4)$$

2 CCA through regression

2.1 The low-dimensional case: high n , low p and q

We begin by analyzing the classical setting where the sample size n is large relative to the covariate dimensions, i.e., $n \gg p \vee q$. This regime provides the basis for the derivation of our algorithm in the high-dimensional setting. We consider the convex objective

$$\mathcal{L}(B) = \frac{1}{2} \left\| \frac{1}{n} X B Y^\top - I_n \right\|_F^2, \quad (5)$$

and show that its minimizer is a consistent estimator of the population matrix $B^\star = U^\star \Lambda^\star V^{\star\top}$, as established in the following theorem.

Theorem 2.1. *Assume that p and q are fixed as n is allowed to grow. Let \hat{B} denote the minimizer of $\mathcal{L}(B)$. Under the canonical pair model, if n grows to infinity, then $\hat{B} \xrightarrow{a.s.} U^\star \Lambda^\star V^{\star\top}$.*

Having established the initial value \hat{B} , estimates of U^\star and V^\star are obtained by first performing a rank- r singular value decomposition (SVD) of the matrix product $\hat{\Sigma}_X^{\frac{1}{2}} \hat{B} \hat{\Sigma}_Y^{\frac{1}{2}} = \hat{U}_0 \hat{\Lambda}_0 \hat{V}_0^\top$, and then normalizing the singular vectors to obtain the canonical direction estimates $\hat{U} = \hat{\Sigma}_X^{-\frac{1}{2}} \hat{U}_0$ and $\hat{V} = \hat{\Sigma}_Y^{-\frac{1}{2}} \hat{V}_0$. The following theorem establishes the consistency of \hat{U} and \hat{V} and the proof can be found in Appendix E.

Theorem 2.2. *Let \hat{B} denote the minimizer of $\mathcal{L}(B)$. Denote by \hat{U}_0 and \hat{V}_0 the left and right singular vector matrices of $\hat{\Sigma}_X^{\frac{1}{2}} \hat{B} \hat{\Sigma}_Y^{\frac{1}{2}}$. Additionally, denote by U_0 and V_0 the left and right singular vector matrices of $\Sigma_X^{\frac{1}{2}} B^\star \Sigma_Y^{\frac{1}{2}}$. Under the canonical pair model,*

$$\lim_{n \rightarrow \infty} \max \left\{ \min_{O \in \mathcal{O}_r} \|\hat{U}_0 - U_0 O\|_F, \min_{\tilde{O} \in \mathcal{O}_r} \|\hat{V}_0 - V_0 \tilde{O}\|_F \right\} = 0, \quad (6)$$

where \mathcal{O}_r denotes the set of rotation matrices in $\mathbb{R}^{r \times r}$. Consequently, the estimates $\hat{U} =$

$\widehat{\Sigma}_X^{-\frac{1}{2}}\widehat{U}_0$ and $\widehat{V} = \widehat{\Sigma}_Y^{-\frac{1}{2}}\widehat{V}_0$ are consistent estimators of U^\star and V^\star in the sense that:

$$\lim_{n \rightarrow \infty} \max \left\{ \min_{O \in \mathcal{O}_{r \times r}} \left\{ \|\widehat{U} - U^\star O\|_F, \min_{\tilde{O} \in \mathcal{O}_{r \times r}} \|\widehat{V} - V^\star \tilde{O}\|_F \right\} \right\} = 0. \quad (7)$$

2.2 The high-dimensional case: low n , high p or q

In the high-dimensional case, the sample estimates $\widehat{\Sigma}_X$, $\widehat{\Sigma}_Y$ and $\widehat{\Sigma}_{XY}$ are no longer guaranteed to provide consistent estimators of the covariance matrices Σ_X , Σ_Y and Σ_{XY} . As a result, the estimators of the CCA directions U^\star and V^\star described in the previous subsection are no longer guaranteed to be consistent without assuming further structure.

In this paper, we consider the case where U^\star and V^\star can be assumed to be row-sparse, i.e. $|\text{supp}(U^\star)| \leq s_u$, $|\text{supp}(V^\star)| \leq s_v$. As in Gao et al. (2017), we note in this case that the row-sparsity of U^\star and V^\star naturally translates into element-wise sparsity of the product $B^\star = U^\star \Lambda^\star V^{\star\top}$. Therefore, to accommodate the structure of the problem, a natural extension of the previous estimator to the high-dimensional setting is to transform Equation 5 into the following loss function:

$$\mathcal{L}(B) = \frac{1}{2} \left\| \frac{1}{n} X B Y^\top - I_n \right\|_F^2 + \rho \|B\|_{11}, \quad (8)$$

where ρ is a tuning parameter controlling the solution sparsity. The sparsity constraint on B^\star is here relaxed to an $\ell_{1,1}$ penalty, thus turning the estimation of B^\star into a convex optimization problem. As in the previous section, estimates of U^\star and V^\star can be obtained by a transformation of the rank- r singular value decomposition of $\widehat{\Sigma}_X^{\frac{1}{2}} \widehat{B} \widehat{\Sigma}_Y^{\frac{1}{2}}$. The full procedure is outlined in Algorithm 1. Moreover, the formulation in Equation 8 provides a flexible framework that can be readily extended to incorporate other types of structural regularization by changing the type of penalty from an ℓ_{11} penalty to a more general function. For instance, one may replace the element-wise penalty with group sparsity constraints or structured norms to reflect known groupings among variables (see Section 2.4).

Algorithm 1 Efficient Sparse CCA via Reduced Rank Regression (ECCAR)

Input: $X \in \mathbb{R}^{n \times p}$, $Y \in \mathbb{R}^{n \times q}$, $\rho \geq 0$, $r \in \mathbb{Z}_{\geq 1}$

Procedure:

- 1: Solve the Lasso problem: $\hat{B} := \operatorname{argmin}_{B \in \mathbb{R}^{p \times q}} \frac{1}{2} \left\| \frac{1}{n} X B Y^\top - I_n \right\|_F^2 + \rho \|B\|_{11}$
- 2: Compute the rank- r SVD of $\hat{\Sigma}_X^{\frac{1}{2}} \hat{B} \hat{\Sigma}_Y^{\frac{1}{2}}$, that is $\hat{U}_0 \hat{\Lambda}_0 \hat{V}_0^\top = \operatorname{svd}_r(\hat{\Sigma}_X^{\frac{1}{2}} \hat{B} \hat{\Sigma}_Y^{\frac{1}{2}})$
- 3: Apply normalization: $\hat{U} = \hat{B} \hat{\Sigma}_Y^{\frac{1}{2}} \hat{V}_0 \hat{\Lambda}_0^{-1}$, $\hat{V} = \hat{B}^\top \hat{\Sigma}_X^{\frac{1}{2}} \hat{U}_0 \hat{\Lambda}_0^{-1}$

Output: \hat{U}, \hat{V}

2.3 Characterizing the computational complexity of our approach

The efficiency of our method is tied to that of the solver of the penalized regression problem of Equation 8. Here, we propose solving it using the Alternating Direction Method of Multipliers (ADMM; Boyd et al. (2011)). Appendix B provides a detailed breakdown of the updates and steps of the algorithm.

Let T denote the number of iterations, and assume $n \leq p, q$. The total computational complexity of our algorithm is then $O(p^2n + q^2n + T(pn^2 + pqn))$, which scales quadratically with the larger dimension. For comparison, the Fantope-based initialization in Gao and Ma (2023) also employs ADMM steps. However, this approach requires computing at each step the SVD of a $(p + q) \times (p + q)$ matrix, resulting in a total complexity of $O(T(p + q)^3)$ that scales cubically with the larger dimension (Gao and Ma, 2023).

2.4 CCA with group sparsity

In many datasets, variables are naturally organized into groups. For example, genes may be grouped by biological function, brain voxels by anatomical region, and geographical measurements by spatial location. In such settings, a common objective is to identify a sparse subset of these covariate groups that captures the key relationships in the data. To

address this, we extend the sparse CCA method introduced in the previous subsection to incorporate group structure. Specifically, we replace the sparsity penalty in Equation 8 by a group-sparse modification leading to:

$$\mathcal{L}(B) = \frac{1}{2} \left\| \frac{1}{n} XBY^\top - I_n \right\|_F^2 + \rho \sum_{g \in G} \sqrt{T_g} \|B_g\|_F. \quad (9)$$

Here G denotes the set of groups, B_g denotes the restriction of the matrix B to the g th group, while T_g denotes the size of group g . As in Section 2.3, the minimizer of Equation 9 can be efficiently found via an ADMM procedure (Appendix B).

3 Theoretical Guarantees

In this section, we first demonstrate that the constrained optimization setting of Equations 8 and 9 allows accurate estimations of the product $B^\star = U^\star \Lambda^\star V^{\star\top}$. Combined with steps 2 and 3 of Algorithm 1, our procedure can thus be shown to produce consistent estimates of the canonical directions U^\star and V^\star . The analogous results for the group sparse setting are available in Appendix F.2.

3.1 Consistency in the sparse high-dimensional setting

The following theorem provides an upper bound on the distance between \hat{B} and B^\star .

Theorem 3.1. *Consider the parameter space $\mathcal{F}(s_u, s_v, p, q, r; M)$ for the covariance matrix Σ (Equation 3 and conditions therein), and let $\Delta = \hat{B} - B^\star$, where \hat{B} is the estimate obtained in step 1 of Algorithm 1 and B^\star is the underlying population quantity $B^\star = U^\star \Lambda^\star V^{\star\top}$. Assume $n \geq cs_u s_v \log(p + q)$ for some sufficiently large constant c . There exist constants a, b, C depending on M and c such that if $\rho \geq a\sqrt{\log(p + q)/n}$, then with probability at*

least $1 - \exp(-bs_u \log(ep/s_u)) - \exp(-bs_v \log(eq/s_v)) - (p+q)^{-b}$, we have:

$$\|\Delta\|_F \leq C\rho\sqrt{s_us_v}.$$

In particular, if ρ is of order of $\sqrt{\log(p+q)/n}$, we have:

$$\|\Delta\|_F \lesssim \sqrt{\frac{s_us_v \log(p+q)}{n}}, \quad (10)$$

and \widehat{B} has sparse entries: $\|\widehat{B}\|_0 \lesssim s_us_v$.

Our approach's error bound compares favorably to that of the initialization procedure proposed by Gao et al. (2017). Their two-step method first estimates the product $A^* = U^*V^{*\top}$ using a Fantope-based approach (Theorem 4.1), resulting in an error bound that scales with the inverse of the square of the signal strength λ_r^* : $\|\widehat{A} - A\|_F \lesssim \frac{1}{\lambda_r^*} \sqrt{\frac{s_us_v \log(p+q)}{n}}$. We achieve the same bound, but without the λ_r^* -term in the denominator. This difference arises because our method directly targets the complete product $U^*\Lambda^*V^{*\top}$.

From a computational standpoint, our method offers a distinct advantage. The approach in Gao et al. (2017) involves a costly projection onto a Fantope set at each iteration. In contrast, our algorithm is projection-free and relies only on efficient matrix multiplications, resulting in significantly improved speed. Building on this, we now demonstrate how our initial estimate of B facilitates the final estimation of U^* and V^* .

Theorem 3.2. *Suppose that the assumptions of Theorem 3.1 are satisfied. Assume $n \geq cs_us_v \log(p+q)/\lambda_r^{*2}$ for some sufficiently large constant c . There exist constants a_1, a_2, b, C depending on M and c such that if $\rho \in \left[a_1\sqrt{\frac{\log(p+q)}{n}}, a_2\sqrt{\frac{\log(p+q)}{n}}\right]$, then with probability at least $1 - \exp(-b(s_u + \log(ep/s_u))) - \exp(-b(s_v + \log(eq/s_v))) - (p+q)^{-b}$, we have*

$$\max \left\{ \min_{W \in \mathcal{O}_r} \|\widehat{U} - U^*W\|_F, \min_{W \in \mathcal{O}_r} \|\widehat{V} - V^*W\|_F \right\} \leq C \frac{1}{\lambda_r^{*2}} \sqrt{\frac{s_us_v \log(p+q)}{n}}.$$

Theorem 3.2 provides error bounds for \widehat{U} and \widehat{V} . We note that our bound scales with the square root of the product $s_u s_v$, thus, is less efficient (from a statistical perspective) than the one in Gao et al. (2017):

$$\min_{W \in \mathcal{O}_r} \left\| \widehat{U} - U^* W \right\|_F \leq C \frac{1}{\lambda_r^* M^{\frac{1}{2}}} \sqrt{\frac{s_u(r + \log(p))}{n}},$$

which is independent of q and s_v and scales with the inherent dimension of the problem $s_u r$ (shown by the authors to be minimax optimal). However, their procedure has practical limitations. It requires splitting the data into three folds, which reduces statistical power, and relies on a computationally intensive Fantope projection — an approach rarely used in practice. While a more recent method by Gao and Ma (2023) avoids sample splitting and achieves a bound of order $s_u + s_v$, it still depends on this computationally expensive initialization and requires tuning multiple hyperparameters. Therefore, our method offers a valuable trade-off: it sacrifices some statistical efficiency in exchange for substantial computational gains, making it a practical and scalable solution for sparse CCA.

3.2 Guarantees on the support recovery

Canonical Correlation Analysis (CCA) is frequently employed to identify associated subsets of variables between two datasets, a process central to scientific discovery. Nevertheless, theoretical guarantees for the validity of support recovery using CCA have not yet been established. The following theorem characterizes the support recovery of \widehat{B} .

Theorem 3.3. *Consider the parameter space $\mathcal{F}(s_u, s_v, p, q, r; M)$ for the covariance matrix Σ (Equation 3 and conditions therein). Assume $n > \max\{s_u, s_v\}$ and*

$$\frac{\|\widehat{\Sigma}_{XY} - \widehat{\Sigma}_X B^* \widehat{\Sigma}_Y\|_\infty}{\rho} + \frac{2(\|\widehat{\Sigma}_{XY} - \widehat{\Sigma}_X B^* \widehat{\Sigma}_Y\|_\infty + \rho)}{\rho} \frac{\widehat{\tau}(X, Y) \sqrt{s_u s_v}}{\sigma_{\min}((\widehat{\Sigma}_X)_{S_u S_u}) \sigma_{\min}((\widehat{\Sigma}_Y)_{S_v S_v})} \leq 1, \quad (11)$$

where $S_u = \text{supp}(U^\star)$ and $S_v = \text{supp}(V^\star)$ and

$$\hat{\tau}(X, Y) = \max \left\{ \left\| (\hat{\Sigma}_X)_{S_u^c S_u} \right\|_{2, \infty} \left\| (\hat{\Sigma}_Y)_{S_v^c S_v} \right\|_{2, \infty}, \left\| (\hat{\Sigma}_X)_{S_u^c S_u} \right\|_{2, \infty} \left\| (\hat{\Sigma}_Y)_{S_v S_v} \right\|_{op}, \right. \\ \left. \left\| (\hat{\Sigma}_X)_{S_u S_u} \right\|_{op} \left\| (\hat{\Sigma}_Y)_{S_v^c S_v} \right\|_{2, \infty} \right\}.$$

Then the minimizer of δ is unique and satisfies $\text{supp}(\hat{B}) \subset S_u \times S_v$.

To make the assumptions more transparent (and deterministic), we refine Theorem 3.3 by the following corollary providing guarantees on the support of \hat{B} with high probability.

Corollary 3.3.1. *Consider the parameter space $\mathcal{F}(s_u, s_v, p, q, r; M)$ for the covariance matrix Σ (Equation 3 and conditions therein), and assume*

$$\frac{2\tau(X, Y)\sqrt{s_u s_v}}{\sigma_{\min}((\Sigma_X)_{S_u S_u})\sigma_{\min}((\Sigma_Y)_{S_v S_v})} < 1 - \alpha \quad (12)$$

for some $\alpha \in (0, 1]$, where $\tau(X, Y)$ is the population version of $\hat{\tau}(X, Y)$. There exist some constants a, b, c depending on M and α such that if $n \geq c(s_u + s_v) \log(p + q)$ and $\rho \geq a\sqrt{\log(p + q)/n}$, then the minimizer of δ is unique and satisfies $\text{supp}(\hat{B}) \subset S_u \times S_v$ with probability at least $1 - \exp(-bs_u \log(ep/s_u)) - \exp(-bs_v \log(eq/s_v)) - (p + q)^{-b}$.

The conditions of Theorem 3.3 and Corollary 3.3.1 ensure that if the covariance between variables within the true support (S_u) and those outside of it (S_u^c) is sufficiently small, then the non-zero entries of the estimator \hat{B} will be contained within the true support of B . This requirement is intuitive: when two variables are highly correlated, a robust method should not assign a large canonical loading to one while excluding the other. Consequently, since by design of our algorithm, sparsity in \hat{B} implies sparsity in \hat{U} and \hat{V} , our theorem's guarantees on support recovery extend directly to \hat{U} and \hat{V} . This implies that the set of non-zero elements in the estimated vectors is a subset of the true support. Table 3 offers a comparison of the theoretical guarantees provided by the different methods.

4 Simulations

We conduct a series of synthetic experiments to evaluate the performance of different sparse CCA approaches in high-dimensional settings. We begin by constructing a block-diagonal covariance matrix Σ_X , defined as $\Sigma_X = \begin{pmatrix} U_X U_X^\top & 0 \\ 0 & I \end{pmatrix}$, where $U_X \in \mathbb{R}^{p_1 \times r_{pca}}$ is a randomly generated matrix with orthonormal columns. This construction induces a non-trivial covariance structure for X , in which the leading r_{pca} principal components are sparse and span only p_1 out of the total p rows. In our experiments, we set $p_1 = 20$ and $r_{pca} = 5$. The covariance matrix Σ_Y is constructed analogously.

Next, we construct the cross-covariance matrix Σ_{XY} as $\Sigma_{XY} = \Sigma_X U^* \Lambda^* V^{*\top} \Sigma_Y$, where $U^* \in \mathbb{R}^{p \times r}$ and $V^* \in \mathbb{R}^{q \times r}$ are random matrices with uniformly sampled entries. Both U^* and V^* are row-sparse, with exactly $s_u = s_v$ non-zero rows. The matrices are then normalized, ensuring that $U^{*\top} \Sigma_X U^* = I_r$ and $V^{*\top} \Sigma_Y V^* = I_r$. We define the canonical correlation matrix as $\Lambda^* = \lambda I_r$ with $\lambda = 0.9$ indicating “high” signal strength, 0.7 for “medium”, and 0.5 for “weak”. Finally, we generate the observations $(X_i, Y_i)_{i=1}^n$ by sampling from the joint multivariate normal distribution $\mathcal{N}_{p+q} \left(0, \begin{pmatrix} \Sigma_X & \Sigma_{XY} \\ \Sigma_{XY}^\top & \Sigma_Y \end{pmatrix} \right)$.

We use this synthetic data to compare the performance of our sparse CCA method with the following four versions of CCA with sparsity: SAR by Wilms and Croux (2016), the sparse CCA approaches by Witten et al. (2009), as well as Waaijenborg and Zwinderman (2009) and Parkhomenko et al. (2009). We also include a comparison of our method against the theory-based approaches, including the Fantope initialization, as well as the full CCA procedure (CoLAR) of Gao et al. (2017), and SGCA (Gao and Ma, 2023). In all versions of our method, we select an optimal regularization parameter ρ by either plugging in the theoretical value of ρ from Theorem 3.1 or by 10-fold cross-validation. Similarly, we select the regularization parameters in all heuristic methods using either 5-fold cross-validation

or a BIC criterion to avoid the need for refitting the method multiple times. Due to the computational complexity of the theory-based methods, we use the theoretical value of ρ in the Fantope initialization procedure instead of relying on cross-validation. We cross-validate on the value of the regularization in the second step of CoLAR, and use the default values in SGCA. To evaluate the resulting CCA reconstructions, we measure the distances between subspaces that span the canonical variates by computing the principal angle (Jordan, 1875) between the subspaces associated with the matrices.

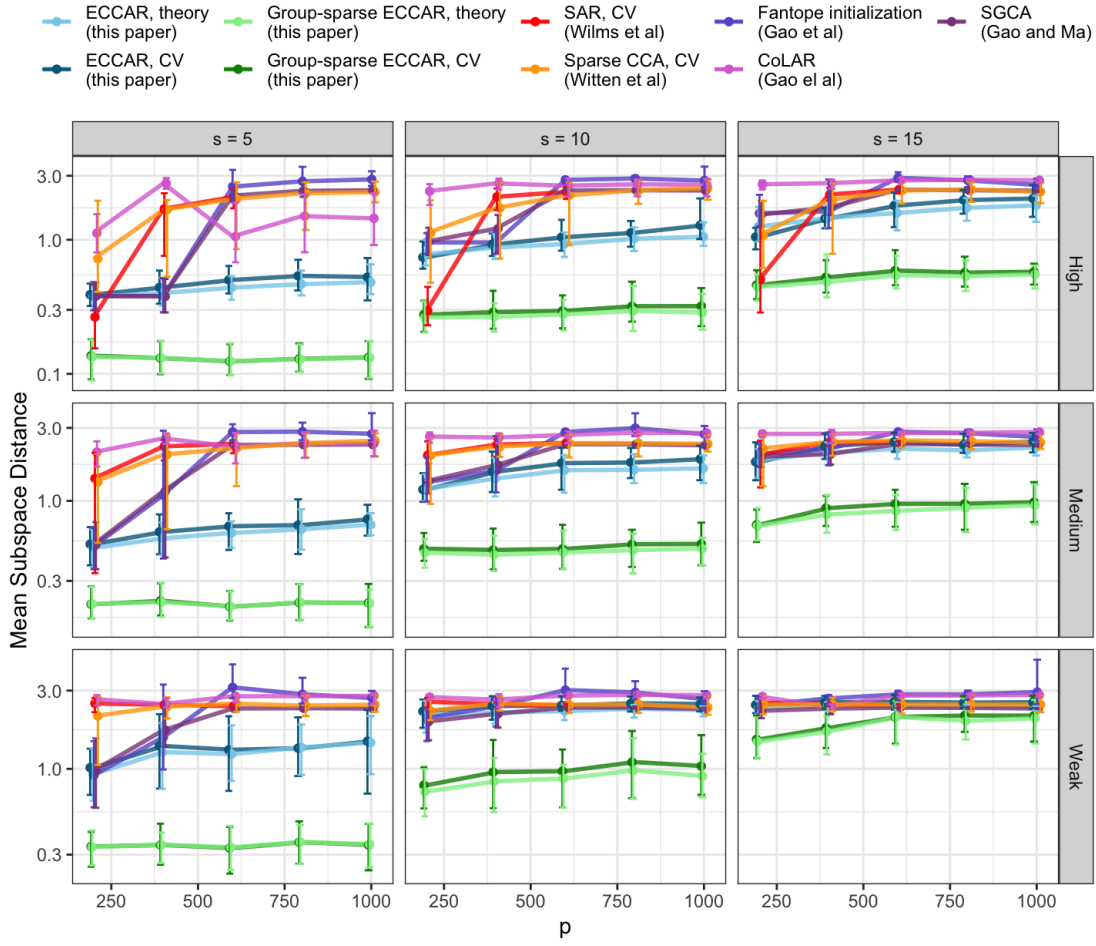


Figure 1: Estimation error as a function of $p(=q)$, the support sizes $s_u = s_v$ (columns) and the strength of the signal (value of λ^* , rows) for $n = 400$. Points indicate mean subspace distance averaged over 25 independent experiments with their interquartile range.

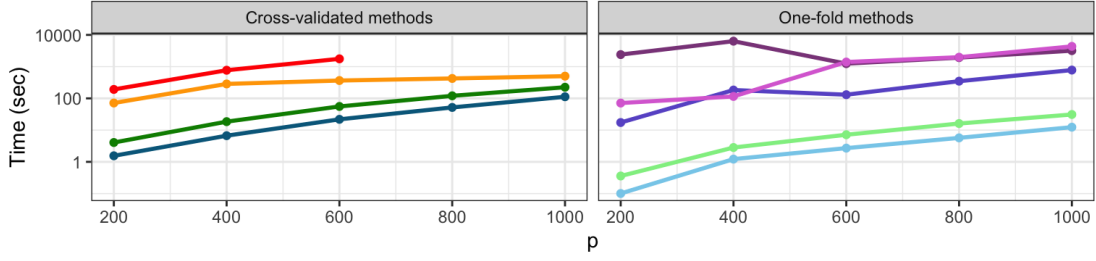


Figure 2: Time as a function of p and q for $n = 400$, $\lambda^* = 0.9$ and $s_u = 15$. Points indicate mean time averaged over 25 independent experiments. The missing values in SAR are caused by computational issues occurred during model fitting.

Estimation error with increasing p . We set $n = 400$ and $p = q = 200, 400, 600, 800, 1000$ with $r = 2$. For the group-sparse ECCAR, we divide the cross covariances into 5 by 5 blocks and treat each block as a group. We consider three sparsity levels, $s_u = s_v = 5, 10, 15$. We estimate the $\sin \Theta$ distance between the stacked $(\begin{smallmatrix} U \\ V \end{smallmatrix})^* \in \mathbb{R}^{(p+q) \times r}$ and the estimates, and the running time based on 25 independent experiments. The results for our method and best performing benchmarks are displayed in Figure 1 (a figure with the full set of benchmarks is provided in Appendix C.1). Our method is able to handle very high-dimensional cases such as $p = q = 1000$, even with weak signals when the canonical variates are sparse enough. In contrast, all other methods fail to achieve reasonable accuracy when $p \geq 400$ compared to others. Strikingly, as shown in Figure 2, our method (using a regularization parameter ρ computed through theory) is 100 times faster than the Fantope and 1,000 times faster than both CoLAR (Gao et al., 2017) and SGCA (Gao and Ma, 2023). Even accounting for cross-validation, our method remains more than 10 times faster than these state-of-the-art methods (which, technically, ought to be cross-validated to ensure an optimal choice of hyperparameters), and is faster than popular heuristic methods such as that of Witten et al. (2009) and Wilms and Croux (2015).

Estimation error with increasing r . We set $n = 400$, $p = q = 200$, and $r = 2, 3, 4, 5$ to examine how the performance of our method changes with respect to r . We consider the same sparsity levels $s_v = s_u$ and signal strength levels as in the previous simulation setting. The results are displayed in Figure 11 of Appendix C.1. Notably, the performance of our method does not deteriorate with increasing r .

5 Real Data Analysis

In this section, we propose to illustrate the benefits of our approach on three real-life examples stemming from different fields: genetics (Subsection 5.1), neuroscience (Subsection 5.2), and natural language processing (Subsection 5.3). We further showcase our method on the Nutrimouse dataset (Appendix C.2), often employed as a benchmark for CCA (Wilms and Croux, 2016; Donnat and Tuzhilina, 2024; Rohart et al., 2017).

5.1 Alcohol Use Disorder

Alcohol-use disorders (AUDs) — encompassing both abuse and dependence — are major drivers of morbidity and premature death. Their etiologies are highly heterogeneous: risk is believed to arise from variation in many genes, gene-gene interactions, and extensive transcriptomic reprogramming triggered by long-term alcohol exposure. To investigate these risk factors, Zhang et al. (2014) profiled genome-wide DNA methylation levels and genome-wide gene expression levels in the postmortem prefrontal cortex of 23 European Australians AUD cases and 23 matched controls. The same dataset was later revisited in Luo et al. (2016) using supervised joint-modeling techniques. Here we re-examine this dataset to assess the validity and efficiency of our proposed CCA approach (ECCAR). As in Witten et al. (2009) and Luo et al. (2016), a marginal test was performed on all genes

Method	Test MSE	Test Correlation	Accuracy (SVM)
ECCAR, CV (this paper)	0.604	0.400	0.958
SAR, CV (Wilms and Croux, 2016)	0.857	0.274	0.869
SAR, BIC (Wilms and Croux, 2016)	0.905	0.311	0.879
Sparse CCA, CV (Witten et al., 2009)	1.070	0.258	0.823
Sparse CCA, permuted (Witten et al., 2009)	0.731	0.483	0.933
Sparse CCA, CV (Waaijenborg and Zwinderman, 2009)	1.825	-0.351	0.955
Sparse CCA, BIC (Waaijenborg and Zwinderman, 2009)	1.865	-0.383	0.955
Fantope Initialization (Gao et al., 2017)	40.081	0.106	0.570
SGCA (Gao and Ma, 2023)	1.617	0.193	0.736

Table 1: Performance comparison of sparse CCA methods on the AUD data.

and CpG sites, and the top $p = 300$ genes and $q = 500$ CpG sites most strongly associated with AUD were selected for further analysis.

We apply ECCAR with $r = 2$ to estimate the first two pairs of canonical directions. The regularization parameter was tuned with an 8-fold cross-validation scheme, where six folds were used for training, one for validation (and selection of the hyperparameter) and one for testing. The optimal penalty parameter ρ was selected by minimizing the average validation mean-squared error (MSE) of the difference $XU - YV$. Table 1 compares the test MSE and correlation of ECCAR approach with benchmark CCA methods. To assess the downstream predictive utility of ECCAR, we projected the genetic data onto the estimated canonical directions and classified the resulting scores XU as either AUD cases or control using support vector machine (SVM). In this case, ECCAR achieved the lowest test MSE and the highest classification accuracy.

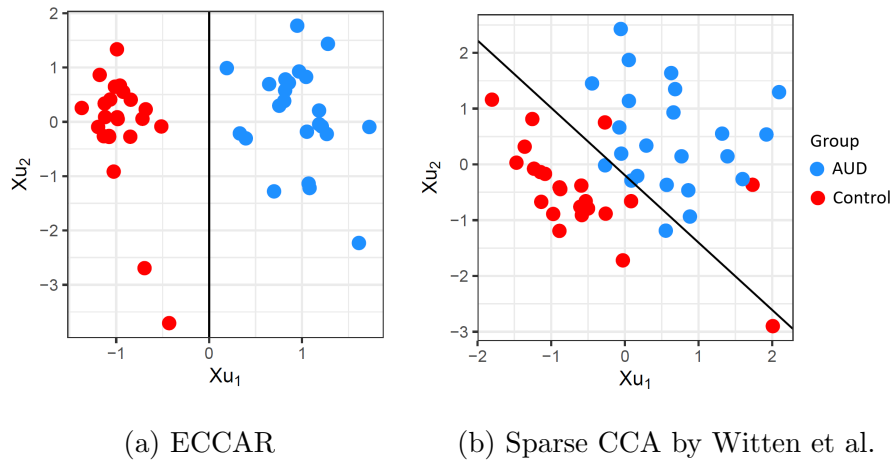


Figure 3: The scatter plot for the first two canonical variates produced for the AUD dataset. (a) The black line $Xu_1 = 0$ perfectly separates two classes. (b) The black line represents the logistic regression decision boundary.

Figure 3 visualizes the separation achieved by ECCAR and by the sparse CCA variant of Witten et al. (2009). Remarkably, the first canonical variate from ECCAR yields a perfect separation between AUD cases and controls, while the approach of Witten et al. (2009) exhibits more mixing between AUD cases and controls.

Turning to the investigation of the first canonical variates, ECCAR identifies 20 genes (Figure 4) and 18 CpG sites (Figure 5) associated with DNA methylation. Since this direction cleanly separates AUD from control cases, we subsequently cross-compare our loadings to existing scientific literature. Notably, ECCAR’s findings echo that of Zhang et al. (2014), who reported the differential expressions of ZNF354A and RASL11A as significantly different between AUD and control cases. Additionally, NDUFAF3 was found to be significantly differentially expressed between alcohol-fed and control pair-fed mice, as noted by Zhang et al. (2018). Gavin et al. (2016) suggested that lower levels of the DNA demethylation protein GADD45G may influence Bdnf expression, potentially altering alcohol consumption behavior. Moreover, GADD45G has been identified as a potential

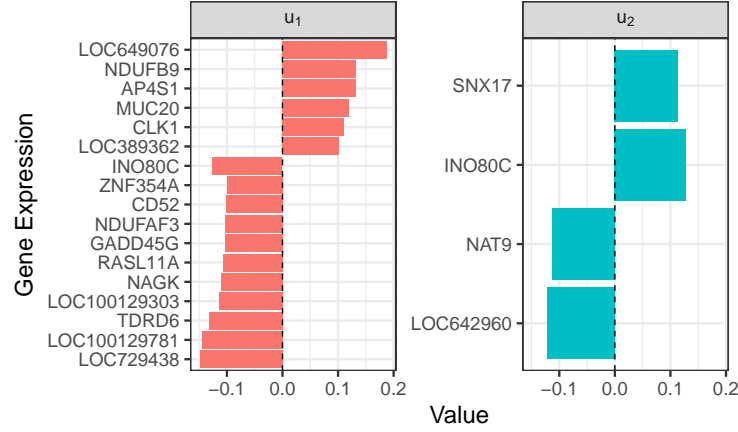


Figure 4: The barplot for the first and second canonical direction vectors u_1 and u_2 corresponding to the genes obtained by ECCAR.

target for the anti-cancer effects of 4MOD in liver cancer (Zeng et al., 2023), which is closely related to alcohol consumption. NUDFB9 was found to be differentially expressed in the medial prefrontal cortex of binge drinkers (McClintick et al., 2018). These results provide more scientific validation for the effectiveness of our method. There is limited evidence regarding the identified CpG sites due to the sparse existing literature on DNA methylation functions. Nevertheless, we found that cg20269537 and cg11562309 are associated with AUD cases, as previously reported by Hu et al. (2018).

5.2 The Autism Brain Imaging Data Exchange

To further evaluate our method, we use preprocessed resting-state fMRI data from the Autism Brain Imaging Data Exchange (ABIDE; Di Martino et al. (2014)) to assess ECCAR’s performance. ABIDE is a multi-site consortium that provides data from subjects with Autism Spectrum Disorder (ASD) and controls. For the purpose of this example, we consider cases for which both fMRI time series and Vineland Adaptive Behavior tests (Sparrow et al., 2005) were available, resulting in a set of 106 patients (65 with an autism

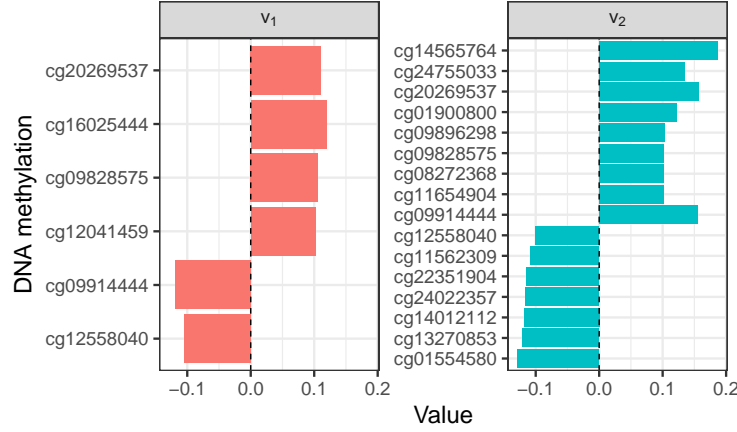


Figure 5: The barplot for the first and second canonical direction vectors v_1 and v_2 corresponding to the CpG sites obtained by ECCAR.

diagnostic, and 41 controls). The Vineland Adaptive Behavior tests consist of 14 behavioral scores measuring such skills as communication, coping, daily living skills, and socialization. The resulting scores were stored row-wise in matrix Y , with $q = 14$.

For each subject, mean fMRI time series were extracted for a set of 110 regions of interest (ROIs) parcellated using the Harvard-Oxford (HO) atlas (Desikan et al., 2006). A 110×110 functional connectivity matrix was then computed by correlating the mean time series between all ROI pairs. The upper-triangular elements of each subject’s connectivity matrix were vectorized and stored row-wise in X , yielding $p = 5995$ features per subject. We subsequently mapped the 110 ROIs to Yeo’s 7-network parcellation (Yeo et al., 2011), supplemented with the Subcortical network. This resulted in 8 functional networks: Subcortical (Scor), Frontoparietal Control Network (FPN), Default Mode Network (DMN), Dorsal Attention Network (DAN), Limbic Network (LIN), Salience/Ventral Attention Network (SAN), Somatomotor Network (SMN), and Visual Network (VIN). Based on these assignments, the features in X were grouped into 36 sets, each corresponding to interactions between pairs of networks (including within-network interactions).

Method	Test MSE	Compute time (s)
ECCAR, CV (this paper)	2.19 (1.84; 2.63)	412s (411; 416)
Group ECCAR, CV (this paper)	1.96 (1.63; 2.19)	411s (410; 419)
Row-sparse ECCAR, CV (this paper)	1.76 (1.39; 2.16)	619s (617; 624)
SAR, CV (Wilms and Croux, 2016)	3.17 (2.16; 3.43)	11372s (10985; 12495)
SAR, BIC (Wilms and Croux, 2016)	3.75 (3.49; 3.77)	10769s (10579; 10839)
Sparse CCA, CV (Witten et al., 2009)	2.48 (2.23; 2.92)	250s (249; 250)
Sparse CCA, permuted (Witten et al., 2009)	2.81 (2.22; 2.97)	57s (57; 57)
SCCA, CV (Parkhomenko et al., 2009)	2.33 (1.81; 2.62)	26s (26; 26)

Table 2: Summary of the performance of the different methods on the ABIDE dataset. Results are reported as the median test MSE and computation time across 10 folds, with interquartile ranges shown in brackets.

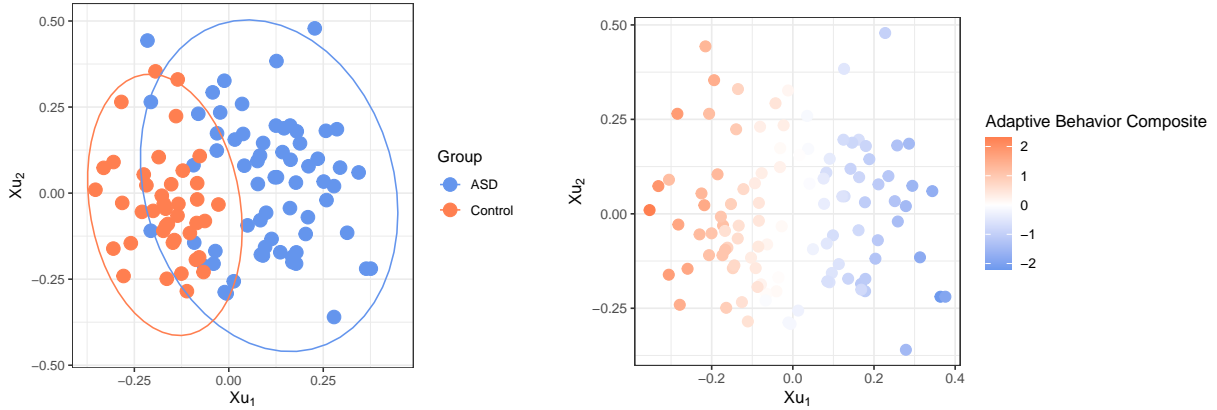


Figure 6: Scatter plots for the first two canonical variates produced by row-sparse ECCAR. Left: The points are colored by diagnosis, the plot includes 95% confidence ellipses for each diagnosis group. Right: the points are colored by Adaptive Behavior Composite.

We run various sparse CCA methods with $r = 2$ on the ABIDE dataset and evaluate the performance using nested 10-fold cross-validation. For our method, we consider three settings: (i) ECCAR, which imposes element-wise sparsity on B ; (ii) row-sparse ECCAR, which encourages sparsity at the row level by grouping elements of B according to their row indices; and (iii) group ECCAR, which groups the rows of B based on predefined network interaction groups (36 in total). We report the average MSE across the folds in Table 2. As shown in the table, the group row-sparse and group ECCAR methods achieve a substantially lower MSE compared to all other approaches.

By analyzing the scatter plot of the canonical variates (left panel of Figure 6) obtained from the row-sparse ECCAR method, we observe a clear separation between ASD patients and controls. This suggests that the first canonical direction effectively captures diagnostic differences between the two groups. The corresponding canonical direction vector u_1 , associated with brain connectivities, is shown in Figure 15 in Appendix C.3. As expected, many connectivity features receive zero weights.

To investigate which network-level interactions are most relevant to disease status, we compute the average absolute loading of u_1 within each of 36 predefined brain network interaction groups and visualize the results as a heatmap. As shown in the left panel of Figure 14, the interaction between the dorsal attention network (DAN) and the somato-motor network (SMN) receives the highest loading, although the difference from other interactions is not pronounced. To more explicitly identify disease-relevant network interactions, we also analyze the same heatmap based on the group-sparse ECCAR method. As shown in Figure 17 (Appendix C.3), the direction u_1 exhibits a block-sparse structure, as expected from the grouping penalty. The corresponding network-level summary, presented in the right panel of Figure 14, indicates that the limbic network (LIN) shows the

strongest involvement, particularly in its interactions with the dorsal attention network (DAN) and the frontoparietal network (FPN). Given that the limbic network is primarily involved in emotion regulation, memory processing, and motivational behavior, its engagement aligns with established neurobiological characteristics of autism spectrum disorder (Haznedar et al., 2000). We also analyze the canonical vector v_1 , associated with the Vineland Adaptive Behavior Scales, as estimated by the row-sparse ECCAR. As shown in Figure 16, the Adaptive Behavior Composite (ABC) receives the highest loading, indicating its primary contribution to the canonical correlation. This observation is supported by the right panel of Figure 6 that shows very clear separation between patients with positive and negative ABC values.

We illustrate the results of the sparse CCA approaches of Parkhomenko et al. (2009) and Witten et al. (2009) in Appendix C.3. The corresponding canonical variate scatter plots (top row of Figure 20) show weaker separation between ASD and control groups compared to our method. The direction vectors u_1 , as well as their network-level summaries are shown in Figures 18, 19, and the middle row of Figure 20. We notice that the method of Parkhomenko et al. (2009) yields a dense u_1 , assigning similar weights across many network interactions and failing to pinpoint specific networks (Figure 18). In contrast, the method of Witten et al. (2009) results in an overly sparse u_1 , highlighting only the interaction between the default mode network (DMN) and the somatomotor network (SMN), potentially overlooking the critical role of the limbic system identified by our method (Figure 19).

5.3 Interpretability of LLM Embeddings

Finally, to show that the application of our method extends beyond biology, we illustrate its utility in the context of algorithm interpretability. While modern foundation models

excel at generating powerful, high-dimensional embeddings from data, the structure of these embeddings is not inherently interpretable. We thus consider the following question: *Given a point cloud of documents embeddings, can we explain its structure?* We propose a principled framework to probe and gain insight in this setting: first, a set of interpretable features is constructed from the data (e.g., document topics or linguistic features from text); second, canonical correlation analysis is employed to identify and quantify the linear relationships between these features and the model’s embeddings. Our approach adapts a paradigm previously used in computer vision to compare internal neural network activations (Raghu et al., 2017; Morcos et al., 2018; Andrew et al., 2013), and repurposes it to directly explain a model’s final output embeddings in terms of external, interpretable variables.

We analyze embeddings of the 20 Newsgroups dataset, a corpus of articles belonging to one of 20 topics, which we further coarsen into 7 main categories (see Table 5 in Appendix C.4). Each document is encoded into a vector of dimensionality $p = 750$ using the `all-mpnet-base-v2` SentenceTransformer model available on Hugging Face. This model is based on MPNet encoder and has been fine-tuned with contrastive and cosine-similarity objectives to produce semantically rich sentence representations that work well in downstream similarity and clustering tasks. To interpret the resulting embedding space, we align these embeddings with a corresponding Term Frequency-Inverse Document Frequency (TF-IDF) representation, constructed using the top q words with the highest TF-IDF frequencies. We then apply CCA to these two data views using ranks $r = 4$ and 10, to uncover structure at various levels of granularity. The performance of different CCA methods is evaluated using MSE on held-out data and running time, as a function of both the number of documents (n) used to train the CCA model and the number of TF-IDF features (q) retained for interpreting the transformer embeddings.

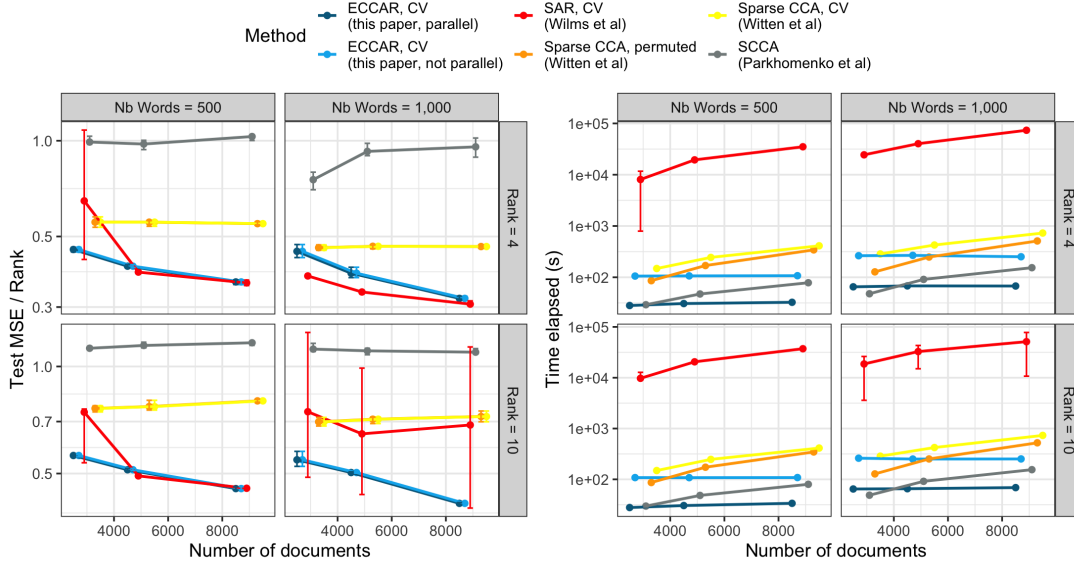


Figure 7: Results of the different sparse CCA methods on the LLM interpretability task. The performance is evaluated using the mean-squared error on a test held-out set (left), and by reporting the compute time (right).

The results presented in Figure 7 show that our proposed estimator ECCAR and SAR (Wilms and Croux, 2016) achieve comparable performances, with SAR having on occasion a slightly smaller test MSE, but displaying higher variability, particularly when the number of documents (n) is small. Crucially, our method offers a significant computational advantage, with a fitting time that is 100 to almost 1,000 times smaller than SAR (even when not resorting to parallelization).

We further visualize the first six canonical variates, colored by coarse category when fitting CCA on $r = 10$ loadings, with $n = 3000$ and $q = 1000$ (see Appendix C.4, Figure 21a). We note that the variates recovered by our method and SAR (Wilms and Croux, 2015) present similar structure (up to a sign flip). This is consistent with the fact that their MSE indicate similar levels of prediction power. Interestingly, the variates exhibit clear streaks corresponding to different topics. By contrast, the approaches of both Witten

et al. (2009) and Parkhomenko et al. (2009) exhibit considerably more mixing and do not seem to yield any clear and interpretable axis of variation in the data.

We also present the loadings of the first 6 canonical directions obtained by ECCAR in Figure 8, where, to help visualization, each word is colored by its main topic (as fitted with a Latent Dirichlet Allocation Model on 7 topics). Overall, it is interesting to observe that the loadings recovered by our method seem to be dominated by one to two main categories (e.g. computers in Loading 4, computers and religion/politics in Loading 1). Interestingly, certain components seem to be able to differentiate between subtopics within each category (see Figure 23 in the Appendix). For instance, CCA direction 4 seems to be strongly associated with distinguishing between hardware-related articles and operating systems/graphics articles, which is reflected in the weights put on certain words (e.g. “windows”, “graphics”, “version” vs “disk”, “scsi”, etc.). Likewise, CCA direction 5 divides political discussions about guns or general policy from those addressing Middle-East politics. This shows that the learned CCA axes are readily interpretable and align closely with the documents’ true labels. For comparison, Figures 22a and 22b in Appendix C show the loadings recovered by the CCA variant of Wilms and Croux (2015) and Witten et al. (2009), respectively. We note again a strong resemblance between the loadings obtained for SAR and ECCAR.

6 Conclusion

Understanding how CCA is used has important implications for method design. In particular, canonical correlation analysis should be *(a) scalable* to enable efficient processing of high-dimensional datasets; *(b) interpretable* to facilitate meaningful scientific conclusions; and *(c) sparsistent* — that is, the variables identified through CCA should come with provable guarantees.

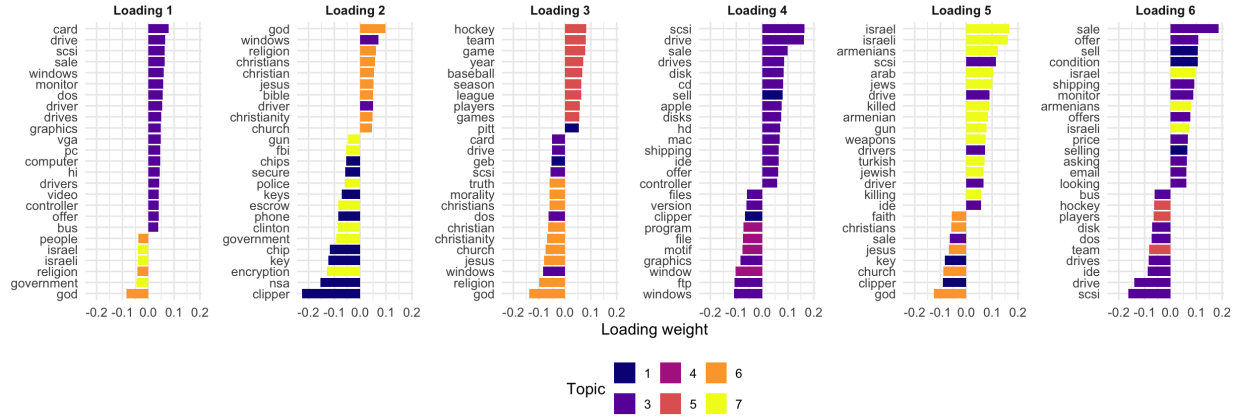


Figure 8: The top 25 loadings for the first 6 canonical directions obtained by ECCAR. Colors were added as a visual aide, and represent each word’s estimated most frequent “topic”, as estimated by the Latent Dirichlet Allocation algorithm.

In this paper, we introduced ECCAR, the first estimator for sparse canonical correlation analysis that provably meets all three criteria. Beyond applications in genetics and neuroscience, we further showcased its practical utility by applying it to the challenging problem of interpreting Large Language Model embeddings. This highlights the continued relevance of classical statistical methods in the era of modern data science. Rather than discarding foundational techniques when faced with new challenges, adapting them through tools such as regularization can lead to practical and powerful solutions. Our work provides not only a scalable and interpretable tool for practitioners, but also a blueprint for how classical multivariate analysis can evolve to meet contemporary demands. In particular, an important future direction is to extend the ECCAR methodology to settings involving more than two datasets, which is particularly relevant in multi-omics studies.

7 Data Availability & Use of AI

All the data used in this paper is publicly available. The Nutrimouse data can be found in the R package `mixomics`. The AUD dataset can be obtained from the R package `CVR`. The ABIDE dataset can be loaded from the ABIDE website. Finally, the 20Newsgroup dataset can be loaded from the Python package `scikit-learn`.

The authors acknowledge the use of AI (ChatGPT 4.5) for improving R plot figures, checking grammar and spelling, and enhancing the flow throughout the manuscript.

References

- Andrew, G., Arora, R., Bilmes, J., and Livescu, K. (2013). Deep canonical correlation analysis. In *International conference on machine learning*, pages 1247–1255. PMLR.
- Avants, B. B., Tustison, N., Song, G., et al. (2009). Advanced normalization tools (ANTs). *Insight j*, 2(365):1–35.
- Behzadi, Y., Restom, K., Liau, J., and Liu, T. T. (2007). A component based noise correction method (compcor) for bold and perfusion based fmri. *Neuroimage*, 37(1):90–101.
- Boyd, S., Parikh, N., Chu, E., Peleato, B., and Eckstein, J. (2011). Distributed optimization and statistical learning via the alternating direction method of multipliers. *Foundations and Trends in Machine Learning*, 3:1–122.
- Chen, M., Gao, C., Ren, Z., and Zhou, H. H. (2013). Sparse CCA via precision adjusted iterative thresholding. *arXiv preprint arXiv:1311.6186*.
- Craddock, C., Sikka, S., Cheung, B., Khanuja, R., Ghosh, S. S., Yan, C., Li, Q., Lurie,

- D., Vogelstein, J., Burns, R., et al. (2013). Towards automated analysis of connectomes: The configurable pipeline for the analysis of connectomes (c-pac). *Front Neuroinform*, 42(10.3389).
- Desikan, R. S., Ségonne, F., Fischl, B., Quinn, B. T., Dickerson, B. C., Blacker, D., Buckner, R. L., Dale, A. M., Maguire, R. P., Hyman, B. T., et al. (2006). An automated labeling system for subdividing the human cerebral cortex on mri scans into gyral based regions of interest. *Neuroimage*, 31(3):968–980.
- Di Martino, A., Yan, C.-G., Li, Q., Denio, E., Castellanos, F. X., Alaerts, K., Anderson, J. S., Assaf, M., Bookheimer, S. Y., Dapretto, M., et al. (2014). The autism brain imaging data exchange: towards a large-scale evaluation of the intrinsic brain architecture in autism. *Molecular psychiatry*, 19(6):659–667.
- Donnat, C. and Tuzhilina, E. (2024). Canonical correlation analysis as reduced rank regression in high dimensions. *arXiv preprint arXiv:2405.19539*.
- Dos Santos, S. F. and Brandi, H. S. (2014). A canonical correlation analysis of the relationship between sustainability and competitiveness. *Clean Technologies and Environmental Policy*, 16:1735–1746.
- Fan, X. and Konold, T. R. (2018). Canonical correlation analysis. In *The reviewer’s guide to quantitative methods in the social sciences*, pages 29–41. Routledge.
- Gao, C., Ma, Z., Ren, Z., and Zhou, H. H. (2015). Minimax estimation in sparse canonical correlation analysis. *The Annals of Statistics*, 43(5):2168–2197.
- Gao, C., Ma, Z., and Zhou, H. H. (2017). Sparse CCA: Adaptive estimation and computational barriers. *The Annals of Statistics*, 45(5):2074–2101.

- Gao, S. and Ma, Z. (2023). Sparse gca and thresholded gradient descent. *Journal of Machine Learning Research*, 24(135):1–61.
- Gavin, D. P., Kusumo, H., Zhang, H., Guidotti, A., and Pandey, S. C. (2016). Role of growth arrest and dna damage-inducible, beta in alcohol-drinking behaviors. *Alcoholism: Clinical and Experimental Research*, 40(2):263–272.
- Haznedar, M. M., Buchsbaum, M. S., Wei, T.-C., Hof, P. R., Cartwright, C., Bienstock, C. A., and Hollander, E. (2000). Limbic Circuitry in Patients With Autism Spectrum Disorders Studied With Positron Emission Tomography and Magnetic Resonance Imaging. *American Journal of Psychiatry*, 157(12):1994–2001.
- Helmer, M., Warrington, S., Mohammadi-Nejad, A.-R., Ji, J. L., Howell, A., Rosand, B., Anticevic, A., Sotiropoulos, S. N., and Murray, J. D. (2024). On the stability of canonical correlation analysis and partial least squares with application to brain-behavior associations. *Communications biology*, 7(1):217.
- Hotelling, H. (1936). Relations between two sets of variates. In *Biometrika*, 28, pages 321–377. Springer.
- Hu, R., Dai, Y., Jia, P., and Zhao, Z. (2018). ANCO-GeneDB: Annotations and comprehensive analysis of candidate genes for alcohol, nicotine, cocaine, and opioid dependence. <https://bioinfo.uth.edu/ancogenedb/views/meDNA.php>. Database; DOI:10.1093/database/bay121.
- Jiang, M.-Z., Aguet, F., Ardlie, K., Chen, J., Cornell, E., Cruz, D., Durda, P., Gabriel, S. B., Gerszten, R. E., Guo, X., et al. (2023). Canonical correlation analysis for multi-omics: Application to cross-cohort analysis. *PLoS genetics*, 19(5):e1010517.

- Jordan, C. (1875). Essai sur la géométrie à n dimensions. *Bulletin de la Société mathématique de France*, 3:103–174.
- Klopp, O., Panov, M., Sigalla, S., and Tsybakov, A. (2021). Assigning topics to documents by successive projections. *arXiv preprint arXiv:2107.03684*.
- Lê Cao, K.-A., Martin, P. G., Robert-Granié, C., and Besse, P. (2009). Sparse canonical methods for biological data integration: application to a cross-platform study. *BMC bioinformatics*, 10:1–17.
- Lin, D., Zhang, J., Li, J., Calhoun, V. D., Deng, H.-W., and Wang, Y.-P. (2013). Group sparse canonical correlation analysis for genomic data integration. *BMC bioinformatics*, 14(1):1–16.
- Lund, T. E., Madsen, K. H., Sidaros, K., Luo, W.-L., and Nichols, T. E. (2006). Non-white noise in fmri: does modelling have an impact? *Neuroimage*, 29(1):54–66.
- Luo, C., Liu, J., Dey, D. K., and Chen, K. (2016). Canonical variate regression. *Biostatistics*, 17(3):468–483.
- Martin, P. G., Guillou, H., Lasserre, F., Déjean, S., Lan, A., Pascussi, J.-M., SanCristobal, M., Legrand, P., Besse, P., and Pineau, T. (2007). Novel aspects of ppar α -mediated regulation of lipid and xenobiotic metabolism revealed through a nutrigenomic study. *Hepatology*, 45(3):767–777.
- Mazuruse, P. (2014). Canonical correlation analysis: Macroeconomic variables versus stock returns. *Journal of Financial Economic Policy*, 6(2):179–196.
- McClintick, J. N., McBride, W. J., Bell, R. L., Ding, Z.-M., Liu, Y., Xuei, X., and Edenberg, H. J. (2018). Gene expression changes in the ventral hippocampus and medial

- prefrontal cortex of adolescent alcohol-preferring (p) rats following binge-like alcohol drinking. *Alcohol*, 68:37–47.
- McIntosh, A. R. (2021). Comparison of canonical correlation and partial least squares analyses of simulated and empirical data. *arXiv preprint arXiv:2107.06867*.
- Morcos, A., Raghu, M., and Bengio, S. (2018). Insights on representational similarity in neural networks with canonical correlation. *Advances in neural information processing systems*, 31.
- Nakua, H., Yu, J.-C., Abdi, H., Hawco, C., Voineskos, A., Hill, S., Lai, M.-C., Wheeler, A. L., McIntosh, A. R., and Ameis, S. H. (2024). Comparing the stability and reproducibility of brain-behavior relationships found using canonical correlation analysis and partial least squares within the abcd sample. *Network Neuroscience*, 8(2):576–596.
- Parkhomenko, E., Tritchler, D., and Beyene, J. (2009). Sparse canonical correlation analysis with application to genomic data integration. *Statistical applications in genetics and molecular biology*, 8(1).
- Raghu, M., Gilmer, J., Yosinski, J., and Sohl-Dickstein, J. (2017). Svcca: Singular vector canonical correlation analysis for deep learning dynamics and interpretability. *Advances in neural information processing systems*, 30.
- Revilla, L., Mayorgas, A., Corraliza, A. M., Masamunt, M. C., Metwaly, A., Haller, D., Tristán, E., Carrasco, A., Esteve, M., Panés, J., et al. (2021). Multi-omic modelling of inflammatory bowel disease with regularized canonical correlation analysis. *Plos one*, 16(2):e0246367.
- Rodosthenous, T., Shahrezaei, V., and Evangelou, M. (2020). Integrating multi-omics

- data through sparse canonical correlation analysis for the prediction of complex traits: a comparison study. *Bioinformatics*, 36(17):4616–4625.
- Rohart, F., Gautier, B., Singh, A., and Lê Cao, K.-A. (2017). mixomics: An r package for ‘omics feature selection and multiple data integration. *PLoS computational biology*, 13(11):e1005752.
- Safo, S. E., Li, S., and Long, Q. (2018). Integrative analysis of transcriptomic and metabolomic data via sparse canonical correlation analysis with incorporation of biological information. *Biometrics*, 74(1):300–312.
- Sparrow, S. S., Cicchetti, D. V., and Balla, D. A. (2005). *Vineland Adaptive Behavior Scales, Second Edition (Vineland-II): Survey Forms Manual*. AGS Publishing.
- Stewart, G. (1969). On the continuity of the generalized inverse. *SIAM Journal on Applied Mathematics*, 17(1):33–45.
- Thorndike, R. M. (2000). Canonical correlation analysis. In *Handbook of applied multivariate statistics and mathematical modeling*, pages 237–263. Elsevier.
- Tibshirani, R. (1996). Regression shrinkage and selection via the lasso. *Journal of the Royal Statistical Society Series B: Statistical Methodology*, 58(1):267–288.
- Waaijenborg, S. and Zwinderman, A. H. (2009). Sparse canonical correlation analysis for identifying, connecting and completing gene-expression networks. *BMC Bioinformatics*, 10.
- Wilms, I. and Croux, C. (2015). Sparse canonical correlation analysis from a predictive point of view. *Biometrical Journal*, 57(5):834–851.

- Wilms, I. and Croux, C. (2016). Robust sparse canonical correlation analysis. *BMC Systems Biology*, 10(72).
- Witten, D. M., Tibshirani, R., and Hastie, T. (2009). A penalized matrix decomposition, with applications to sparse principal components and canonical correlation analysis. *Biostatistics*, 10(3):515–534.
- Witten, D. M. and Tibshirani, R. J. (2009). Extensions of sparse canonical correlation analysis with applications to genomic data. *Statistical applications in genetics and molecular biology*, 8(1).
- Yeo, B. T., Krienen, F. M., Sepulcre, J., Sabuncu, M. R., Lashkari, D., Hollinshead, M., Roffman, J. L., Smoller, J. W., Zöllei, L., Polimeni, J. R., et al. (2011). The organization of the human cerebral cortex estimated by intrinsic functional connectivity. *Journal of neurophysiology*.
- Yu, Y., Wang, T., and Samworth, R. J. (2015). A useful variant of the Davis–Kahan theorem for statisticians. *Biometrika*, 102(2):315–323.
- Zeng, L.-P., Qin, Y.-Q., Lu, X.-M., Feng, Z.-B., and Fang, X.-L. (2023). Identify gadd45g as a potential target of 4-methoxydalbergione in treatment of liver cancer: bioinformatics analysis and in vivo experiment. *World Journal of Surgical Oncology*, 21(1):324.
- Zhang, H., Wang, F., Xu, H., Liu, Y., Liu, J., Zhao, H., and Gelernter, J. (2014). Differentially co-expressed genes in postmortem prefrontal cortex of individuals with alcohol use disorders: influence on alcohol metabolism-related pathways. *Human genetics*, 133:1383–1394.
- Zhang, Y., Zhan, C., Chen, G., and Sun, J. (2018). Label-free quantitative proteomics and

bioinformatics analyses of alcoholic liver disease in a chronic and binge mouse model.

Molecular Medicine Reports, 18(2):2079–2087.

A Related Works

Sparse CCA methods assume that only a subset of coefficients in the canonical directions are non-zero. In recent years, these methods have gained significant traction, particularly due to the greater interpretability of the results—a crucial feature given CCA’s role in discovering associations between datasets. From a methodological perspective, sparse CCA methods can typically be classified into two categories: (a) *heuristic-based* and (b) *theory-based* approaches.

Heuristic-based approaches (Wilms and Croux, 2015, 2016; Parkhomenko et al., 2009) build on the success of the lasso (Tibshirani, 1996) by adding an ℓ_1 -penalty to the objective function in Equation 1. The canonical directions are then fitted in an alternating fashion, fixing one direction and solving for the other until convergence. When the number of canonical directions r is greater than 1, they are typically computed sequentially by progressively deflating the matrices X and Y . Although these methods are generally fast, questions regarding their accuracy remain unresolved. Notably, to our knowledge, the consistency of these methods has not been rigorously analyzed. Furthermore, due to the reliance on alternating fitting procedures, sensitivity to initialization has not been thoroughly investigated. To ensure computational efficiency, these methods (e.g., Witten et al., 2009) can also make simplifying assumptions, such as neglecting correlations between variables and assuming that $\Sigma_X = I$ and $\Sigma_Y = I$. As we demonstrate in Section 4, these assumptions can introduce substantial bias in the results.

In contrast, theory-based methods provide formal guarantees for estimation accuracy. To the best of our knowledge, the only theoretical treatment of sparse CCA consists in the series of works by Gao and coauthors (Chen et al., 2013; Gao et al., 2015, 2017), as well as more recent contributions by Gao and Ma (2023) and Donnat and Tuzhilina (2024).

These works attempt to formally characterize the estimation error with high-probability, and derive a corresponding algorithm. Framing the recovery of sparse components as a prediction problem, Gao et al. (2017) propose a sparsity-adaptive method that achieves optimal minimax rates for estimating both U^\star and V^\star . They consider a regime where the true canonical directions are sparse, with support sizes satisfying $|\text{supp}(U^\star)| \leq s_u$ and $|\text{supp}(V^\star)| \leq s_v$, for some $s_u \leq p$ and $s_v \leq q$. In this setting, Gao et al. (2015) establish that the minimax rate for estimating U^\star and V^\star under the joint prediction loss $\|\widehat{U}\widehat{V}^\top - U^\star V^{\star\top}\|_F^2$ is given by

$$\frac{1}{n\lambda_r^{\star 2}} \left(r(s_u + s_v) + s_u \log \left(\frac{ep}{s_u} \right) + s_v \log \left(\frac{eq}{s_v} \right) \right),$$

where λ_r^\star denotes the r -th largest canonical correlation.

Follow-up work further refines this minimax rate to the loss on each of the component which, in this case, is provided by:

$$\inf_{W \in \mathcal{O}_r} \mathbb{E} \|W^\top \widehat{U}^\top X - U^{\star\top} X\|^2 \leq C \frac{s_u(r + \log(p))}{n\lambda_r^2}$$

To obtain this rate, the authors propose a three-step procedure. In step 1, they transform the sparse CCA problem into a convex optimization problem:

$$\text{minimize } \text{Tr}(\widehat{\Sigma}_{XY}C) - \lambda \|C\|_{11}$$

The constraint set here is known as the Fantope, and had already been used in the context of sparse PCA estimation. In step 2, the estimators are refined using linear regression. The last step involves normalization of the result. More recent work by Gao and Ma (2023) expands upon the framework introduced in Gao et al. (2015, 2017), replacing the second step of their procedure with a thresholded gradient descent algorithm. This modification has been shown to yield improved empirical performance over the original method.

Feature	Our method (ECCAR)	Gao et al. (2017)	Gao & Ma (2023)
Statistical Rate ($\min_{O \in \mathcal{O}_r} \ \hat{U} - UO\ _F$)	$O\left(\frac{1}{\lambda_r^{*2}} \sqrt{\frac{s_u s_v \log(p+q)}{n}}\right)$	$O\left(\frac{1}{\lambda_r^*} \sqrt{\frac{s_u r \log(p)}{n}}\right)$	$O\left(\frac{1}{\lambda_r^*} \sqrt{\frac{(s_u + s_v) r \log(p+q)}{n}}\right)$
Computational Cost	$O(T(pn^2 + pqn))$	$O(T(p+q)^3)$	Prohibitive due to Fantope and multi-parameter tuning
Key Algorithmic Step	ADMM on a penalized regression problem	Fantope Projection	Thresholded Gradient Descent
Sample Splitting?	No	Yes (3-fold)	No

Table 3: Comparison of theoretical guarantees and computational costs of sparse CCA.

Finally, Donnat and Tuzhilina (2024) propose a theoretically-grounded alternative to CCA that is computationally tractable and specifically tailored for settings in which only one of the datasets is high-dimensional. By leveraging the low-dimensional structure of the second dataset, they are able to reformulate the Fantope optimization problem as a more tractable regression problem. However, this approach is only applicable when one dataset has relatively low dimension.

B Algorithms

B.1 Algorithm for the sparse CCA setting

We detail the steps of the ADMM Algorithm. To this end, we first transform our original loss function into the following ADMM Lagrangian:

$$\mathcal{L}(B, Z, H) = \frac{1}{2} \left\| \frac{1}{n} XBY^\top - I_n \right\|_F^2 + \lambda \mathcal{P}(Z) + \rho \langle H, B - Z \rangle + \frac{\rho}{2} \|B - Z\|_F^2.$$

where $\mathcal{P}(Z)$ represents a penalty function (for instance, an ℓ_{11} penalty or a group penalty).

Below we demonstrate how to solve the ADMM steps efficiently.

Pre-computations: Before running the algorithm, we first compute the eigen-decompositions

$\widehat{\Sigma}_X = U_X \Lambda_1 U_X^\top$, and $\widehat{\Sigma}_Y = U_Y \Lambda_2 U_Y^\top$. These operations have cost $O(p^2 \times (p \wedge n))$ and $O(q^2 \times (q \wedge n))$, respectively.

ADMM procedure: We then repeat the following steps until convergence.

1. *Updating B.* Setting $\nabla_B \mathcal{L}(B, Z, H) = 0$, we have

$$\widehat{\Sigma}_X B \widehat{\Sigma}_Y - \widehat{\Sigma}_{XY} + \rho H + \rho(B - Z) = 0$$

$$U_X \Lambda_1 U_X^\top B U_Y \Lambda_2 U_Y^\top + \rho B = \widehat{\Sigma}_{XY} + \rho(Z - H)$$

$$\Lambda_1 U_X^\top B U_Y \Lambda_2 + \rho U_X^\top B U_Y = U_X^\top (\widehat{\Sigma}_{XY} + \rho(Z - H)) U_Y.$$

Let $\tilde{B} = U_X^\top B U_Y$. Rewriting the equation, we obtain

$$\Lambda_1 \tilde{B} \Lambda_2 + \rho \tilde{B} = U_X^\top (\widehat{\Sigma}_{XY} + \rho(Z - H)) U_Y.$$

Equivalently, for each entry $i \in [p], j \in [q]$,

$$((\Lambda_1)_{ii}(\Lambda_2)_{jj} + \rho) \tilde{B}_{ij} = (U_X^\top (\widehat{\Sigma}_{XY} + \rho(Z - H)) U_Y)_{ij}.$$

Thus, \tilde{B} can be easily computed through element-wise division of the entries of the matrix $U_X^\top (\widehat{\Sigma}_{XY} + \rho(Z - H)) U_Y$ by the corresponding values $(\Lambda_1)_{ii}(\Lambda_2)_{jj} + \rho$. The operations for computing this matrix is $O(pq)$ for the matrix additions, $O((p \wedge n)pq)$ and $O((p \wedge n)q(q \wedge n))$ for the multiplications by U_X and U_Y , respectively. The matrix B , which is obtained as $B = U_X \tilde{B} U_Y^\top$, can then be computed in $O(p(p \wedge n)(q \wedge n) + p(q \wedge n)q)$.

2. *Updating Z.* We consider the objective function as a function of Z :

$$\mathcal{L}(Z) = \begin{cases} \lambda \|Z\|_{11} + \frac{\rho}{2} \|H + C - Z\|_F^2, & \text{with } \ell_1 \text{ sparsity;} \\ \lambda \sum_g \sqrt{T_g} \|Z\|_F + \frac{\rho}{2} \|H + C - Z\|_F^2, & \text{with group sparsity.} \end{cases}$$

The solution, thus, has a closed form:

$$Z_{ij} := S_{\lambda/\rho}(H_{ij} + B_{ij}) = \left(1 - \lambda/(\rho|H_{ij} + B_{ij}|)\right)_+(H_{ij} + B_{ij}) \quad \text{with } \ell_1 \text{ sparsity;}$$

$$Z_g := S_{\lambda/\rho}(H_g + B_g) = \left(1 - \sqrt{T_g}\lambda/(\rho\|H_g + B_g\|_F)\right)_+(H_g + B_g) \quad \text{with group sparsity.}$$

3. *Updating* H . $H := H + \rho(B - Z)$

The same algorithm can be adapted to the group-sparse setting by simply replacing the thresholding step of Step 2 by a group-thresholding step.

C Simulation and real data experiments

C.1 Synthetic Experiments

Below, we present a figure comparing all existing sparse CCA methods based on simulation results.

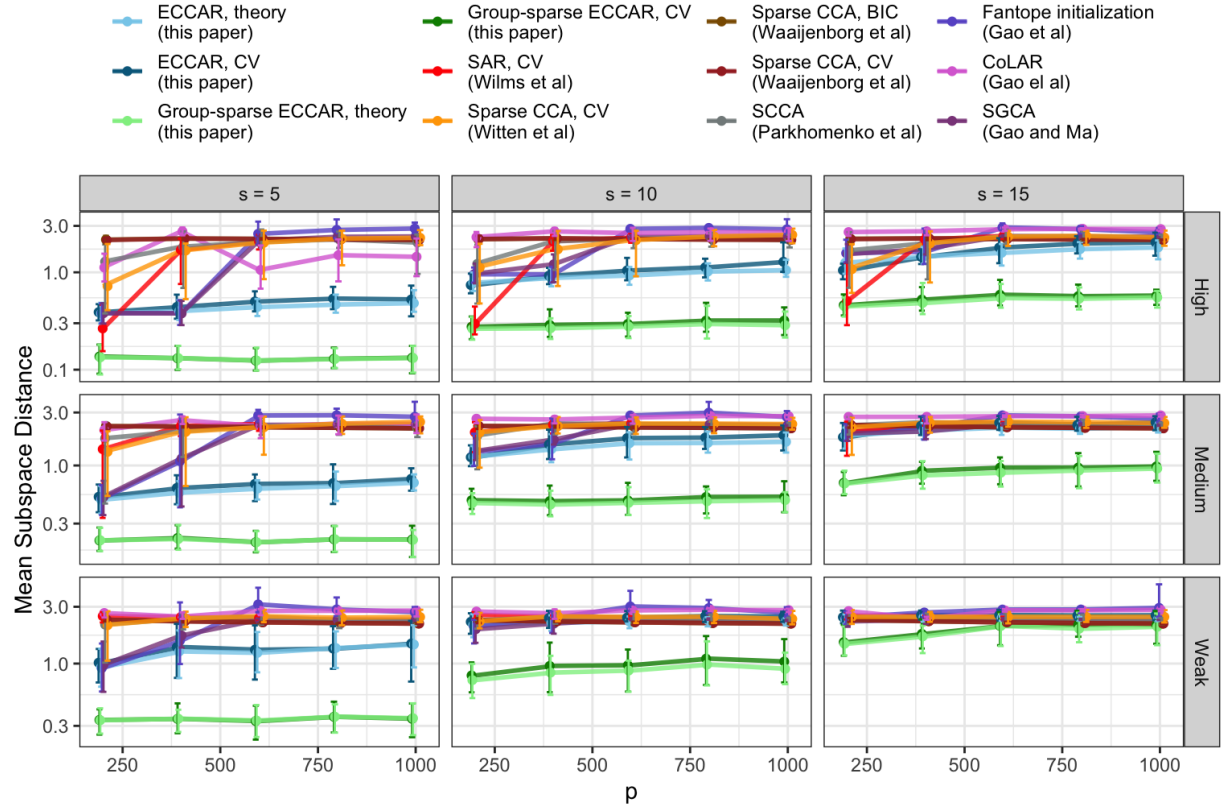


Figure 9: Estimation error as a function of p and q , and the support sizes $s_u = s_v$. Points indicate mean subspace distance averaged over 25 independent experiments with error bars representing the 25th and 75th percentiles.

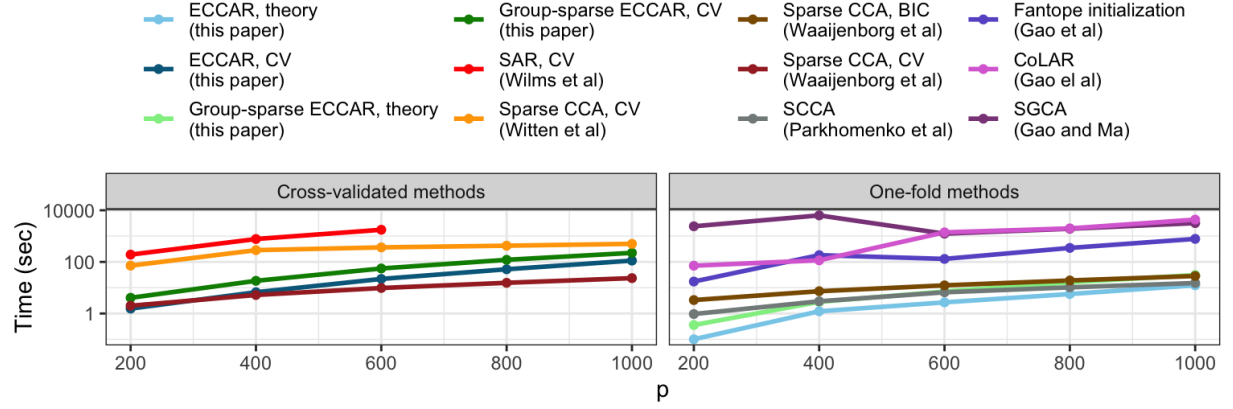


Figure 10: Estimation Time as a function of p and q , and the support sizes $s_u = s_v$. Points indicate mean running time averaged over 25 independent experiments.

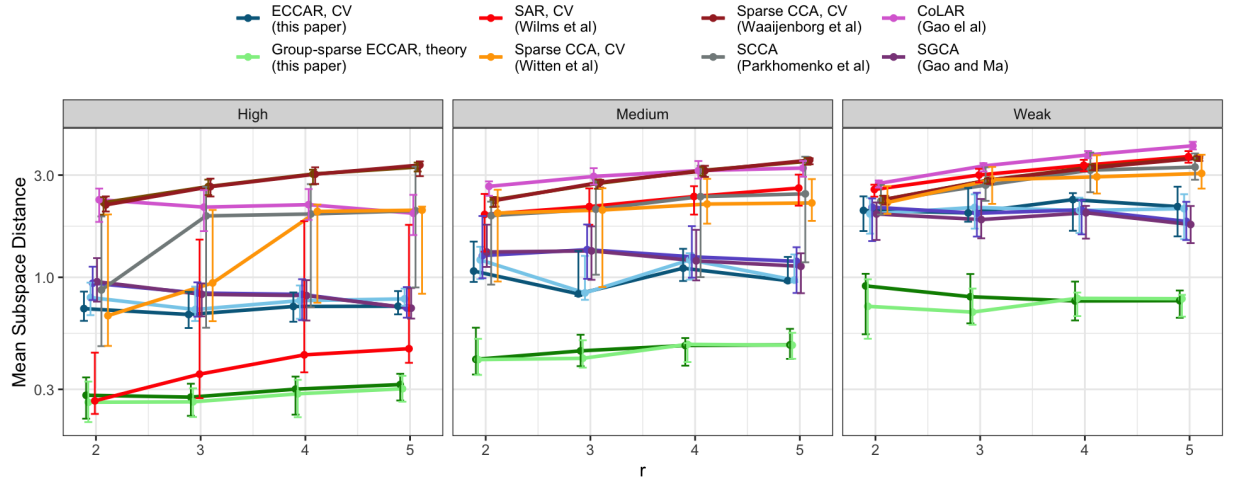


Figure 11: Simulations with $s = 10$ and increasing r . Median distance with error bars representing the 95th and 5th percentiles.

C.2 The Nutrimouse data

The Nutrimouse dataset includes the expression measurements of $p = 120$ genes potentially involved in nutritional issues and the concentrations of $q = 21$ hepatic fatty acids for $n = 40$ mice. Additionally, it contains two categorical variables: genotype, indicating whether the mouse is wildtype or genetically modified (PPAR), and diet, indicating the oils used in the experimental diets. We test our proposed method on the Nutrimouse dataset and compare its performance to the benchmarks introduced in the previous section except SGCA by Gao and Ma (2023) due to its long running time. We set the number of canonical directions to $r = 5$ based on the scree plot showing the eigenvalues of Σ_{XY} .

When applying our sparse ECCAR method to the genes X and fatty acids Y , we determine the appropriate regularization parameter for our method using 8-fold cross-validation: six folds were used for training, one for testing, and one for validation. The optimal penalty λ is chosen using the average test mean squared error (MSE) between canonical variates $X\hat{U}$ and $Y\hat{V}$. For other methods the hyper-parameters are chosen by the default implementation. The performance is assessed using four metrics computed through cross-validation: the average MSE between the canonical variates $X\hat{U}$ and $Y\hat{V}$; the average correlation between $X\hat{U}$ and $Y\hat{V}$; the classification loss for genotype using transformed genes; the classification loss for diet using transformed fatty acids. Classification is performed using support vector machines (SVM) or random forests (RF).

As shown in the Table 4, our method outperforms the competing approaches in terms of test MSE, test correlation, and prediction accuracy for diet. For genotype prediction, our method performs nearly as well as the best-performing alternative, SAR. We visualize the clustering patterns produced by our method and SAR (see Figure 12). Notably, our method provides a clear separation of both genotype and diet groups.

Method	Test MSE	Test Corelation	Genotype Acc SVM / RF	Diet Acc SVM / RF
Sparse eccar, CV (this paper)	0.827	0.529	0.969 / 0.927	0.727 / 0.563
SAR, CV (Wilms and Croux, 2016)	0.844	0.524	0.979 / 0.969	0.656 / 0.696
SAR, BIC (Wilms and Croux, 2016)	0.935	0.443	0.979 / 0.902	0.521 / 0.540
SCCA, CV (Parkhomenko et al., 2009)	0.945	0.418	0.958 / 0.875	0.317 / 0.417
Sparse CCA, CV (Witten et al., 2009)	1.470	0.301	0.969 / 0.948	0.338 / 0.288
Sparse CCA, permuted (Witten et al., 2009)	1.350	0.362	0.969 / 0.913	0.423 / 0.542
Sparse CCA, CV (Waaijenborg and Zwinderman, 2009)	2.140	-0.275	0.969 / 0.892	0.458 / 0.417
Sparse CCA, BIC (Waaijenborg and Zwinderman, 2009)	2.140	-0.261	0.969 / 0.917	0.490 / 0.473
Fantope initialization (Gao et al., 2017)	1.320	0.384	0.954 / 0.885	0.310 / 0.433

Table 4: Performance comparison of different methods on the Nutrimouse dataset using 8-fold cross-validation.

We evaluate the concordance between the genes and fatty acids selected by sparse ECCAR and the findings reported by Martin et al. (2007). Based on the first component, our method identifies the following fatty acids as most influential: C20:2n-6, C20:1n-9, C18:3n-3, C18:3n-6, C16:1n-9, C14:0, C22:5n-3, C18:1n-7, C16:0, and C20:3n-9. Among these, Martin et al. reported that C18:3n-3 exhibited a “robust increase” in expression in PPAR α genotypes compared to the wild type—consistent with our observation that this loading effectively separates genotypes. They also noted that changes in C16:1n-9 levels mirrored diet-induced changes within each genotype, and that C22:5n-3 was a major constituent of the fish oil used in their diet intervention. Regarding gene selection, our method highlights *CAR1*, *HPNCL*, *CPT2*, *CYP3A11*, *CYP4A10*, and *GSTmu* as the most influential. Martin et al. observed a consistent downregulation of *CYP3A11* in PPAR α livers, alongside an overexpression of *CAR1*, that is in agreement with our findings.

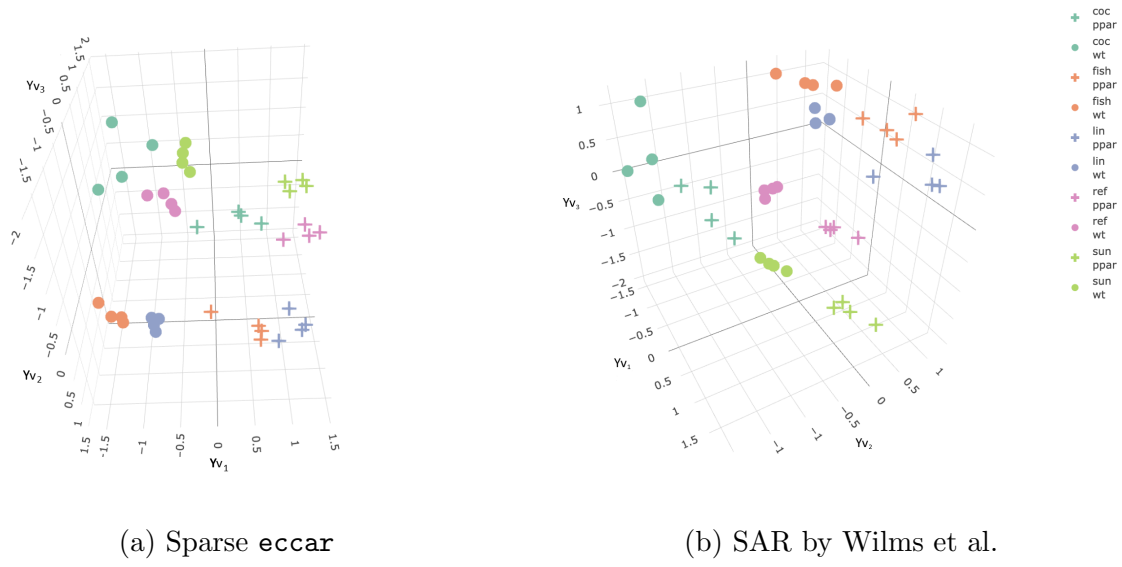


Figure 12: Scatter plots for first three canonical variates produced for the Nutrimouse dataset. Colors represent diet and shapes represent genotype.

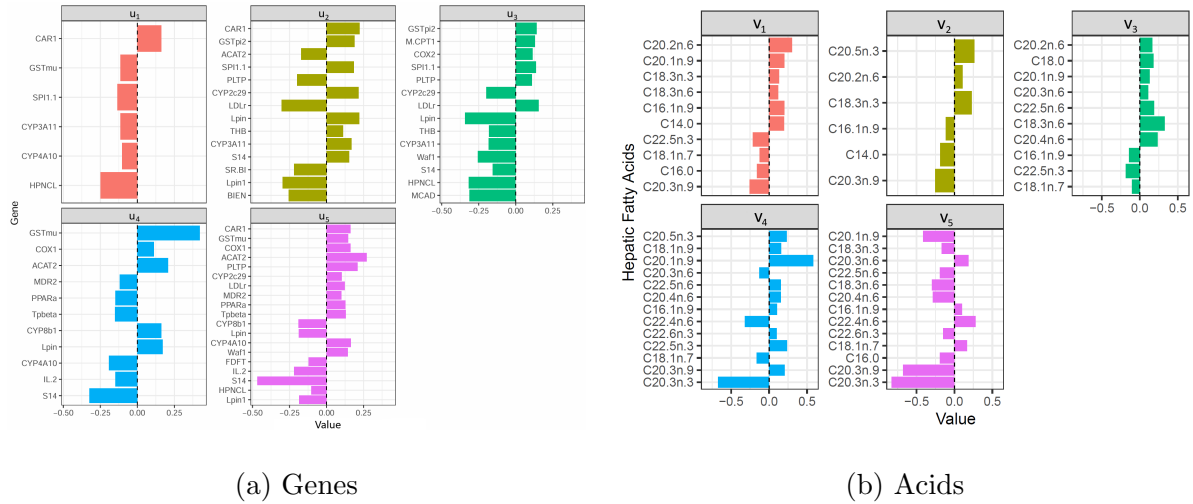


Figure 13: Five canonical directions produced for the Nutrimouse dataset obtained by sparse ECCAR.

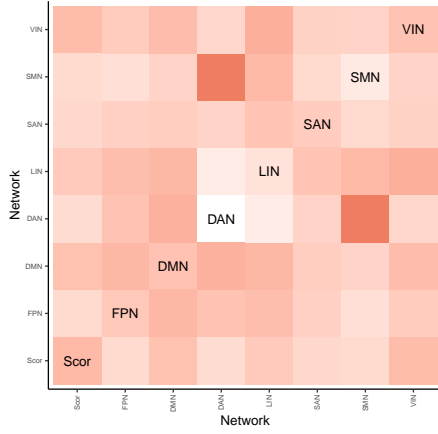
C.3 The Autism Brain Imaging Data Exchange

Preprocessing. We preprocess the ABIDE dataset using the Configurable Pipeline for the Analysis of Connectomes (C-PAC; Craddock et al. (2013)), a standardized workflow for fMRI data. The initial steps include slice-timing correction, realignment for motion, and normalization of signal intensities. To reduce noise from non-neuronal sources, we apply nuisance regression (Lund et al., 2006), targeting several confounding factors such as physiological artifacts (e.g., cardiac and respiratory cycles), head motion, and scanner drift.

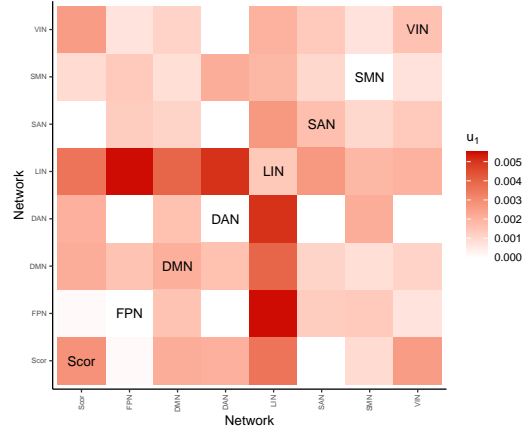
Head motion artifacts are modeled with 24 motion parameters, while scanner drift is addressed using both linear and quadratic terms. Physiological noise is controlled using the CompCor approach (Behzadi et al., 2007), which extracts the top five principal components from signals within white matter and cerebrospinal fluid (CSF). After nuisance correction, the data undergo band-pass filtering in the 0.01–0.1 Hz range and global signal regression to further isolate neural fluctuations.

For spatial normalization, functional images are aligned to anatomical scans using FSL’s Boundary-Based Registration (BBR), followed by non-linear warping to MNI space with the Advanced Normalization Tools (ANTs; Avants et al. (2009)).

Figures. We include additional plots for the analysis of the ABIDE data, such as the heatmaps for the first canonical direction u_1 (Figures 15-19) and the supplementary graphs for the sparse CCA benchmarks of Parkhomenko et al. (2009) and Witten and Tibshirani (2009) (Figure 20).



(a) row-sparse ECCAR



(b) group ECCAR

Figure 14: The heatmap for the first canonical direction vector u_1 corresponding to the brain signal. The plot represents the average of absolute values of loadings within each network.

C.4 LLM Interpretability

In this subsection, we present additional tables and plots for the LLM interpretability example.

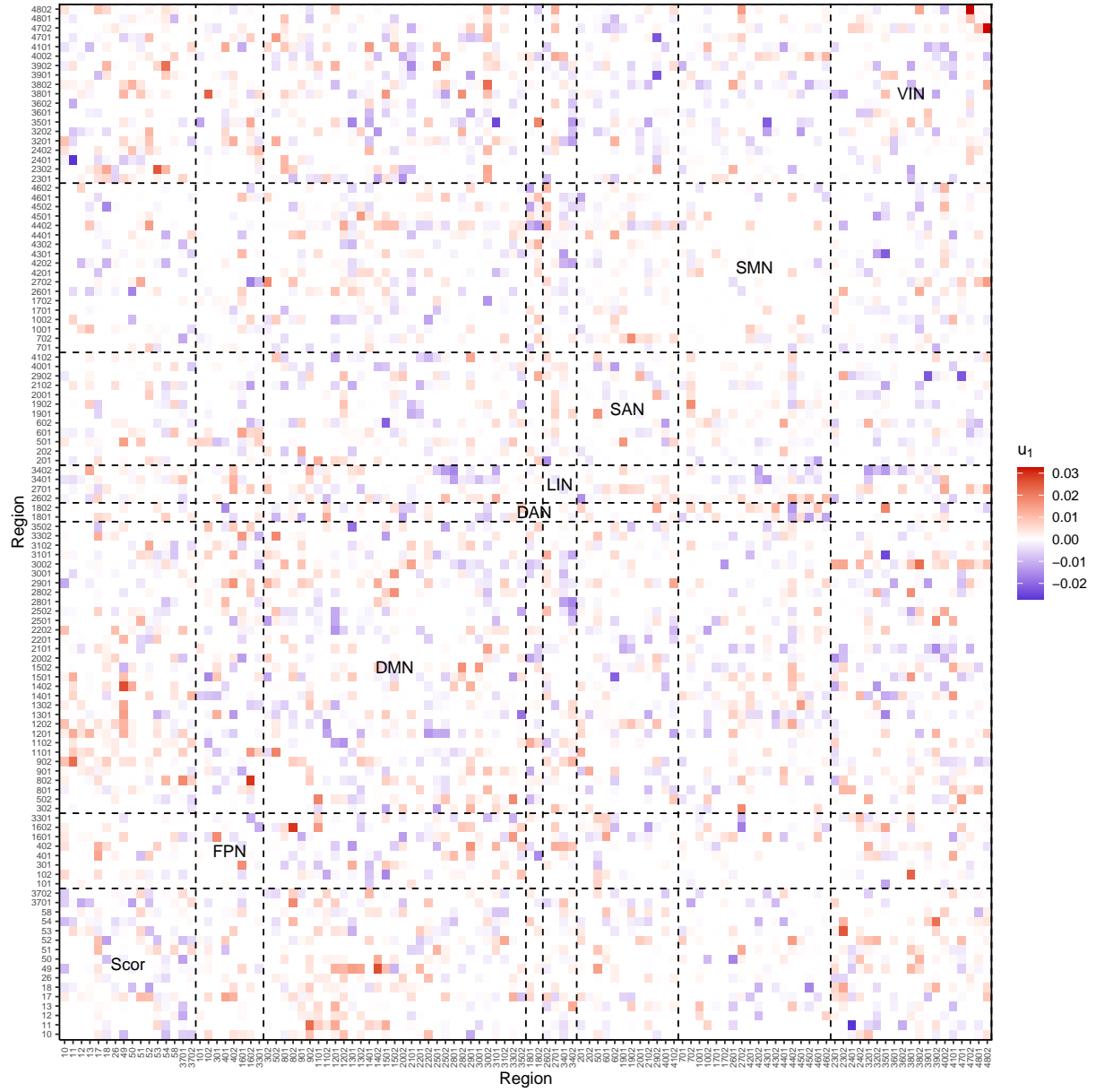


Figure 15: Heatmap of the first canonical direction vector u_1 from row-sparse ECCAR on ABIDE data. The x- and y-axes indicate brain region indices. Horizontal and vertical lines separate the eight brain networks, the name of each network is represented in the diagonal blocks.

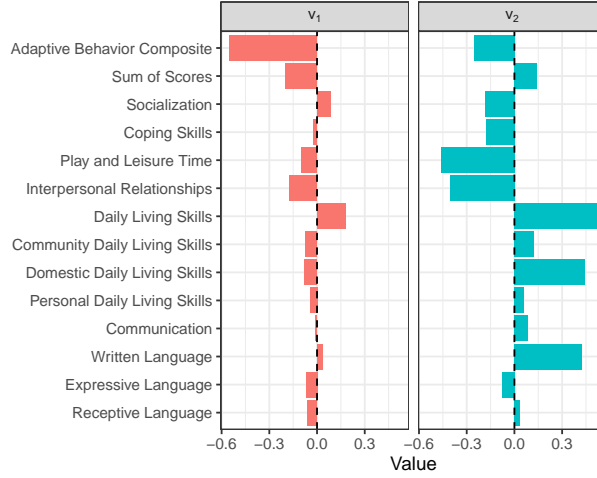


Figure 16: The barplot for the first and second canonical direction vectors v_1 and v_2 corresponding to the Vineland behavioral scores obtained by row-sparse ECCAR.

Category	Fine-grain topics
Religion	alt.atheism; soc.religion.christian; talk.religion.misc
Computer	comp.graphics; comp.os.ms-windows.misc; comp.sys.ibm.pc.hardware; comp.sys.mac.hardware; comp.windows.x
Misc	misc.forsale
Cars	rec.autos; rec.motorcycles
Sport	rec.sport.baseball; rec.sport.hockey
Science	sci.crypt; sci.electronics; sci.med; sci.space
Politics	talk.politics.guns; talk.politics.mideast; talk.politics.misc

Table 5: 20-Newsgroups coarse categories and constituent topics.

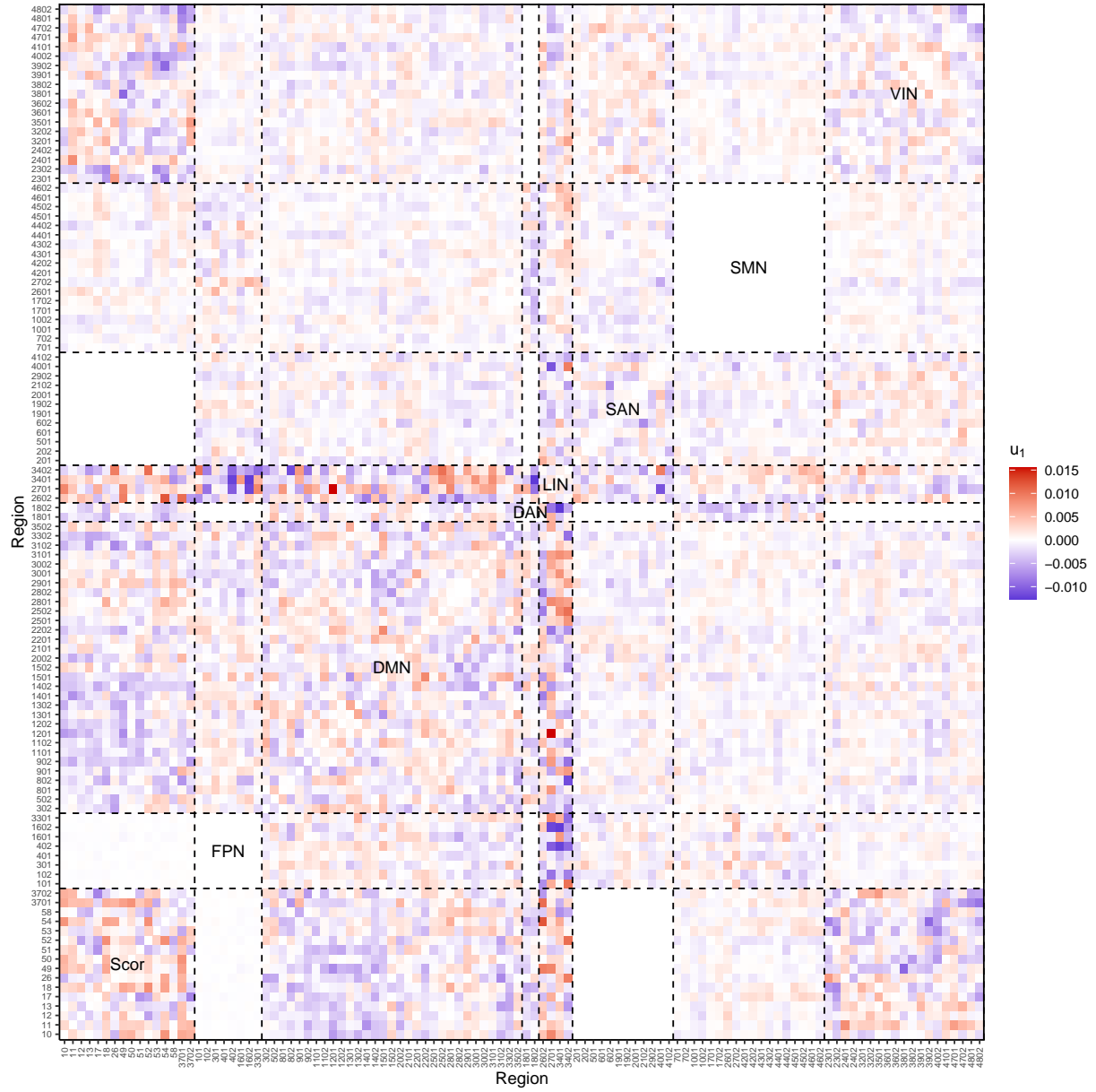


Figure 17: Heatmap of the first canonical direction vector u_1 from group-sparse ECCAR on ABIDE data. The x- and y-axes indicate brain region indices. Horizontal and vertical lines separate the eight brain networks, the name of each network is represented in the diagonal blocks.

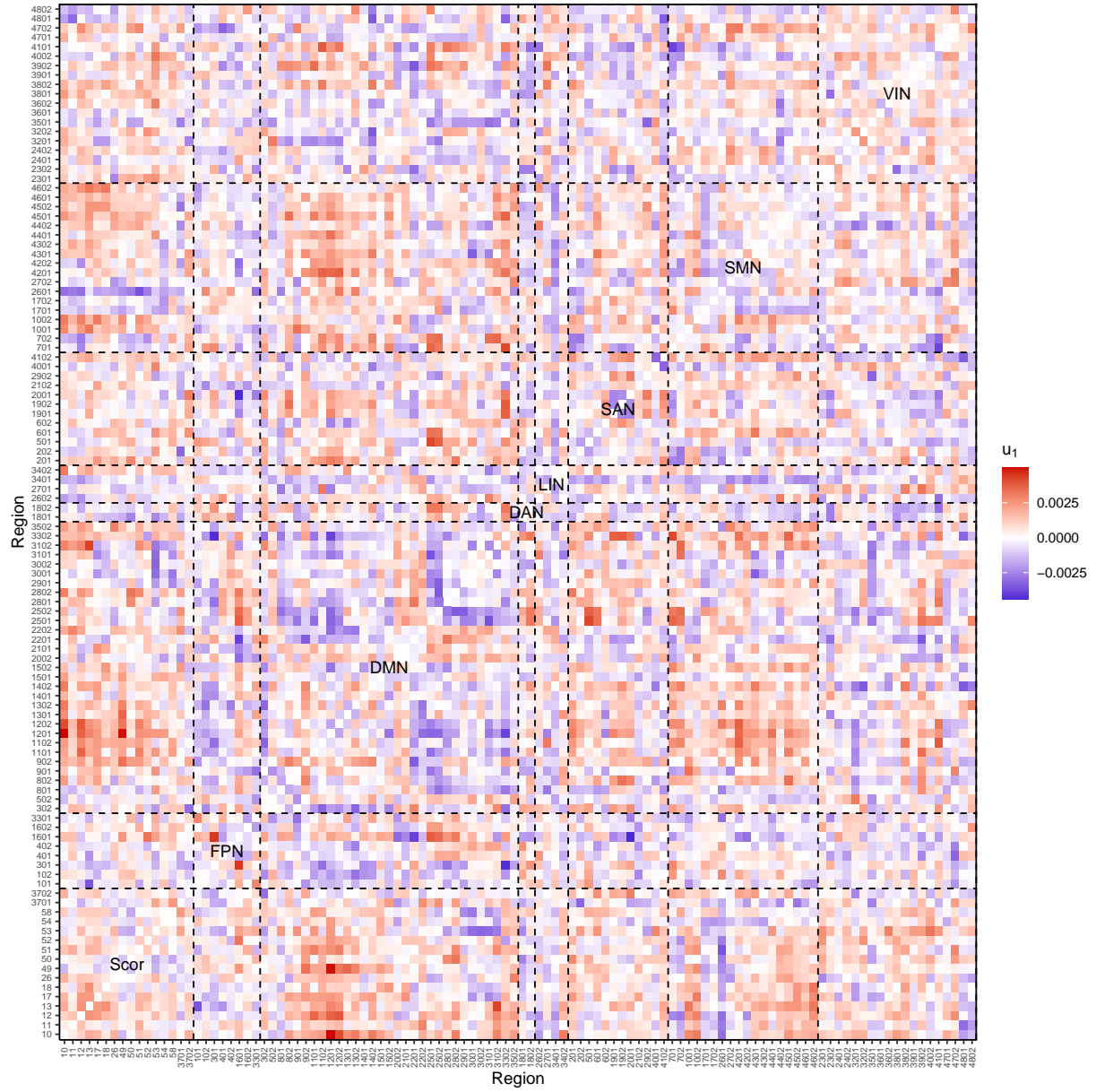


Figure 18: Heatmap of the first canonical direction vector u_1 from sparse CCA by Parkhomenko et al. (2009) on ABIDE data. The x- and y-axes indicate brain region indices. Horizontal and vertical lines separate the eight brain networks, the name of each network is represented in the diagonal blocks.

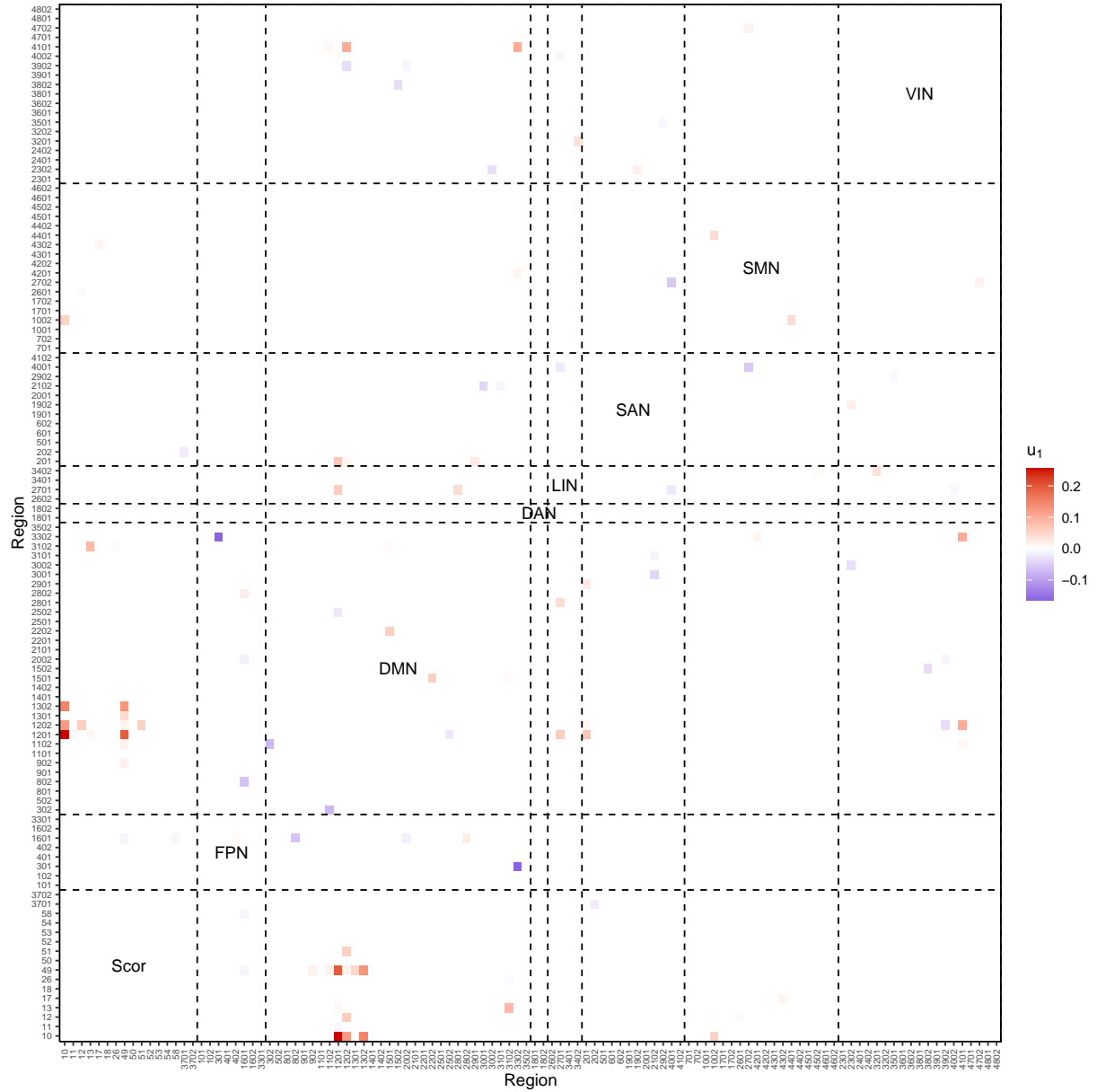
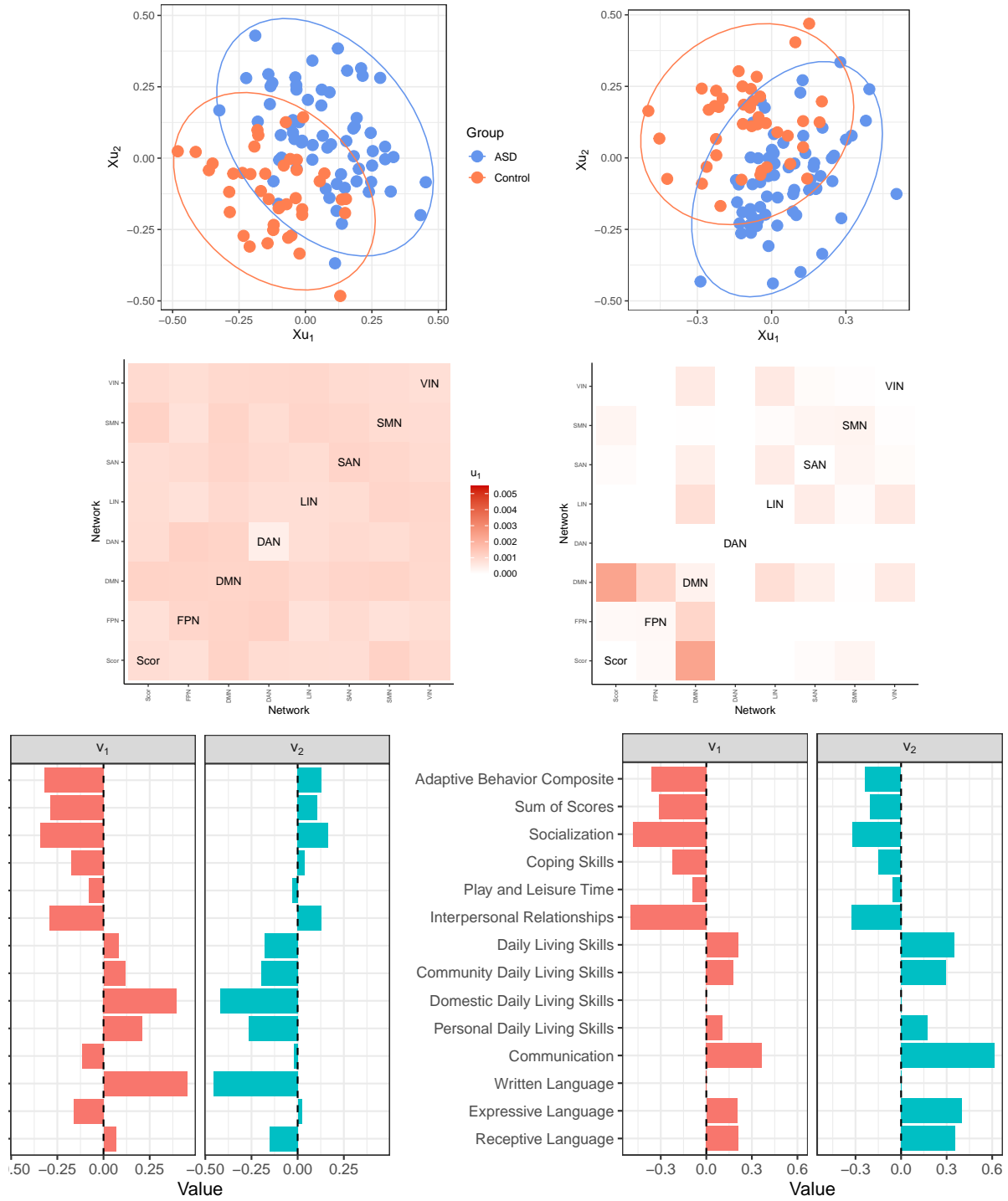


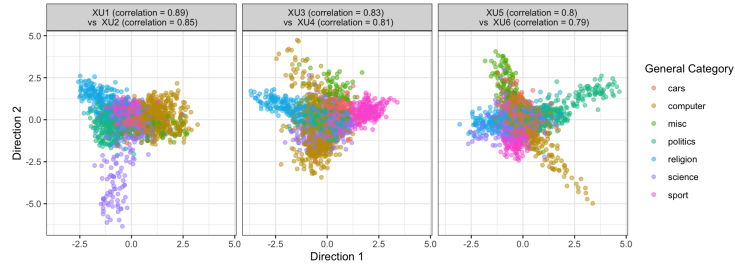
Figure 19: Heatmap of the first canonical direction vector u_1 from sparse CCA by Witten et al. (2009) on ABIDE data. The x- and y-axes indicate brain region indices. Horizontal and vertical lines separate the eight brain networks, the name of each network is represented in the diagonal blocks.



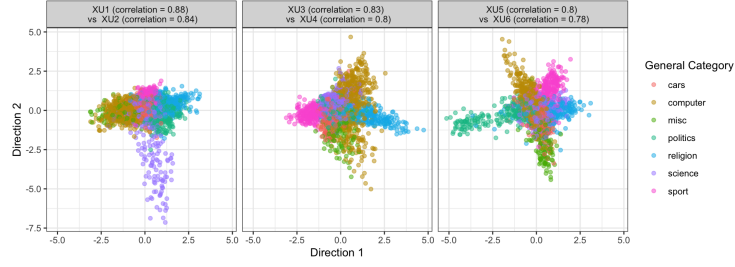
(a) SCCA by Parkhomenko et al.

(b) Sparse CCA by Witten et al.

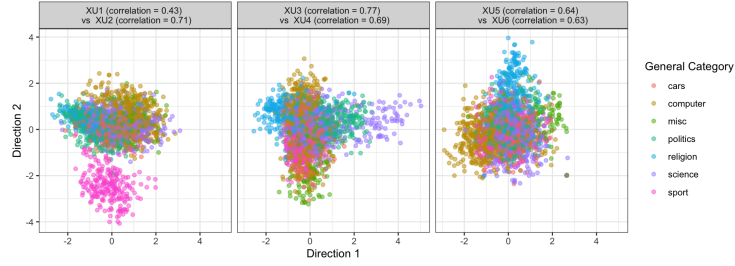
Figure 20: The results for the ABIDE data. Top: the projection of the data onto the space of the first two canonical variates colored by the disease status. Middle: the heatmap for u_1 (average of absolute values within each network). Bottom: the bar plot for v_1 and v_2 .



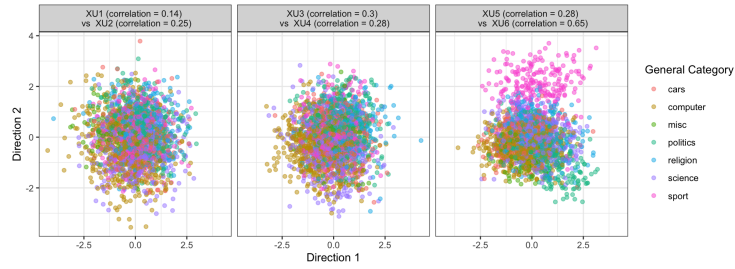
(a) Sparse eccar.



(b) SAR Wilms and Croux (2016)



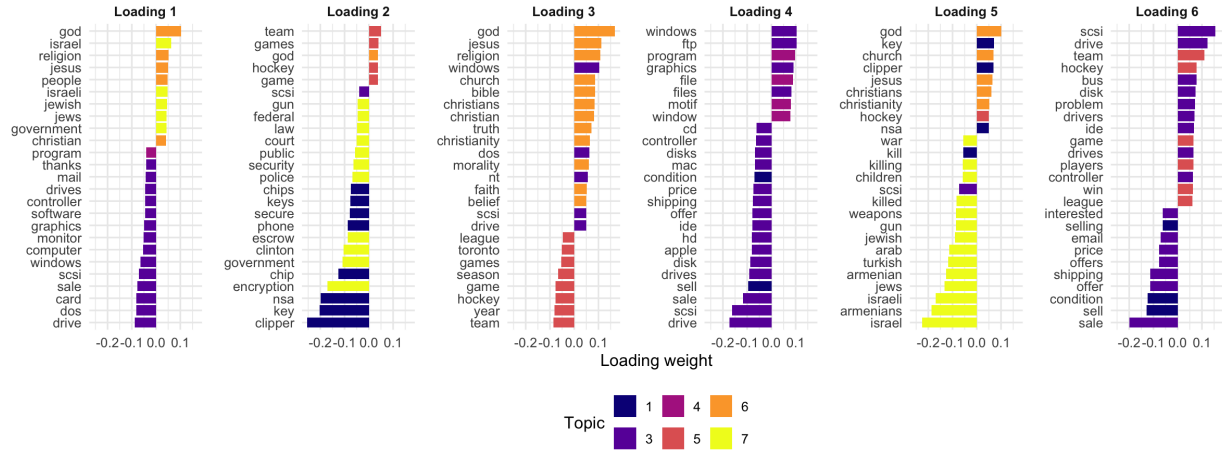
(c) Sparse CCA method of Witten et al. (2009).



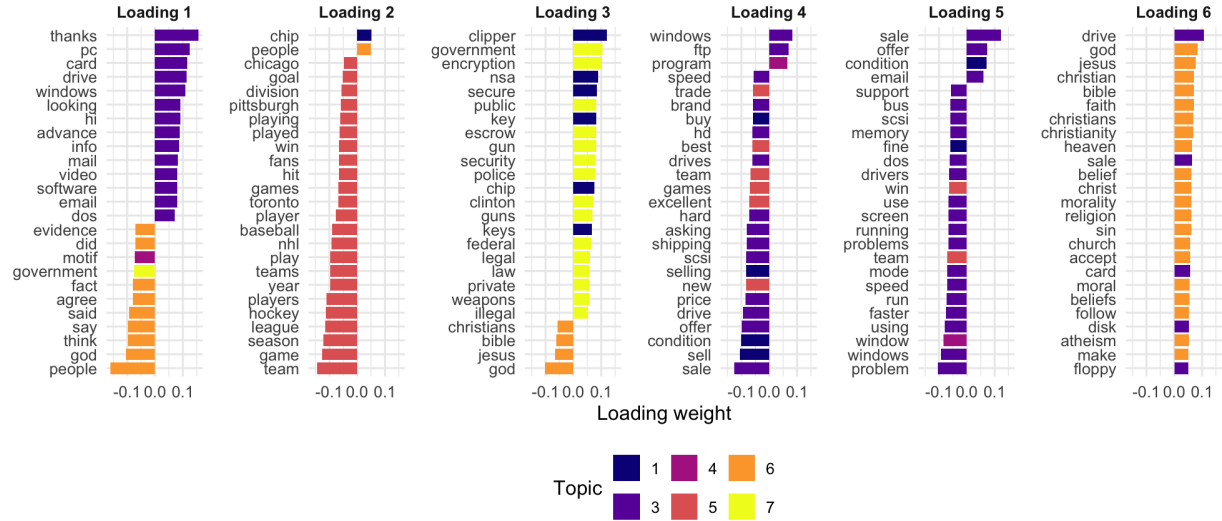
(d) Sparse CCA of Parkhomenko et al. (2009).

Figure 21: CCA variates produced by sparse CCA for our LLM interpretability example:

Alignment XU of the LLM document embeddings with the TF IDF frequencies.

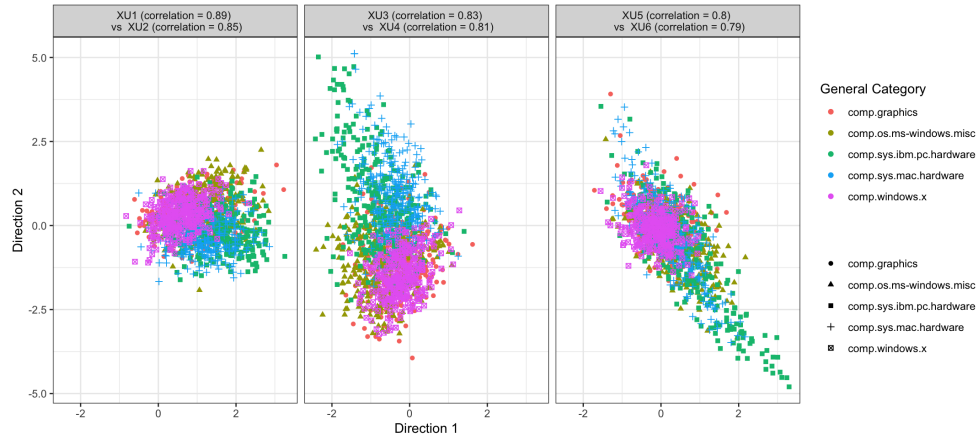


(a) Loadings obtained using SAR (Wilms and Croux, 2015)

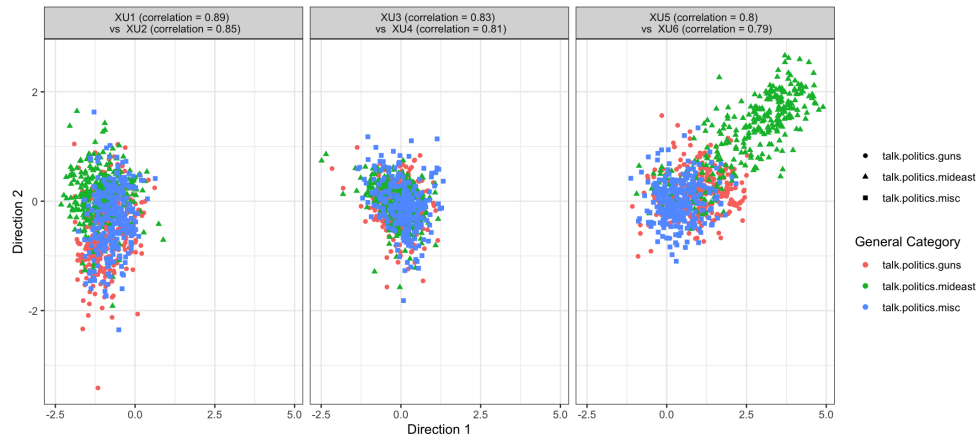


(b) Loadings obtained using the Sparse CCA of Witten and Tibshirani (2009)

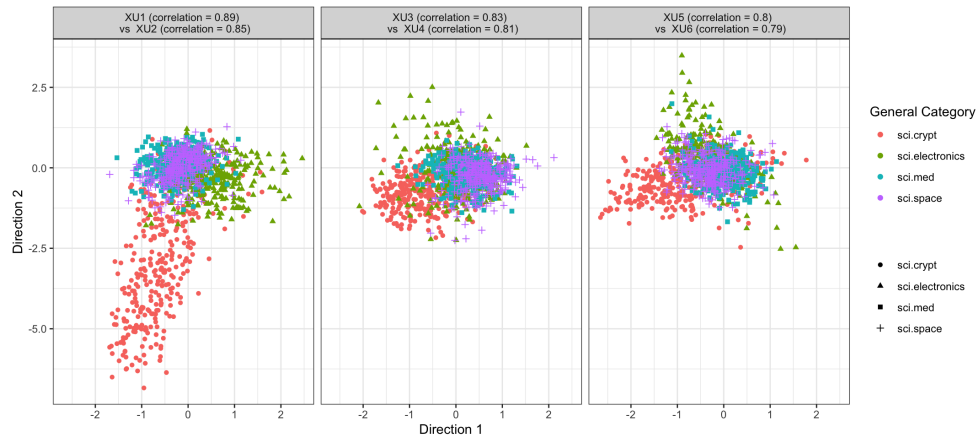
Figure 22: CCA loadings as recovered by the sparse CCA method for the first 6 canonical directions. Colors indicate the word's main topics, as estimated by the Latent Dirichlet Allocation algorithm.



(a) Computers



(b) Politics



(c) Science

Figure 23: CCA projections of points belonging to a category, using `eccar`.

D Technical lemmas

D.1 Matrix Perturbation Bounds

In this section, we provide facts about matrix perturbation that we have used in the proofs.

We start with the following theorem, which is a variant of Davis-Kahan theorem.

Theorem D.1 (Theorem 2 in Yu et al. (2015)). *Let $M \in \mathbb{R}^{n \times n}$ be a rank K symmetric matrix with smallest nonzero eigenvalue $\lambda_K(M)$, and let $\widehat{M} \in \mathbb{R}^{n \times n}$ be any symmetric matrix. Let $\widehat{U}(\widehat{M}) \in \mathbb{R}^{n \times K}$ and $U(M) \in \mathbb{R}^{n \times K}$ be the matrices of K leading eigenvectors of \widehat{M} and M , respectively. Then there exists a $K \times K$ orthogonal matrix O such that*

$$\|\widehat{U}(\widehat{M}) - U(M)O\|_F \leq \frac{2\sqrt{2}\|\widehat{M} - M\|_F}{\lambda_K(M)}. \quad (13)$$

The following corollary and lemma are taken from Klopp et al. (2021) and very slightly adapted in terms of the Frobenius norm. The proof is provided to make this manuscript self contained, but it is essentially the same as the original proof of Klopp et al. (2021).

Corollary D.1.1 (Adapted from Corollary 4 of Klopp et al. (2021)). *Let M and X be matrices with singular value decompositions given by $M = U\Lambda V^\top$ and $X = \widehat{U}\widehat{\Lambda}(\widehat{V})^\top$ where \widehat{U} and \widehat{V} are the left and right singular vectors of X corresponding to its K leading singular values. Then there exists $K \times K$ orthogonal matrices O and \tilde{O} such that*

$$\begin{aligned} \|\widehat{U} - UO\|_F &\leq \frac{2\sqrt{2}(\|X\|_{op} + \|M\|_{op})\|X - M\|_F}{\lambda_K^2(M)} \\ \|\widehat{V} - V\tilde{O}\|_F &\leq \frac{2\sqrt{2}(\|X\|_{op} + \|M\|_{op})\|X - M\|_F}{\lambda_K^2(M)} \end{aligned} \quad (14)$$

Furthermore, if $\|X - M\| \leq \frac{1}{2}\lambda_K(M)$ then

$$\max \left\{ \|\widehat{U} - UO\|_F, \|\widehat{V} - V\tilde{O}\|_F \right\} \leq \frac{5\sqrt{2}\kappa(M)\|X - M\|_F}{\lambda_K(M)}. \quad (15)$$

Proof. Applying Theorem D.1 to matrices MM^\top and XX^\top we get

$$\|\hat{U} - UO\|_F \leq \frac{2\sqrt{2}\|MM^\top - XX^\top\|_F}{\lambda_K(MM^\top)} \leq \frac{2\sqrt{2}(\|X\|_{op} + \|M\|_{op})\|X - M\|_F}{\lambda_K^2(M)}. \quad (16)$$

The last line follows by observing that:

$$\begin{aligned} \|MM^\top - XX^\top\|_F &= \|MM^\top - MX^\top + MX^\top - XX^\top\|_F = \|M(M^\top - X^\top) + (M - X)X^\top\|_F \\ &\leq \|M(M^\top - X^\top)\|_F + \|(M - X)X^\top\|_F \\ &\leq \|M\|_{op}\|M^\top - X^\top\|_F + \|X^\top\|_{op}\|M - X\|_F \end{aligned} \quad (17)$$

Similarly, the inequality on \hat{V} is obtained by applying Proposition D.1 to matrices $M^\top M$ and $X^\top X$. Next, if $\|X - M\|_{op} \leq \frac{1}{2}\lambda_K(M)$ then due to the triangle inequality we have $\|X\|_{op} \leq \|M\|_{op} + \frac{1}{2}\lambda_K(M) \leq \frac{3}{2}\|M\|_{op}$. Combining this fact with (14), we obtain (15). \square

Lemma D.2 (Adapted from Lemma 3 of Klopp et al. (2021)). *Let the assumption of Corollary 13 hold. Let $\hat{\Lambda}$ and Λ be diagonal $K \times K$ matrices of K largest singular values of X and M . If $\|X - M\| \leq \frac{1}{2}\lambda_K(M)$ then*

$$\|\hat{\Lambda} - O^\top \Lambda \tilde{O}\| \leq C\kappa^2(M)\sqrt{K}\|X - M\| \quad (18)$$

and

$$\|\hat{\Lambda}^{-1} - \tilde{O}^\top \hat{\Lambda}^{-1} O\| \leq C\kappa^2(M)\sqrt{K}\frac{\|X - M\|}{\lambda_K^2(M)} \quad (19)$$

The following Lemmas D.3, D.4, and D.5 correspond to Lemmas 6.4 and 6.5 in Gao et al. (2017), and Lemma 9.7 in its supplementary material.

Lemma D.3. *Assume $r\sqrt{\log(p+q)}/n \leq c$ for some sufficiently small constant $c \in (0,1)$*

Then there exist some constants $a, a' > 0$ only depending on M and c such that $\|\hat{\Sigma}_{XY} - \hat{\Sigma}_X C \hat{\Sigma}_Y\|_\infty \leq a\sqrt{\log(p+q)/n}$ with probability at least $1 - (p+q)^{-a'}$.

For any positive semi-definite matrix B , define

$$\phi_{max}^B(k) = \max_{\|u\|_0 \leq k, \|u\|_2=1} u^\top B u, \quad \phi_{min}^B(k) = \min_{\|u\|_0 \leq k, \|u\|_2=1} u^\top B u$$

Lemma D.4. Assume $\frac{1}{n} \left((k_u \wedge p) \log \left(\frac{ep}{k_u \wedge p} \right) + (k_v \wedge q) \log \left(\frac{eq}{k_v \wedge q} \right) \right) \leq c$ for some sufficiently small constant $c > 0$. Then there exist some constants $b, b' > 0$ only depending on M and c such that for

$$\delta_u(k_u) = \sqrt{\frac{1}{n} \left((k_u \wedge p) \log \left(\frac{ep}{k_u \wedge p} \right) \right)}$$

and

$$\delta_v(k_v) = \sqrt{\frac{1}{n} \left((k_v \wedge q) \log \left(\frac{eq}{k_v \wedge q} \right) \right)}$$

we have

$$M^{-1} - b\delta_u(k_u) \leq \phi_{min}^{\hat{\Sigma}_X}(k_u) \leq \phi_{max}^{\hat{\Sigma}_X}(k_v) \leq M + b\delta_u(k_u),$$

$$M^{-1} - b\delta_v(k_v) \leq \phi_{min}^{\hat{\Sigma}_Y}(k_u) \leq \phi_{max}^{\hat{\Sigma}_Y}(k_v) \leq M + b\delta_v(k_v),$$

with probability at least $1 - \exp \left(-b'(k_u \wedge p) \log \left(\frac{ep}{k_u \wedge p} \right) \right) - \exp \left(-b'(k_v \wedge q) \log \left(\frac{eq}{k_v \wedge q} \right) \right)$

Lemma D.5. Assume $n \geq c(s_u + s_v + \log(ep/s_u) + \log(eq/s_v))$ for some sufficiently large constant c . Then there exists constant C, C' only depending on c such that

$$\begin{aligned} \|U^\top \hat{\Sigma}_X U - I\|_{op} \vee \|(U^\top \hat{\Sigma}_X U)^{1/2} - I\|_{op} &\leq C \sqrt{\frac{1}{n}(s_u + \log(ep/s_u))} \\ \|V^\top \hat{\Sigma}_Y V - I\|_{op} \vee \|(V^\top \hat{\Sigma}_Y V)^{1/2} - I\|_{op} &\leq C \sqrt{\frac{1}{n}(s_v + \log(eq/s_v))} \end{aligned}$$

with probability at least $1 - \exp(-C'(s_u + \log(ep/s_u))) - \exp(-C'(s_v + \log(eq/s_v)))$

Lemma D.6. Consider the parameter spaces $F(s_u, s_v, p, q, r; M)$ of all covariance matrices Σ that satisfy the condition. Assume $n > s_u s_v$. Then the solution of

$$\min_{B \in \mathbb{R}^{s_u \times s_v}} \frac{1}{2} \|X_{s_u} B Y_{s_v}^\top - I_n\|_F^2 + \lambda \|B\|_1,$$

satisfies

$$\|\tilde{\Delta}\|_F \leq \frac{2(\|\widehat{\Sigma}_{XY} - \widehat{\Sigma}_X B \widehat{\Sigma}_Y\|_\infty + \lambda)}{\sigma_{\min}((\widehat{\Sigma}_X)_{S_u S_u}) \sigma_{\min}((\widehat{\Sigma}_Y)_{S_v S_v})} \sqrt{s_u s_v}$$

Proof of Lemma D.6. Following the step 1 of the proof of Theorem 3.1, we have

$$\frac{1}{2} \|X_{S_u} \tilde{\Delta} Y_{S_v}\|_F^2 \leq \|\widehat{\Sigma}_{XY} - \widehat{\Sigma}_X B \widehat{\Sigma}_Y\|_\infty \|\tilde{\Delta}\|_1 + \lambda \|\tilde{\Delta}\|_1$$

Therefore

$$\|X_{S_u} \tilde{\Delta} Y_{S_v}\|_F^2 \leq 2(\|\widehat{\Sigma}_{XY} - \widehat{\Sigma}_X B \widehat{\Sigma}_Y\|_\infty + \lambda) \|\tilde{\Delta}\|_1 \leq 2(\|\widehat{\Sigma}_{XY} - \widehat{\Sigma}_X B \widehat{\Sigma}_Y\|_\infty + \lambda) \sqrt{s_u s_v} \|\tilde{\Delta}\|_F$$

On the other hand,

$$\|X_{S_u} \tilde{\Delta} Y_{S_v}\|_F^2 \geq \sigma_{\min}((\widehat{\Sigma}_X)_{S_u S_u}) \sigma_{\min}((\widehat{\Sigma}_Y)_{S_v S_v}) \|\tilde{\Delta}\|_F^2,$$

Therefore

$$\sigma_{\min}((\widehat{\Sigma}_X)_{S_u S_u}) \sigma_{\min}((\widehat{\Sigma}_Y)_{S_v S_v}) \|\tilde{\Delta}\|_F^2 \leq \|X_{S_u} \tilde{\Delta} Y_{S_v}\|_F^2 \leq 2(\|\widehat{\Sigma}_{XY} - \widehat{\Sigma}_X B \widehat{\Sigma}_Y\|_\infty + \lambda) \sqrt{s_u s_v} \|\tilde{\Delta}\|_F$$

This implies

$$\|\tilde{\Delta}\|_F \leq \frac{2(\|\widehat{\Sigma}_{XY} - \widehat{\Sigma}_X B \widehat{\Sigma}_Y\|_\infty + \lambda)}{\sigma_{\min}((\widehat{\Sigma}_X)_{S_u S_u}) \sigma_{\min}((\widehat{\Sigma}_Y)_{S_v S_v})} \sqrt{s_u s_v}$$

□

E Proofs of the consistency of ECCAR in low dimensions

E.1 Proof of Theorem 2.1

Proof. A derivation of the Karush–Kuhn–Tucker conditions (KKT) for minimizing $\mathcal{L}(B)$ reveals that the solution \widehat{B} can be expressed as a function of the sample covariance matrices

$\widehat{\Sigma}_X$, $\widehat{\Sigma}_Y$ and $\widehat{\Sigma}_{XY}$:

$$\nabla_B \mathcal{L}(\widehat{B}) = 0 \iff \frac{X^\top X}{n} \widehat{B} \frac{Y^\top Y}{n} - \frac{X^\top Y}{n} = 0 \iff \widehat{B} = \widehat{\Sigma}_X^{-1} \widehat{\Sigma}_{XY} \widehat{\Sigma}_Y^{-1}. \quad (20)$$

Since X and Y are assumed to be Gaussian and thus have finite second moments, the Law of Large Numbers implies that:

$$\widehat{\Sigma}_X \xrightarrow{a.s.} \Sigma_X, \quad \widehat{\Sigma}_Y \xrightarrow{a.s.} \Sigma_Y \quad \text{and} \quad \widehat{\Sigma}_{XY} \xrightarrow{a.s.} \Sigma_{XY}. \quad (21)$$

Since the matrix inversion $A \mapsto A^{-1} = \frac{1}{\det(A)} \text{adj}(A)$ is a continuous function on the set of positive definite matrices (Stewart, 1969), due to the continuity of the determinant and adjugate functions, and since, for sufficiently large n , the sample covariance matrices $\widehat{\Sigma}_X$ and $\widehat{\Sigma}_Y$ are almost surely positive definite, it follows that

$$\widehat{\Sigma}_X^{-1} \xrightarrow{a.s.} \Sigma_X^{-1}, \quad \widehat{\Sigma}_Y^{-1} \xrightarrow{a.s.} \Sigma_Y^{-1}.$$

Therefore, by the continuous mapping theorem, the matrix $\widehat{\Sigma}_X^{-1} \widehat{\Sigma}_{XY} \widehat{\Sigma}_Y^{-1}$ converges entry-wise almost surely to $\Sigma_X^{-1} \Sigma_{XY} \Sigma_Y^{-1}$. Under the canonical pair model (Equation 3), this implies that $\lim_{n \rightarrow \infty} \widehat{B} = \lim_{n \rightarrow \infty} \widehat{\Sigma}_X^{-1} \widehat{\Sigma}_{XY} \widehat{\Sigma}_Y^{-1} = U^* \Lambda^* V^{*\top} = B^*$. Hence, \widehat{B} is a consistent estimator for B^* . \square

E.2 Proof of Theorem 2.2

Proof. By theorem 2.1, we know that \widehat{B} is a consistent estimator of B^* . Since, additionally, the matrix square root $A \mapsto A^{\frac{1}{2}}$ is a continuous function on the set of positive definite matrices, by the continuous mapping theorem, $\widehat{\Sigma}_X^{\frac{1}{2}} \widehat{B} \widehat{\Sigma}_Y^{\frac{1}{2}}$ is a consistent estimator of $\Sigma_X^{\frac{1}{2}} B^* \Sigma_Y^{\frac{1}{2}}$. Equation 6 can be proved by application of known properties of the singular subspaces in perturbation theory (e.g. Corollary D.1.1 in Appendix D). A second application of the continuous mapping theorem, coupled with the fact that $\widehat{\Sigma}_X^{-\frac{1}{2}}$ and $\widehat{\Sigma}_Y^{-\frac{1}{2}}$ converge almost

surely to $\Sigma_X^{-\frac{1}{2}}$ and $\Sigma_Y^{-\frac{1}{2}}$ (see proof of Theorem 2.1) establishes the consistency result of Equation 7. \square

F Proofs of the consistency of ECCAR in high dimensions

F.1 The sparse Setting

F.1.1 Theorem 3.1

Consider the parameter space $F(s_u, s_v, p, q, r; M)$ for the covariance matrix Σ (Equation 3 and conditions here therein), and let $\Delta = \hat{B} - B^$, where \hat{B} is the estimate obtained in step 1 of Algorithm 1. Assume $n \geq cs_u s_v \log(p+q)$ for some sufficiently large constant c . There exist constants a, b, C depending on M and c such that if $\rho \geq a\sqrt{\log(p+q)/n}$, then with probability at least $1 - \exp(-bs_u \log(ep/s_u)) - \exp(-bs_v \log(eq/s_v)) - (p+q)^{-b}$, we have:*

$$\|\Delta\|_F \leq C\rho\sqrt{s_u s_v}.$$

In particular, if ρ is of order $\sqrt{\log(p+q)/n}$, we have:

$$\|\Delta\|_F \lesssim \sqrt{\frac{s_u s_v \log(p+q)}{n}},$$

and \hat{B} has sparse entries:

$$\|\hat{B}\|_0 \lesssim s_u s_v.$$

Proof of Theorem 3.1. We first prove the bound on $\|\Delta\|_F$. The proof consists here of three main steps.

Step 1. Showing that $\|\Delta_{(S_u S_v)^c}\|_1 \leq 3\|\Delta_{S_u S_v}\|_1$: By the basic inequality, we have

$$\begin{aligned}
L(\widehat{B}) + \rho\|\widehat{B}\|_1 &\leq L(B^\star) + \rho\|B^\star\|_1 \\
\frac{1}{2}\|\frac{1}{n}X\widehat{B}Y^\top - I_n\|_F^2 + \rho\|\widehat{B}\|_1 &\leq \frac{1}{2}\|\frac{1}{n}XB^\star Y^\top - I_n\|_F^2 + \rho\|B^\star\|_1 \\
\frac{1}{2}\|X\widehat{B}Y^\top/n\|_F^2 - \text{tr}(X\widehat{B}Y^\top)/n &\leq \frac{1}{2}\|XB^\star Y^\top/n\|_F^2 - \text{tr}(XB^\star Y^\top)/n + \rho\|B^\star\|_1 - \rho\|\widehat{B}\|_1 \\
\frac{1}{2}(\|X(B^\star + \Delta)Y^\top/n\|_F^2 - \|XB^\star Y^\top/n\|_F^2) &\leq \text{tr}(\Delta^\top \widehat{\Sigma}_{XY}) + \rho\|B^\star\|_1 - \rho\|\widehat{B}\|_1 \\
\frac{1}{2}\|X\Delta Y^\top/n\|_F^2 + \text{tr}(YB^{\star\top}X^\top X\Delta Y^\top)/n^2 &\leq \text{tr}(\Delta^\top \widehat{\Sigma}_{XY}) + \rho\|B^\star\|_1 - \rho\|\widehat{B}\|_1 \\
\frac{1}{2}\|X\Delta Y^\top/n\|_F^2 + \text{tr}(\widehat{\Sigma}_Y B^{\star\top} \widehat{\Sigma}_X \Delta) &\leq \text{tr}(\Delta^\top \widehat{\Sigma}_{XY}) + \rho\|B^\star\|_1 - \rho\|\widehat{B}\|_1 \\
\frac{1}{2}\|X\Delta Y^\top/n\|_F^2 &\leq \langle \widehat{\Sigma}_{XY} - \widehat{\Sigma}_X B^\star \widehat{\Sigma}_Y, \Delta \rangle + \rho\|B^\star\|_1 - \rho\|\widehat{B}\|_1 \\
\frac{1}{2}\|X\Delta Y^\top/n\|_F^2 &\leq \langle \widehat{\Sigma}_{XY} - \widehat{\Sigma}_X B^\star \widehat{\Sigma}_Y, \Delta \rangle + \rho\|B_{S_u S_v}^\star\|_1 \\
&\quad - \rho\|\widehat{B}_{S_u S_v}\|_1 - \rho\|\widehat{B}_{(S_u S_v)^c}\|_1 \\
\frac{1}{2}\|X\Delta Y^\top/n\|_F^2 &\leq \langle \widehat{\Sigma}_{XY} - \widehat{\Sigma}_X B^\star \widehat{\Sigma}_Y, \Delta \rangle + \rho\|\Delta_{S_u S_v}\|_1 - \rho\|\Delta_{(S_u S_v)^c}\|_1 \\
\frac{1}{2}\|X\Delta Y^\top/n\|_F^2 &\leq \|\widehat{\Sigma}_{XY} - \widehat{\Sigma}_X B^\star \widehat{\Sigma}_Y\|_\infty \|\Delta\|_1 + \rho\|\Delta_{S_u S_v}\|_1 - \rho\|\Delta_{(S_u S_v)^c}\|_1
\end{aligned}$$

By our choice of ρ and Lemma D.3 we have

$$\begin{aligned}
0 &\leq \frac{\rho}{2}\|\Delta\|_1 + \rho\|\Delta_{S_u S_v}\|_1 - \rho\|\Delta_{(S_u S_v)^c}\|_1 \\
0 &\leq \frac{3}{2}\|\Delta_{S_u S_v}\|_1 - \frac{1}{2}\|\Delta_{(S_u S_v)^c}\|_1
\end{aligned}$$

Therefore we have

$$\|\Delta_{(S_u S_v)^c}\|_1 \leq 3\|\Delta_{S_u S_v}\|_1$$

Step 2. Showing that $\|X\Delta Y^\top/n\|_F^2 \lesssim \rho\sqrt{s_us_v}\|\Delta_{S_uS_v}\|_F$: This is directly implied by the conclusion of **Step 1**:

$$\begin{aligned}
\frac{1}{2}\|X\Delta Y^\top/n\|_F^2 &\leq \frac{\rho}{2}\|\Delta\|_1 + \rho\|\Delta_{S_uS_v}\|_1 \\
&= \frac{\rho}{2}(\|\Delta_{S_uS_v}\|_1 + \|\Delta_{(S_uS_v)^c}\|_1) + \rho\|\Delta_{S_uS_v}\|_1 \\
&\leq \frac{\rho}{2}(\|\Delta_{S_uS_v}\|_1 + 3\|\Delta_{S_uS_v}\|_1) + \rho\|\Delta_{S_uS_v}\|_1 \\
&= 3\rho\|\Delta_{S_uS_v}\|_1 \\
&\leq 3\rho\sqrt{s_us_v}\|\Delta_{S_uS_v}\|_F
\end{aligned}$$

Step 3. Showing that $\|X\Delta Y^\top/n\|_F \gtrsim \|\Delta_{S_uS_v}\|_F$: Now let us look at $\|X\Delta Y^\top/n\|_F^2 = \text{tr}(\Delta^\top \hat{\Sigma}_X \Delta \hat{\Sigma}_Y) = \|\hat{\Sigma}_X^{1/2} \Delta \hat{\Sigma}_Y^{1/2}\|_F^2$. Let the index set $J_1 = \{(i_k, j_k)\}_{k=1}^\top$ in $(S_u \times S_v)^c$ correspond to the entries with the largest absolute values in Δ . and we define the set $\tilde{J} = (S_u \times S_v) \cup J_1$. Now we partition \tilde{J}^c into disjoint subsets J_2, \dots, J_K of size t (with $|J_K| \leq t$), such that J_k is the set of (double) indices corresponding to the entries of t largest absolute values in Δ outside $\tilde{J} \cup \bigcup_{j=2}^{K-1} J_j$. By the triangle inequality,

$$\begin{aligned}
\|\hat{\Sigma}_X^{1/2} \Delta \hat{\Sigma}_Y^{1/2}\|_F &\geq \|\hat{\Sigma}_X^{1/2} \Delta_{\tilde{J}} \hat{\Sigma}_Y^{1/2}\|_F - \sum_{k=2}^K \|\hat{\Sigma}_X^{1/2} \Delta_{J_k} \hat{\Sigma}_Y^{1/2}\|_F \\
&\geq \sqrt{\phi_{\min}^{\hat{\Sigma}_X}(s_u + t) \phi_{\min}^{\hat{\Sigma}_Y}(s_v + t)} \|\Delta_{\tilde{J}}\|_F - \sqrt{\phi_{\max}^{\hat{\Sigma}_X}(t) \phi_{\max}^{\hat{\Sigma}_Y}(t)} \sum_{k=2}^K \|\Delta_{J_k}\|_F
\end{aligned}$$

Also we have

$$\sum_{k=2}^K \|\Delta_{J_k}\|_F \leq \sqrt{t} \sum_{k=2}^K \|\Delta_{J_k}\|_\infty \leq \frac{1}{\sqrt{t}} \sum_{k=1}^{K-1} \|\Delta_{J_k}\|_1 \leq \frac{1}{\sqrt{t}} \|\Delta_{(S_uS_v)^c}\|_1 \leq \frac{3}{\sqrt{t}} \|\Delta_{S_uS_v}\|_1 \leq \frac{3\sqrt{s_us_v}}{\sqrt{t}} \|\Delta_{\tilde{J}}\|_F$$

Therefore

$$\|\hat{\Sigma}_X^{1/2} \Delta \hat{\Sigma}_Y^{1/2}\|_F \geq \left(\sqrt{\phi_{\min}^{\hat{\Sigma}_X}(s_u + t) \phi_{\min}^{\hat{\Sigma}_Y}(s_v + t)} - \frac{3\sqrt{s_us_v}}{\sqrt{t}} \sqrt{\phi_{\max}^{\hat{\Sigma}_X}(t) \phi_{\max}^{\hat{\Sigma}_Y}(t)} \right) \|\Delta_{\tilde{J}}\|_F$$

Take $t = c_1 s_u s_v$ for some sufficiently large constant $c_1 > 1$. Then with high probability,

$$\left(\sqrt{\phi_{\min}^{\hat{\Sigma}_X}(s_u + t) \phi_{\min}^{\hat{\Sigma}_Y}(s_v + t)} - \frac{3\sqrt{s_us_v}}{\sqrt{t}} \sqrt{\phi_{\max}^{\hat{\Sigma}_X}(t) \phi_{\max}^{\hat{\Sigma}_Y}(t)} \right) \geq \kappa,$$

where κ is some positive constant that depends only on M . To see this, note by Lemma D.4, $\delta_u(s_u + t)$ and $\delta_v(s_v + t)$ are bounded by $\frac{2c_1 s_u s_v \log(p)}{n}$ and $\frac{2c_1 s_u s_v \log(q)}{n}$, which are small by assumption. The same arguments hold for $\delta_u(t)$ and $\delta_v(t)$. Therefore taking c_1 to be large leads to the lower bound κ .

Combining this result with the upper bound on the right-hand side, we have

$$\kappa^2 \|\Delta_{\tilde{J}}\|_F^2 \leq \|\widehat{\Sigma}_X^{1/2} \Delta \widehat{\Sigma}_Y^{1/2}\|_F^2 \leq 3\rho \sqrt{s_u s_v} \|\Delta_{S_u S_v}\|_F \leq 3\rho \sqrt{s_u s_v} \|\Delta_{\tilde{J}}\|_F$$

Therefore

$$\|\Delta_{\tilde{J}}\|_F \leq \frac{3\rho \sqrt{s_u s_v}}{\kappa^2}$$

On the other hand,

$$\|\Delta_{\tilde{J}^c}\|_F = \sum_{k=2}^K \|\Delta_{J_k}\|_F \leq \frac{3\sqrt{s_u s_v}}{\sqrt{t}} \|\Delta_{\tilde{J}}\|_F = \frac{3\sqrt{s_u s_v}}{\sqrt{c_1 s_u s_v}} \|\Delta_{\tilde{J}}\|_F$$

Combining the results from steps 1 through 3, the bound on $\|\Delta\|_F$ in Equation 10 follows.

Then we prove the support of \widehat{B} is sparse. By the KKT conditions, we have

$$\left(\widehat{\Sigma}_X \widehat{B} \widehat{\Sigma}_Y - \widehat{\Sigma}_{XY} \right)_{ij} = \rho \frac{\partial |B_{ij}|}{\partial B}$$

Therefore

$$\left| \left(\widehat{\Sigma}_X \Delta \widehat{\Sigma}_Y \right)_{ij} \right| \geq \rho^* - \|\widehat{\Sigma}_X B^* \widehat{\Sigma}_Y - \widehat{\Sigma}_{XY}\|_\infty \geq \frac{\rho}{2},$$

where the last inequality follows from Lemma D.3. Let T be the set of non-zero elements

in \widehat{B} , T_u be the non-zero rows of \widehat{B} and T_v be the non-zero columns of \widehat{B} . Then

$$\begin{aligned}
\frac{\rho^2}{4}T &\leq \sum_{(i,j) \in T} \left(\widehat{\Sigma}_X \Delta \widehat{\Sigma}_Y \right)_{ij}^2 \\
&\leq \delta_u(T_u) \delta_v(T_v) \|\Delta\|_F^2 \\
&\lesssim \left(M + \sqrt{\frac{T_u \log(p)}{n}} \right) \left(M + \sqrt{\frac{T_v \log(q)}{n}} \right) \rho^2 s_u s_v \\
&\lesssim \left(M^2 + M \sqrt{\frac{(T_u + T_v) \log(p+q)}{n}} + \sqrt{\frac{T_u T_v \log(p) \log(q)}{n^2}} \right) \rho^2 s_u s_v \\
&\lesssim \left(M^2 + M \sqrt{\frac{T \log(p+q)}{n}} + \frac{T \log(p+q)}{n} \right) \rho^2 s_u s_v
\end{aligned}$$

Here the second inequality is implied by Lemma D.4. It follows that

$$\left(\frac{1}{4} - \frac{s_u s_v \log(p+q)}{n} \right) T \leq \left(M^2 + M \sqrt{\frac{T \log(p+q)}{n}} \right) s_u s_v$$

By assumption,

$$\frac{1}{4} - \frac{s_u s_v \log(p+q)}{n} \geq \frac{1}{8}$$

for sufficiently large c . Solving

$$\frac{1}{8}T \leq \left(M^2 + M \sqrt{\frac{T \log(p+q)}{n}} \right) s_u s_v$$

gives

$$\sqrt{T} \lesssim \sqrt{\frac{\log(p+q)}{n}} s_u s_v + \sqrt{s_u s_v}$$

Again, as long as $n \geq c s_u s_v \log(p+q)$ for sufficiently large constant c , we have

$$T \lesssim \frac{\log(p+q) s_u s_v}{n} s_u s_v + s_u s_v \lesssim s_u s_v$$

□

F.1.2 Theorem 3.3

Consider the parameter space $\mathcal{F}(s_u, s_v, p, q, r; M)$ for the covariance matrix Σ (Equation 3 and conditions here therein). Assume $n > \max\{s_u, s_v\}$ and

$$\frac{\|\widehat{\Sigma}_{XY} - \widehat{\Sigma}_X B^* \widehat{\Sigma}_Y\|_\infty}{\rho} + \frac{2(\|\widehat{\Sigma}_{XY} - \widehat{\Sigma}_X B^* \widehat{\Sigma}_Y\|_\infty + \rho)}{\rho} \frac{\widehat{\tau}(X, Y) \sqrt{s_u s_v}}{\sigma_{\min}((\widehat{\Sigma}_X)_{S_u S_u}) \sigma_{\min}((\widehat{\Sigma}_Y)_{S_v S_v})} \leq 1, \quad (22)$$

where $S_u = \text{supp}(U^*)$ and $S_v = \text{supp}(V^*)$ and

$$\begin{aligned} \widehat{\tau}(X, Y) = \max \Big\{ & \|(\widehat{\Sigma}_X)_{S_u^c S_u}\|_{2, \infty} \|(\widehat{\Sigma}_Y)_{S_v^c S_v}\|_{2, \infty}, \\ & \|(\widehat{\Sigma}_X)_{S_u^c S_u}\|_{2, \infty} \|(\widehat{\Sigma}_Y)_{S_v S_v}\|_{op}, \\ & \|(\widehat{\Sigma}_X)_{S_u S_u}\|_{op} \|(\widehat{\Sigma}_Y)_{S_v^c S_v}\|_{2, \infty} \Big\}. \end{aligned}$$

Then the minimizer of 8 is unique and satisfies

$$\text{supp}(\widehat{B}) \subset S_u \times S_v.$$

Proof of Theorem 3.3. We first prove the existence of solution with support $S_u \times S_v$. Using strong duality, we can write the objective in a equivalent min-max form:

$$\begin{aligned} \min_{B^* \in \mathbb{R}^{p \times q}} \frac{1}{2} \|XBY^\top - I_n\|_F^2 + \rho \|B^*\|_1 & \iff \min_{B^* \in \mathbb{R}^{p \times q}} \max_{Z \in \mathbb{B}_{p, q}} \frac{1}{2} \|XBY^\top - I_n\|_F^2 + \rho \langle B, Z \rangle \\ & \iff \max_{Z \in \mathbb{B}_{p, q}} \min_{B^* \in \mathbb{R}^{p \times q}} \frac{1}{2} \|XBY^\top - I_n\|_F^2 + \rho \langle B, Z \rangle \end{aligned}$$

where

$$\mathbb{B}_{p, q} := \{Z \in \mathbb{R}^{p \times q}, \|Z\|_\infty \leq 1\}.$$

Then from the KKT condition, a pair $(\widehat{B}, \widehat{Z})$ is an optimal solution if and only if

$$Z_{ij} = \text{sign}(\widehat{B}_{ij}) \quad \widehat{B}_{ij} \neq 0 \quad (23)$$

$$Z_{ij} \in [-1, 1] \quad \widehat{B}_{ij} = 0 \quad (24)$$

$$B^* = \underset{B \in \mathbb{R}^{p \times q}}{\text{argmin}} \frac{1}{2} \|XBY^\top - I_n\|_F^2 + \rho \langle B, Z \rangle. \quad (25)$$

Let $S = S_u \times S_v$ be the support of the true solution. Consider the constrained solution \tilde{B} that solves the following problem

$$\min_{B^* \in \mathbb{R}^{p \times q}, \text{supp}(B) \in S} \frac{1}{2} \|XBY^\top - I_n\|_F^2 + \rho \|B^*\|_1 \quad (26)$$

One can easily show that this is equivalent to first solving

$$\min_{B^* \in \mathbb{R}^{s_u \times s_v}} \frac{1}{2} \|X_{S_u} B Y_{S_v}^\top - I_n\|_F^2 + \rho \|B^*\|_1,$$

then setting entries to be zero. By Lemma D.6, we have

$$\|\tilde{B} - B^*\|_F = \|\tilde{\Delta}\|_F \leq \frac{2(\|\hat{\Sigma}_{XY} - \hat{\Sigma}_X B^* \hat{\Sigma}_Y\|_\infty + \rho)}{\sigma_{\min}((\hat{\Sigma}_X)_{S_u S_u}) \sigma_{\min}((\hat{\Sigma}_Y)_{S_v S_v})} \sqrt{s_u s_v}.$$

Define a modified primal dual pair (\hat{B}, \hat{Z}) as follows

$$\begin{aligned} \hat{B} &= \tilde{B} \\ \hat{Z}_{S_u S_v} &= \tilde{Z}_{S_u S_v} \\ \hat{Z}_{S_u S_v^c} &= \frac{1}{\rho} \left((\hat{\Sigma}_{XY})_{S_u S_v^c} - (\hat{\Sigma}_X)_{S_u S_u} \tilde{B}_{S_u S_v} (\hat{\Sigma}_Y)_{S_v S_v^c} \right) \\ \hat{Z}_{S_u^c S_v} &= \frac{1}{\rho} \left((\hat{\Sigma}_{XY})_{S_u^c S_v} - (\hat{\Sigma}_X)_{S_u^c S_u} \tilde{B}_{S_u S_v} (\hat{\Sigma}_Y)_{S_v S_v} \right) \\ \hat{Z}_{S_u^c S_v^c} &= \frac{1}{\rho} \left((\hat{\Sigma}_{XY})_{S_u^c S_v^c} - (\hat{\Sigma}_X)_{S_u^c S_u} \tilde{B}_{S_u S_v} (\hat{\Sigma}_Y)_{S_v S_v^c} \right) \end{aligned} \quad (27)$$

We shall show that both \hat{B} and \hat{Z} satisfy the KKT conditions 23, 24, 25. Note that conditions 23 and 25 are automatically satisfied by the construction. So it suffices to verify condition 24.

Note that for $(i, j) \in S_u^c \times S_v$, we have:

$$\begin{aligned}
\rho|\hat{Z}_{ij}| &= |(\hat{\Sigma}_{XY})_{ij} - (\hat{\Sigma}_X)_{i,S_u} \tilde{B}_{S_u S_v} (\hat{\Sigma}_Y)_{S_v,j}| \\
&= |(\hat{\Sigma}_{XY})_{ij} - (\hat{\Sigma}_X)_{i,S_u} B_{S_u S_v}^* (\hat{\Sigma}_Y)_{S_v,j} + (\hat{\Sigma}_X)_{i,S_u} B_{S_u S_v}^* (\hat{\Sigma}_Y)_{S_v,j} - |(\hat{\Sigma}_X)_{i,S_u} \tilde{B}_{S_u S_v} (\hat{\Sigma}_Y)_{S_v,j}| \\
&\leq \|\hat{\Sigma}_{XY} - \hat{\Sigma}_X B^* \hat{\Sigma}_Y\|_\infty + |(\hat{\Sigma}_X)_{i,S_u} \tilde{\Delta}_{S_u S_v} (\hat{\Sigma}_Y)_{S_v,j}| \\
&= \|\hat{\Sigma}_{XY} - \hat{\Sigma}_X B^* \hat{\Sigma}_Y\|_\infty + |(\hat{\Sigma}_X)_{i,S_u} \tilde{\Delta}_{S_u S_v} (\hat{\Sigma}_Y)_{S_v,j}| \\
&\leq \|\hat{\Sigma}_{XY} - \hat{\Sigma}_X B^* \hat{\Sigma}_Y\|_\infty + \|(\hat{\Sigma}_X)_{i,S_u}\|_F \|\tilde{\Delta}_{S_u S_v}\|_F \|(\hat{\Sigma}_Y)_{S_v,j}\|_{op} \\
&\leq \|\hat{\Sigma}_{XY} - \hat{\Sigma}_X B^* \hat{\Sigma}_Y\|_\infty + \|(\hat{\Sigma}_X)_{i,S_u}\|_F \|(\hat{\Sigma}_Y)_{S_v,j}\|_{op} \|\tilde{\Delta}_{S_u S_v}\|_F \\
&\leq \|\hat{\Sigma}_{XY} - \hat{\Sigma}_X B^* \hat{\Sigma}_Y\|_\infty + \|(\hat{\Sigma}_X)_{S_u^c S_u}\|_{2,\infty} \|(\hat{\Sigma}_Y)_{S_v S_v}\|_{op} \|\tilde{\Delta}_{S_u S_v}\|_F
\end{aligned}$$

Therefore

$$|\hat{Z}_{ij}| \leq \frac{\|\hat{\Sigma}_{XY} - \hat{\Sigma}_X B^* \hat{\Sigma}_Y\|_\infty}{\rho} + \|(\hat{\Sigma}_X)_{S_u^c S_u}\|_{2,\infty} \|(\hat{\Sigma}_Y)_{S_v S_v}\|_{op} \frac{\|\tilde{\Delta}_{S_u S_v}\|_F}{\rho}$$

Similarly, for $\hat{Z}_{S_u S_v^c}$, we have

$$|\hat{Z}_{ij}| \leq \frac{\|\hat{\Sigma}_{XY} - \hat{\Sigma}_X B^* \hat{\Sigma}_Y\|_\infty}{\rho} + \|(\hat{\Sigma}_Y)_{S_v^c S_v}\|_{2,\infty} \|(\hat{\Sigma}_X)_{S_u S_u}\|_{op} \frac{\|\tilde{\Delta}_{S_u S_v}\|_F}{\rho}$$

And, for $\hat{Z}_{S_u^c S_v^c}$, we have

$$|\hat{Z}_{ij}| \leq \frac{\|\hat{\Sigma}_{XY} - \hat{\Sigma}_X B^* \hat{\Sigma}_Y\|_\infty}{\rho} + \|(\hat{\Sigma}_Y)_{S_v^c S_v}\|_{2,\infty} \|(\hat{\Sigma}_X)_{S_u^c S_u}\|_{2,\infty} \frac{\|\tilde{\Delta}_{S_u S_v}\|_F}{\rho}$$

Define

$$\hat{\tau}(X, Y) = \max\{\|(\hat{\Sigma}_X)_{S_u^c S_u}\|_{2,\infty} \|(\hat{\Sigma}_Y)_{S_v^c S_v}\|_{2,\infty}, \|(\hat{\Sigma}_X)_{S_u^c S_u}\|_{2,\infty} \|(\hat{\Sigma}_Y)_{S_v S_v}\|_{op}, \|(\hat{\Sigma}_X)_{S_u S_u}\|_{op} \|(\hat{\Sigma}_Y)_{S_v^c S_v}\|_{2,\infty}\}$$

Then by Lemma D.6, the KKT condition is satisfied when

$$\frac{\|\hat{\Sigma}_{XY} - \hat{\Sigma}_X B^* \hat{\Sigma}_Y\|_\infty}{\rho} + \frac{2(\|\hat{\Sigma}_{XY} - \hat{\Sigma}_X B^* \hat{\Sigma}_Y\|_\infty + \rho)}{\rho} \frac{\hat{\tau}(X, Y) \sqrt{s_u s_v}}{\sigma_{\min}((\hat{\Sigma}_X)_{S_u S_u}) \sigma_{\min}((\hat{\Sigma}_Y)_{S_v S_v})} \leq 1$$

We then prove the uniqueness of the solution (\hat{B}, \hat{Z}) . Let (\hat{B}', \hat{Z}') be another pair of solutions. Let $F(B) = \frac{1}{2} \|XBY^\top/n - I_n\|_F^2$. Then we must have:

$$\begin{aligned} F(\hat{B}) + \rho \langle \hat{B}, \hat{Z} \rangle &= F(\hat{B}') + \rho \langle \hat{B}', \hat{Z}' \rangle \\ F(\hat{B}) + \rho \langle \hat{B} - \hat{B}', \hat{Z} \rangle &= F(\hat{B}') + \rho \langle \hat{B}', \hat{Z}' - \hat{Z} \rangle \end{aligned}$$

By the KKT conditions, we know $\rho \hat{Z} = -\nabla F(\hat{B})$. Therefore

$$F(\hat{B}) - F(\hat{B}') - \langle \hat{B} - \hat{B}', \nabla F(\hat{B}) \rangle = \rho \langle \hat{B}', \hat{Z}' - \hat{Z} \rangle = \rho \|\hat{B}'\|_1 - \rho \langle \hat{B}', \hat{Z} \rangle$$

By convexity of F , the left-hand side is non-positive. This implies $\|\hat{B}'\|_1 \leq \langle \hat{B}', \hat{Z} \rangle$. But we also have $\langle \hat{B}', \hat{Z} \rangle \leq \|\hat{B}'\|_1$ by the min-max formulation. This suggests $\|\hat{B}'\|_1 = \langle \hat{B}', \hat{Z} \rangle$. On the other hand, this inequality only occurs when $\hat{B}'_{i,j} = 0$ if $(i, j) \notin S_u \times S_v$. This implies \hat{B}' also has support inside $S_u \times S_v$. The proof is finished by the strict convexity of the objective inside $S_u \times S_v$. \square

F.1.3 Corollary 3.3.1

Consider the parameter space $\mathcal{F}(s_u, s_v, p, q, r; M)$ for the covariance matrix Σ (Equation 3 and conditions therein), and assume

$$\frac{2\tau(X, Y)\sqrt{s_u s_v}}{\sigma_{\min}((\Sigma_X)_{S_u S_u})\sigma_{\min}((\Sigma_Y)_{S_v S_v})} < 1 - \alpha, \quad (28)$$

for some $\alpha \in (0, 1]$, where

$$\begin{aligned} \tau(X, Y) = \max \Big\{ & \|(\Sigma_X)_{S_u^c S_u}\|_{2,\infty} \|(\Sigma_Y)_{S_v^c S_v}\|_{2,\infty}, \\ & \|(\Sigma_X)_{S_u^c S_u}\|_{2,\infty} \|(\Sigma_Y)_{S_v S_v}\|_{op}, \\ & \|(\Sigma_X)_{S_u S_u}\|_{op} \|(\Sigma_Y)_{S_v^c S_v}\|_{2,\infty} \Big\}. \end{aligned}$$

There exist some constants a, b, c depending on M and α such that if $n \geq c(s_u + s_v) \log(p+q)$ and $\rho \geq a\sqrt{\log(p+q)/n}$, then the minimizer of δ is unique and satisfies

$$\text{supp}(\widehat{B}) \subset S_u \times S_v$$

with probability at least $1 - \exp(-bs_u \log(ep/s_u)) - \exp(-bs_v \log(eq/s_v)) - (p+q)^{-b}$.

Proof of Corollary 3.3.1. By Lemma D.3, there exist constants a and b such that with probability at least $1 - (p+q)^{-b}$,

$$\|\widehat{\Sigma}_{XY} - \widehat{\Sigma}_X \widehat{\Sigma}_Y\|_\infty \leq a\sqrt{\log(p+q)/n}.$$

It follows that

$$\|(\widehat{\Sigma}_X)_{S_u^c S_u}\|_{2,\infty} \leq \|(\Sigma_X)_{S_u^c S_u}\|_{2,\infty} + a\sqrt{s_u} \sqrt{\log(p+q)/n}$$

$$\|(\widehat{\Sigma}_Y)_{S_v^c S_v}\|_{2,\infty} \leq \|(\Sigma_Y)_{S_v^c S_v}\|_{2,\infty} + a\sqrt{s_v} \sqrt{\log(p+q)/n}$$

On the other hand, by Lemma D.4, there exist constants a' and b' such that with probability at least $1 - \exp(-b's_u \log(ep/s_u)) - \exp(-b's_v \log(eq/s_v))$, we have

$$\sigma_{\max}(\widehat{\Sigma}_X) \leq \sigma_{\max}(\Sigma_X) + a'\sqrt{s_u \log(ep/s_u)/n}$$

$$\sigma_{\min}(\widehat{\Sigma}_Y) \geq \sigma_{\min}(\Sigma_Y) - a'\sqrt{s_v \log(ep/s_v)/n}$$

$$\sigma_{\max}(\widehat{\Sigma}_X) \leq \sigma_{\max}(\Sigma_X) + a'\sqrt{s_v \log(eq/s_u)/n}$$

$$\sigma_{\min}(\widehat{\Sigma}_Y) \geq \sigma_{\min}(\Sigma_Y) - a'\sqrt{s_v \log(eq/s_v)/n}$$

Then as a consequence of Theorem 3.3, the proof is done by choosing $n \geq c_n(s_u + s_v) \log(p+q)$ and $\rho \geq c_\rho \sqrt{\log(p+q)/n}$ for sufficiently large constants c_n and c_ρ

F.1.4 Theorem 3.2

Suppose that all the assumptions stated in Theorem 3.1 are satisfied. In addition, assume $n \geq cs_u s_v \log(p+q)/\rho_r^{\star 2}$ for some sufficiently large constant c . There exist constants a_1, a_2, b , and C depending on M and c such that if $\rho \in \left[a_1 \sqrt{\frac{\log(p+q)}{n}}, a_2 \sqrt{\frac{\log(p+q)}{n}} \right]$, then with probability at least $1 - \exp(-B^*(s_u + \log(ep/s_u))) - \exp(-B^*(s_v + \log(eq/s_v))) - (p+q)^{-b}$, we have

$$\max \left\{ \min_{W \in \mathcal{O}_r} \|\widehat{U} - U^* W\|_F, \min_{\tilde{W} \in \mathcal{O}_r} \|\widehat{V} - V^* \tilde{W}\|_F \right\} \leq C \frac{1}{\rho_r^{\star 2}} \sqrt{\frac{s_u s_v \log(p+q)}{n}}.$$

□

Proof of Theorem 3.2. Let

$$\begin{aligned} \tilde{U} &= U^*(U^{\star \top} \widehat{\Sigma}_X U^*)^{-1/2}, \\ \tilde{V} &= V^*(V^{\star \top} \widehat{\Sigma}_Y V^*)^{-1/2}, \\ \tilde{\Lambda} &= (U^{\star \top} \widehat{\Sigma}_X U^*)^{1/2} \Lambda^* (V^{\star \top} \widehat{\Sigma}_Y V^*)^{1/2} \end{aligned}$$

so that

$$B^* = U^* \Lambda^* V^{\star \top} = \tilde{U} \tilde{\Lambda} \tilde{V}^{\top}$$

We first show that $\widehat{\Sigma}_X^{1/2} \widehat{B} \widehat{\Sigma}_Y^{1/2}$ is close to $\widehat{\Sigma}_X^{1/2} \tilde{U} \Lambda^* \tilde{V}^{\top} \widehat{\Sigma}_Y^{1/2}$. Note

$$\begin{aligned} \|\widehat{\Sigma}_X^{1/2} \widehat{B} \widehat{\Sigma}_Y^{1/2} - \widehat{\Sigma}_X^{1/2} \tilde{U} \Lambda^* \tilde{V}^{\top} \widehat{\Sigma}_Y^{1/2}\|_F &\leq \|\widehat{\Sigma}_X^{1/2} \Delta \widehat{\Sigma}_Y^{1/2}\|_F + \|\widehat{\Sigma}_X^{1/2} B^* \widehat{\Sigma}_Y^{1/2} - \widehat{\Sigma}_X^{1/2} \tilde{U} \Lambda^* \tilde{V}^{\top} \widehat{\Sigma}_Y^{1/2}\|_F \\ &\leq \|\widehat{\Sigma}_X^{1/2} \Delta \widehat{\Sigma}_Y^{1/2}\|_F + \|\widehat{\Sigma}_X^{1/2} \tilde{U} (\Lambda^* - \tilde{\Lambda}) \tilde{V}^{\top} \widehat{\Sigma}_Y^{1/2}\|_F \\ &\leq \|\widehat{\Sigma}_X^{1/2} \Delta \widehat{\Sigma}_Y^{1/2}\|_F + \|\widehat{\Sigma}_X^{1/2} \tilde{U}\|_{op} \|(\Lambda^* - \tilde{\Lambda})\|_{op} \|\tilde{V}^{\top} \widehat{\Sigma}_Y^{1/2}\|_F \\ &\leq \|\widehat{\Sigma}_X^{1/2} \Delta \widehat{\Sigma}_Y^{1/2}\|_F + \sqrt{r} \|\Lambda^* - \tilde{\Lambda}\|_{op} \end{aligned}$$

Following the same logic as in the proof of Theorem 3.2, there exists a constant κ such that

$$\|\widehat{\Sigma}_X^{1/2} \Delta \widehat{\Sigma}_Y^{1/2}\|_F \leq \kappa \|\Delta\|_F \lesssim \sqrt{\frac{s_u s_v \log(p+q)}{n}},$$

where the last inequality is a consequence of Theorem 3.2. By Lemma D.5 , with high probability we know

$$\begin{aligned}
\|\Lambda^* - \tilde{\Lambda}\|_{op} &\leq \|(I - (U^{\star\top} \hat{\Sigma}_X U^*)^{1/2}) \Lambda^*\|_{op} + \|(U^{\star\top} \hat{\Sigma}_X U^*)^{1/2} \Lambda^* (I - (V^{\star\top} \hat{\Sigma}_Y V)^{1/2})\|_{op} \\
&\lesssim \sqrt{\frac{s_u + \log(ep/s_u)}{n}} + \left(1 + \sqrt{\frac{s_u + \log(ep/s_u)}{n}}\right) \sqrt{\frac{s_v + \log(eq/s_v)}{n}} \\
&\lesssim \left(\sqrt{\frac{s_u + \log(ep/s_u)}{n}} + \sqrt{\frac{s_v + \log(eq/s_v)}{n}}\right)
\end{aligned}$$

Therefore

$$\begin{aligned}
\|\hat{\Sigma}_X^{1/2} \hat{B} \hat{\Sigma}_Y^{1/2} - \hat{\Sigma}_X^{1/2} \tilde{U} \Lambda^* \tilde{V}^\top \hat{\Sigma}_Y^{1/2}\|_F &\lesssim \sqrt{\frac{s_u s_v \log(p+q)}{n}} + \sqrt{r} \left(\sqrt{\frac{s_u + \log(ep/s_u)}{n}} + \sqrt{\frac{s_v + \log(eq/s_v)}{n}}\right) \\
&\lesssim \sqrt{\frac{s_u s_v \log(p+q)}{n}}
\end{aligned}$$

Denote the rank- r SVD of $\hat{\Sigma}_X^{1/2} \hat{B} \hat{\Sigma}_Y^{1/2}$ by $U_0 \Lambda_0 V_0^\top$. By Wedin's theorem, since $n \geq c \frac{s_u s_v \log(p+q)}{\lambda_r^2}$ for some sufficiently large constant c , we know

$$\begin{aligned}
\min_{W \in O^{r \times r}} \|U_0 - \hat{\Sigma}_X^{1/2} \tilde{U} W\|_F &\lesssim \frac{1}{\left(\lambda_r - \sqrt{\frac{s_u s_v \log(p+q)}{n}}\right)} \sqrt{\frac{s_u s_v \log(p+q)}{n}} \lesssim \frac{1}{\lambda_r} \sqrt{\frac{s_u s_v \log(p+q)}{n}} \\
\min_{W \in O^{r \times r}} \|V_0 - \hat{\Sigma}_Y^{1/2} \tilde{V} W\|_F &\lesssim \frac{1}{\left(\lambda_r - \sqrt{\frac{s_u s_v \log(p+q)}{n}}\right)} \sqrt{\frac{s_u s_v \log(p+q)}{n}} \lesssim \frac{1}{\lambda_r} \sqrt{\frac{s_u s_v \log(p+q)}{n}} \\
\|\Lambda_0 - \Lambda^*\|_{op} &\lesssim \sqrt{\frac{s_u s_v \log(p+q)}{n}} \leq \frac{\lambda_r}{2}
\end{aligned}$$

Let

$$W_{U^*} := \operatorname{argmin}_{W \in O^{r \times r}} \|U_0 - \hat{\Sigma}_X^{1/2} \tilde{U} W\|_F$$

$$W_{V^*} := \operatorname{argmin}_{W \in O^{r \times r}} \|V_0 - \hat{\Sigma}_Y^{1/2} \tilde{V} W\|_F$$

Note that:

$$\begin{aligned}
U_0 \Lambda_0 V_0^\top - \widehat{\Sigma}_X^{1/2} \tilde{U} \Lambda^* \tilde{V}^\top \widehat{\Sigma}_Y^{1/2} &= (U_0 - \widehat{\Sigma}_X^{1/2} \tilde{U} W_{U^*}) \Lambda_0 V_0^\top + \left(\widehat{\Sigma}_X^{1/2} \tilde{U} W_{U^*} \Lambda_0 V_0^\top - \widehat{\Sigma}_X^{1/2} \tilde{U} \Lambda^* \tilde{V}^\top \widehat{\Sigma}_Y^{1/2} \right) \\
&= (U_0 - \widehat{\Sigma}_X^{1/2} \tilde{U} W_{U^*}) \Lambda_0 V_0^\top + \left(\widehat{\Sigma}_X^{1/2} \tilde{U} W_{U^*} \Lambda_0 V_0^\top - \widehat{\Sigma}_X^{1/2} \tilde{U} \Lambda^* W_{V^*} V_0^\top \right) \\
&\quad + \left(\widehat{\Sigma}_X^{1/2} \tilde{U} \Lambda^* W_{V^*} V_0^\top - \widehat{\Sigma}_X^{1/2} \tilde{U} \Lambda^* \tilde{V}^\top \widehat{\Sigma}_Y^{1/2} \right) \\
&= (U_0 - \widehat{\Sigma}_X^{1/2} \tilde{U} W_{U^*}) \Lambda_0 V_0^\top + \left(\widehat{\Sigma}_X^{1/2} \tilde{U} W_{U^*} (\Lambda_0 - W_{U^*}^\top \Lambda^* W_{V^*}) V_0^\top \right) \\
&\quad + \left(\widehat{\Sigma}_X^{1/2} \tilde{U} \Lambda^* (W_{V^*} V_0^\top - \tilde{V}^\top \widehat{\Sigma}_Y^{1/2}) \right)
\end{aligned}$$

Therefore

$$\begin{aligned}
\|\Lambda_0 - \Lambda^* W_{V^*}\|_F &= \|\widehat{\Sigma}_X^{1/2} \tilde{U} W_{U^*} (\Lambda_0 - W_{U^*}^\top \Lambda^* W_{V^*}) V_0^\top\|_F \\
&\leq \|U_0 \Lambda_0 V_0^\top - \widehat{\Sigma}_X^{1/2} \tilde{U} \Lambda^* \tilde{V}^\top \widehat{\Sigma}_Y^{1/2}\|_F + \|(U_0 - \widehat{\Sigma}_X^{1/2} \tilde{U} W_{U^*}) \Lambda_0\|_F + \|\Lambda^* (W_{V^*} V_0^\top - \tilde{V}^\top \widehat{\Sigma}_Y^{1/2})\|_F \\
&\lesssim \frac{1}{\lambda_r} \sqrt{\frac{s_u s_v \log(p+q)}{n}}
\end{aligned}$$

Note that:

$$\begin{aligned}
\|\widehat{B} \widehat{\Sigma}_Y^{1/2} - \tilde{U} \Lambda^* \tilde{V}^\top \widehat{\Sigma}_Y^{1/2}\|_F &= \|\widehat{B} \widehat{\Sigma}_Y^{1/2} V_0 - B^* \widehat{\Sigma}_Y^{1/2} + B^* \widehat{\Sigma}_Y^{1/2} - \tilde{U} \Lambda^* \tilde{V}^\top \widehat{\Sigma}_Y^{1/2}\|_F \\
&\leq \|\widehat{\Sigma}_Y^{1/2} \Delta\|_F + \|\tilde{U} \tilde{\Lambda} \tilde{V}^\top \widehat{\Sigma}_Y^{1/2} - \tilde{U} \Lambda^* \tilde{V}^\top \widehat{\Sigma}_Y^{1/2}\|_F \\
&\leq \|\widehat{\Sigma}_Y^{1/2} \Delta\|_F + \|\tilde{U}\|_{op} \|\tilde{\Lambda} - \Lambda^*\|_{op} \|\tilde{V}^\top \widehat{\Sigma}_Y^{1/2}\|_F \\
&\leq \|\widehat{\Sigma}_Y^{1/2} \Delta\|_F + \sqrt{r} \|\Sigma_X^{-1/2}\|_{op} \|\Sigma_X^{1/2} U\|_{op} \|(U^* \widehat{\Sigma}_X U^*)^{-1/2}\|_{op} \|\tilde{\Lambda} - \Lambda^*\|_{op} \|\tilde{V}^\top \widehat{\Sigma}_Y^{1/2}\|_{op} \\
&\lesssim \sqrt{\frac{s_u s_v \log(p+q)}{n}}
\end{aligned}$$

And

$$\begin{aligned}
\|\tilde{U} \Lambda^* \tilde{V}^\top \widehat{\Sigma}_Y^{1/2} - \tilde{U} W_{U^*} \Lambda_0 V_0^\top\|_F &\leq \|\tilde{U} \Lambda^* \tilde{V}^\top \widehat{\Sigma}_Y^{1/2} - \tilde{U} \Lambda^* W_{V^*} V_0^\top\|_F + \|\tilde{U} \Lambda^* W_{V^*} V_0^\top - \tilde{U} W_{U^*} \Lambda_0 V_0^\top\|_F \\
&\leq \|\tilde{U}\|_{op} \|\Lambda^*\|_{op} \|\widehat{\Sigma}_Y^{1/2} - W_{V^*} V_0^\top\|_F + \|\tilde{U}\|_{op} \|\Lambda^* - W_{U^*} \Lambda_0 W_{V^*}^\top\|_F \|W_{V^*}^\top\|_{op} \\
&\lesssim \frac{1}{\lambda_r} \sqrt{\frac{s_u s_v \log(p+q)}{n}}
\end{aligned}$$

Therefore

$$\begin{aligned} \|\widehat{B}\widehat{\Sigma}_Y^{1/2} - U^\star W_{U^\star} \Lambda_0 V_0^\top\|_F &= \|\widehat{B}\widehat{\Sigma}_Y^{1/2} - \tilde{U} \Lambda^\star \tilde{V}^\top \widehat{\Sigma}_Y^{1/2} + \tilde{U} \Lambda^\star \tilde{V}^\top \widehat{\Sigma}_Y^{1/2} - \tilde{U} W_{U^\star} \Lambda_0 V_0^\top + (\tilde{U} - U^\star) W_{U^\star} \Lambda_0 V_0^\top\|_F \\ &\lesssim \frac{1}{\lambda_r} \sqrt{\frac{s_u s_v \log(p+q)}{n}} \end{aligned}$$

Hence

$$\|\widehat{B}\widehat{\Sigma}_Y^{1/2} V_0 \Lambda_0^{-1} - U^\star W_{U^\star}\| \leq \|\widehat{B}\widehat{\Sigma}_Y^{1/2} - U^\star W_{U^\star} \Lambda_0 V_0^\top\|_F \|V_0\|_{op} \|\Lambda_0^{-1}\|_{op} \lesssim \frac{1}{\lambda_r^2} \sqrt{\frac{s_u s_v \log(p+q)}{n}}$$

□

F.2 The group-sparse setting

We have the following error bound on estimating B^\star for the group sparse CCA setting.

Theorem F.1. *Consider the parameter spaces $\mathcal{F}(s_u, s_v, p, q, r; M)$ of all covariance matrices Σ that satisfy the condition and denote by s the number of groups. Assume $n \geq cs \log(p+q)$ for some sufficiently large constant c . Define $\Delta = \widehat{B} - B^\star$. Then there exist some constants a, b, C depending on M and c such that if $\rho \geq a \sqrt{\log(p+q)/n}$, Then with probability at least $1 - \exp(-B^\star s_u \log(ep/s_u)) - \exp(-B^\star s_v \log(eq/s_v)) - (p+q)^{-b}$, we have*

$$\|\Delta\|_F \leq C \rho \sqrt{s}$$

In particular, if ρ is of order $\sqrt{\log(p+q)/n}$, we have

$$\|\Delta\|_F \lesssim \sqrt{\frac{s \log(p+q)}{n}}$$

And \widehat{B} has sparse entries:

$$\|\widehat{B}\|_0 \lesssim s$$

Proof of Theorem F.1. Following a similar argument as in the proof of Theorem 3.1, we have

$$\begin{aligned}
L(\widehat{B}) + \rho \sum_{g \in G} \sqrt{T_g} \|\widehat{B}_g\|_F &\leq L(B) + \rho \sum_{g \in G} \sqrt{T_g} \|B_g^*\|_F \\
\frac{1}{2} \|X \widehat{B} Y^\top / n - I_n\|_F^2 + \rho \sum_{g \in G} \sqrt{T_g} \|\widehat{B}_g\|_F &\leq \frac{1}{2} \left\| \frac{1}{n} X B^* Y^\top - I_n \right\|_F^2 + \rho \sum_{g \in G} \sqrt{T_g} \|B_g^*\|_F \\
\frac{1}{2} \|X \widehat{B} Y^\top / n\|_F^2 - \text{tr}(X \widehat{B} Y^\top) / n &\leq \frac{1}{2} \|X B Y^\top / n\|_F^2 - \text{tr}(X B Y^\top) / n + \rho \sum_{g \in G} \sqrt{T_g} (\|B_g^*\|_1 - \|\widehat{B}_g\|_F) \\
\frac{1}{2} \|X(B^* + \Delta) Y^\top / n\|_F^2 - \frac{1}{2} \|X B Y^\top / n\|_F^2 &\leq \text{tr}(\Delta^\top \widehat{\Sigma}_{XY}) + \rho \sum_{g \in G} \sqrt{T_g} (\|B_g^*\|_F - \|\widehat{B}_g\|_F) \\
\frac{1}{2} \|X \Delta Y^\top / n\|_F^2 + \text{tr}(Y B^{*\top} X^\top X \Delta Y^\top) / n^2 &\leq \text{tr}(\Delta^\top \widehat{\Sigma}_{XY}) + \rho \sum_{g \in G} \sqrt{T_g} (\|B_g^*\|_F - \|\widehat{B}_g\|_F) \\
\frac{1}{2} \|X \Delta Y^\top / n\|_F^2 + \text{tr}(\widehat{\Sigma}_Y B^{*\top} \widehat{\Sigma}_X \Delta) &\leq \text{tr}(\Delta^\top \widehat{\Sigma}_{XY}) + \rho \sum_{g \in G} \sqrt{T_g} (\|B_g^*\|_F - \|\widehat{B}_g\|_F) \\
\frac{1}{2} \|X \Delta Y^\top / n\|_F^2 &\leq \langle \widehat{\Sigma}_{XY} - \widehat{\Sigma}_X B^* \widehat{\Sigma}_Y, \Delta \rangle + \rho \sum_{g \in G} \sqrt{T_g} (\|B_g^*\|_F - \|\widehat{B}_g\|_F)
\end{aligned}$$

By the triangle inequality, we have

$$\begin{aligned}
\frac{1}{2} \|X \Delta Y^\top / n\|_F^2 &\leq \langle \widehat{\Sigma}_{XY} - \widehat{\Sigma}_X B^* \widehat{\Sigma}_Y, \Delta \rangle + \rho \sum_{g \in G_0} \sqrt{T_g} (\|B_g^*\|_F - \|\widehat{B}_g\|_F) - \rho \sum_{g \notin G_0} \sqrt{T_g} \|\widehat{B}_g\|_F \\
\frac{1}{2} \|X \Delta Y^\top / n\|_F^2 &\leq \langle \widehat{\Sigma}_{XY} - \widehat{\Sigma}_X B^* \widehat{\Sigma}_Y, \Delta \rangle + \rho \sum_{g \in G_0} \sqrt{T_g} \|\Delta_g\|_F - \rho \sum_{g \notin G_0} \sqrt{T_g} \|\Delta_g\|_F
\end{aligned}$$

On the other hand, we have

$$\begin{aligned}
\langle \widehat{\Sigma}_{XY} - \widehat{\Sigma}_X B^* \widehat{\Sigma}_Y, \Delta \rangle &= \sum_{g \in G} \left\langle \left(\widehat{\Sigma}_{XY} - \widehat{\Sigma}_X B^* \widehat{\Sigma}_Y \right)_g, \Delta_g \right\rangle \\
&\leq \sum_{g \in G} \left\| \left(\widehat{\Sigma}_{XY} - \widehat{\Sigma}_X B^* \widehat{\Sigma}_Y \right)_g \right\|_F \|\Delta_g\|_F \\
&\leq \max_{g \in G} \left(\left\| \left(\widehat{\Sigma}_{XY} - \widehat{\Sigma}_X B^* \widehat{\Sigma}_Y \right)_g \right\|_F / \sqrt{T_g} \right) \left(\sum_{g \in G} \sqrt{T_g} \|\Delta_g\|_F \right) \\
&\leq \|\widehat{\Sigma}_{XY} - \widehat{\Sigma}_X B^* \widehat{\Sigma}_Y\|_\infty \left(\sum_{g \in G} \sqrt{T_g} \|\Delta_g\|_F \right)
\end{aligned}$$

By our choice of ρ and Lemma D.3 we have

$$0 \leq \frac{\rho}{2} \sum_{g \in G} \sqrt{T_g} \|\Delta_g\|_F + \rho \sum_{g \in G_0} \sqrt{T_g} \|\Delta_g\|_F - \rho \sum_{g \notin G_0} \sqrt{T_g} \|\Delta_g\|_F$$

Therefore

$$\sum_{g \in G} \sqrt{T_g} \|\Delta_g\|_F \leq 3 \sum_{g \notin G_0} \sqrt{T_g} \|\Delta_g\|_F$$

Then

$$\begin{aligned} \frac{1}{2} \|X \Delta Y^\top / n\|_F^2 &\leq \frac{\rho}{2} \sum_{g \in G} \sqrt{T_g} \|\Delta_g\|_F + \rho \sum_{g \in G_0} \sqrt{T_g} \|\Delta_g\|_F \\ &= \frac{3\rho}{2} \sum_{g \in G_0} \sqrt{T_g} \|\Delta_g\|_F + \frac{\rho}{2} \sum_{g \notin G_0} \sqrt{T_g} \|\Delta_g\|_F \\ &\leq 3\rho \sum_{g \in G_0} \sqrt{T_g} \|\Delta_g\|_F \\ &\leq 3\rho \sqrt{\left(\sum_{g \in G_0} T_g\right) \left(\sum_{g \in G_0} \|\Delta_g\|_F^2\right)} \\ &\leq 3\rho \sqrt{s} \|\Delta_S\|_F \end{aligned}$$

Now let us look at $\|X \Delta Y^\top / n\|_F^2 = \text{tr}(\Delta^\top \hat{\Sigma}_X \Delta \hat{\Sigma}_Y) = \|\hat{\Sigma}_X^{1/2} \Delta \hat{\Sigma}_Y^{1/2}\|_F^2$. Let $G_0^c = \{g_1, g_2, \dots, g_r\}$ and without loss of generality assume $\|\Delta_{g_1}\|_1 \geq \|\Delta_{g_2}\|_1 \geq \dots \geq \|\Delta_{g_r}\|_1$. Let the index set $J_1 = \{(i_k, j_k)\}_{k=1}^\top \in S^c$ that correspond to the entries with the largest absolute values in Δ_{g_1} . If $t \geq T_{g_1}$, then J_1 first includes all entries from g_1 and then the largest $t - T_{g_1}$ entries from g_2 , and so on. We define the set $\tilde{J} = S \cup J_1$. Now we partition \tilde{J}^c into disjoint subsets J_2, \dots, J_K of size t (with $|J_K| \leq t$) following the rules we used to construct J_1 . By triangle inequality,

$$\begin{aligned} \|\hat{\Sigma}_X^{1/2} \Delta \hat{\Sigma}_Y^{1/2}\|_F &\geq \|\hat{\Sigma}_X^{1/2} \Delta_{\tilde{J}} \hat{\Sigma}_Y^{1/2}\|_F - \sum_{k=2}^K \|\hat{\Sigma}_X^{1/2} \Delta_{J_k} \hat{\Sigma}_Y^{1/2}\|_F \\ &\geq \sqrt{\phi_{\min}^{\hat{\Sigma}_X}(s+t) \phi_{\min}^{\hat{\Sigma}_Y}(s+t)} \|\Delta_{\tilde{J}}\|_F - \sqrt{\phi_{\max}^{\hat{\Sigma}_X}(t) \phi_{\max}^{\hat{\Sigma}_Y}(t)} \sum_{k=2}^K \|\Delta_{J_k}\|_F \end{aligned}$$

Also we have

$$\sum_{k=2}^K \|\Delta_{J_k}\|_F = \frac{1}{\sqrt{t}} \sum_{k=2}^K \sqrt{t} \|\Delta_{J_k}\|_F \leq \frac{1}{\sqrt{t}} \sum_{g \in G_0^c} \sqrt{T_g} \|\Delta_g\|_F \leq \frac{3}{\sqrt{t}} \sum_{g \in G_0} \sqrt{T_g} \|\Delta_g\|_F \leq \frac{3\sqrt{s}}{\sqrt{t}} \|\Delta_{\bar{J}}\|_F$$

Therefore

$$\|\hat{\Sigma}_X^{1/2} \Delta \hat{\Sigma}_Y^{1/2}\|_F \geq \left(\sqrt{\phi_{\min}^{\hat{\Sigma}_X}(s+t) \phi_{\min}^{\hat{\Sigma}_Y}(s+t)} - \frac{3\sqrt{s}}{\sqrt{t}} \sqrt{\phi_{\max}^{\hat{\Sigma}_X}(t) \phi_{\max}^{\hat{\Sigma}_Y}(t)} \right) \|\Delta_{\bar{J}}\|_F$$

Take $t = c_1 s$ for some sufficiently large constant $c_1 > 1$. Then with high probability,

$$\left(\sqrt{\phi_{\min}^{\hat{\Sigma}_X}(s+t) \phi_{\min}^{\hat{\Sigma}_Y}(s+t)} - \frac{3\sqrt{s}}{\sqrt{t}} \sqrt{\phi_{\max}^{\hat{\Sigma}_X}(t) \phi_{\max}^{\hat{\Sigma}_Y}(t)} \right) \geq \kappa,$$

where κ is some positive constant that depends only on M . To see this, note by Lemma D.4, $\delta_u(s+t)$ and $\delta_v(s+t)$ are bounded by $\frac{2c_1 s \log(p)}{n}$ and $\frac{2c_1 s \log(q)}{n}$, which are small by assumption. The same arguments hold for $\delta_u(t)$ and $\delta_v(t)$. Therefore taking c_1 to be large leads to the lower bound κ . Combining this result with the upper bound on the right-hand side, we have

$$\kappa^2 \|\Delta_{\bar{J}}\|_F^2 \leq \|\hat{\Sigma}_X^{1/2} \Delta \hat{\Sigma}_Y^{1/2}\|_F^2 \leq 3\rho\sqrt{s} \|\Delta_S\|_F \leq 3\rho\sqrt{s} \|\Delta_{\bar{J}}\|_F$$

Therefore

$$\|\Delta_{\bar{J}}\|_F \leq \frac{3\rho\sqrt{s}}{\kappa^2}$$

On the other hand,

$$\|\Delta_{\bar{J}^c}\|_F = \sum_{k=2}^K \|\Delta_{J_k}\|_F \leq \frac{3\sqrt{s}}{\sqrt{t}} \|\Delta_{\bar{J}}\|_F = \frac{3\sqrt{s}}{\sqrt{c_1 s}} \|\Delta_{\bar{J}}\|_F$$

Combining all the results from steps 1, 2 and 3, we showed the bound on $\|\Delta\|_F$.

Then we prove the support of \hat{B} is sparse. By the KKT conditions, we have

$$\left(\hat{\Sigma}_X \hat{B} \hat{\Sigma}_Y - \hat{\Sigma}_{XY} \right)_g = \rho \sqrt{T_g} \frac{\partial \|B_g\|_F}{\partial B}$$

Therefore

$$\left\| \left(\widehat{\Sigma}_X \Delta \widehat{\Sigma}_Y \right)_g \right\|_F \geq \rho \sqrt{T_g} - \|\widehat{\Sigma}_X B^\star \widehat{\Sigma}_Y - \widehat{\Sigma}_{XY}\|_\infty \sqrt{T_g} \geq \frac{\rho \sqrt{T_g}}{2},$$

where the last inequality follows from Lemma D.3. Let T be the set of non-zero elements

in \widehat{B} , T_u be the non-zero rows of \widehat{B} and T_v be the non-zero columns of \widehat{B} . Then

$$\begin{aligned} \frac{\rho^2}{4} T &= \sum_{g \in G_0} \frac{\rho^2}{4} T_g \leq \sum_{g \in G_0} \left\| \left(\widehat{\Sigma}_X \Delta \widehat{\Sigma}_Y \right)_g \right\|_F^2 \\ &\leq \delta_u(T_u) \delta_v(T_v) \|\Delta\|_F^2 \\ &\lesssim \left(M + \sqrt{\frac{T_u \log(p)}{n}} \right) \left(M + \sqrt{\frac{T_v \log(q)}{n}} \right) \rho^2 s \\ &\lesssim \left(M^2 + M \sqrt{\frac{(T_u + T_v) \log(p+q)}{n}} + \sqrt{\frac{T_u T_v \log(p) \log(q)}{n^2}} \right) \rho^2 s \\ &\lesssim \left(M^2 + M \sqrt{\frac{T \log(p+q)}{n}} + \frac{T \log(p+q)}{n} \right) \rho^2 s \end{aligned}$$

Here the fourth inequality is implied by Lemma D.4. It follows that

$$\left(\frac{1}{4} - \frac{s \log(p+q)}{n} \right) T \leq \left(M^2 + M \sqrt{\frac{T \log(p+q)}{n}} \right) s$$

By assumption,

$$\frac{1}{4} - \frac{s \log(p+q)}{n} \geq \frac{1}{8}$$

for sufficiently large c . Solving

$$\frac{1}{8} T \leq \left(M^2 + M \sqrt{\frac{T \log(p+q)}{n}} \right) s$$

gives

$$\sqrt{T} \lesssim \sqrt{\frac{\log(p+q)}{n}} s + \sqrt{s}$$

Again, as long as $n \geq cs \log(p+q)$ for sufficiently large constant c , we have

$$T \lesssim \frac{\log(p+q)s}{n} s + s \lesssim s$$

□

Following a similar analysis, we are able to show the following results for the estimates \widehat{U} and \widehat{V} .

Theorem F.2. *Suppose that all the assumptions stated in Theorem F.1 are satisfied. In addition, assume $n \geq cs_us_v \log(p+q)/\rho_r^{\star 2}$ for some sufficiently large constant c . There exist constants a_1, a_2, b, C depending on M and c such that if $\rho \in \left[a_1 \sqrt{\frac{\log(p+q)}{n}}, a_2 \sqrt{\frac{\log(p+q)}{n}} \right]$, then with probability at least $1 - \exp(-B^\star(s_u + \log(ep/s_u))) - \exp(-B^\star(s_v + \log(eq/s_v))) - (p+q)^{-b}$, we have*

$$\max \left\{ \min_{W \in \mathcal{O}_r} \|\widehat{U}^\star - U^\star W\|_F, \min_{W \in \mathcal{O}_r} \|\widehat{V} - V^\star W\|_F \right\} \leq C \frac{1}{\rho_r^{\star 2}} \sqrt{\frac{s \log(p+q)}{n}}, .$$

Proof of Theorem F.2. This directly follows from the consequence of Theorem F.1 and the proof of Theorem 3.2. □